Block Copolymers for Sustainable Thermoplastic Elastomers and Nanoparticle Fabrication

A Dissertation
SUBMITTED TO THE FACULTY OF
UNIVERSITY OF MINNESOTA
BY

Mohammadreza Nasiri

IN PARTIAL FULFILLMENT OF THE REQUIREMENTS
FOR THE DEGREE OF
DOCTOR OF PHILOSOPHY

Theresa M. Reineke

December, 2017

Acknowledgements

First and foremost, I would like to extend my sincere gratitude to my advisor, Professor Theresa Reineke. It has been a privilege to be mentored by such an amazing person. She was a wonderful mentor full of encouragement and support and gave me great latitude in determining my own direction and played a significant role in my intellectual growth. Then, I would like to thank my graduate committee members Professor Marc Hillmyer, Professor Mark Distefano, and Professor Chris Macosko for their help and feedbacks along the way. Also, thanks to the Center for Sustainable Polymers (CSP) for giving me the opportunity to be a part of their great mission. Working in CSP was an amazing experience.

A big thank you goes to the Reineke Group members, past and present, for the wonderful support they have provided me during these years. As in particular, Dr. Yaoying Wu, Dr. Jeff Ting, Dr. James Gallagher, Leon Lillie, Anatolii Purchel, and Derek Saxon, thank you for your help along the way. I would also like to thank Dr. Arthur Bertrand for mentoring me in beginning of my PhD and his contribution to the Nanoskiving project. Thank you, Dr. David Giles, for the helpful discussions. I would also like to thank Laura Seifert and Nancy Tao for being very helpful and always finding a solution.

I have been fortunate to have made many wonderful friends during my PhD and I am very appreciative of the fun experiences shared with these friends as well as their incredible support at difficult times. To all of my wonderful friends in Minneapolis and around the world; thank you for your encouragement and help, I am blessed and thankful to have you as my friends.

Furthermore, I want to give my sincerest gratitude to my mother, my father, my sisters, and my brothers for their unconditional love and support. You have always been a great source of inspiration, motivation, and encouragement for me. I love you and this thesis is all dedicated to you.

Finally, I acknowledge all the funding supports from the Chemistry Department and the Graduate School at University of Minnesota, Center for Sustainable Polymers and National Science Foundation (NSF), and National Institutes of Health (NIH).

To My Wonderful Loving Family

For your undying love, encouragement, and sacrifices

Abstract

Sugars have proven to be an excellent resource for building blocks of sustainable polymeric materials. The first area of research presented in this thesis focuses on the preparation of sugar-derived monomers and polymers as well as investigation of their properties. Chapter 2 describes direct modification of glucose to produce new sustainable and functional polymers. Glucose acrylate tetraacetate (GATA) was synthesized and shown to provide a useful glassy component for developing an innovative family of elastomeric and adhesive materials. A series of diblock and triblock copolymers of GATA and *n*-butyl acrylate (nBA) were created via Reversible Addition-Fragmentation Chain Transfer (RAFT) polymerization. These block copolymers were investigated as thermoplastic elastomers (TPE) and while the peel adhesion results were desirable, only moderate mechanical properties were observed. As described in Chapter 3, further structural and chemical modifications were employed to improve the performance of these block copolymers. Isosorbide was also modified to prepare acetylated acrylic isosorbide (AAI), as another sugar-based glassy component. RAFT polymerization was employed to prepare ABA triblock copolymers of GATA and AAI with nBA. Comprehensive adhesion testings were conducted and adhesion properties comparable to many commercial pressure sensitive adhesives were observed. Additionally, GATA-derived triblock copolymers were chemically modified to promote self-complementary hydrogen bonding in their glassy domains, resulting in significant enhancement in their mechanical strength. The improvements observed in the properties of these materials as a result of such non-covalent

interactions allows for improved design of sustainable, sugar-derived polymers as high performance TPEs.

The second area of research focuses on controlled fabrication of cylindrical nanoparticles. A new facile fabrication approach to generate polymeric nanostructures is described in Chapter 4. Block copolymers containing immiscible segments can self-assemble to generate ordered nanostructures, such as cylinders of one block in a matrix of the other in the bulk, which can then be sectioned on the nanoscale using a microtome (nanoskiving). Dispersing these sections in a selective solvent for the matrix block results in nanocylinders. In one example, we utilized a poly(N,N-dimethylacrylamide)-*block*-poly(styrene) (PDMA-PS) copolymer containing 36% by volume of PS. This composition was selected as it self-assembles into cylinders of PS in a matrix of PDMA. The cylinders were aligned using a channel die and the aligned samples were subsequently sectioned using a microtome containing a diamond knife. The resulting sections were dispersed in water, a selective solvent for the PDMA matrix, affording PS nanocylinders with a PDMA corona. This technique allows for tuning of nanocyliders without the requirement of specialty equipment and can be employed for fabrication of therapeutics in nanomedicine.

Table of Contents

List of Figures

List of Schemes

List of Tables

Chapter 1

General Introduction

1.1 Sustainable Materials

Due to their extraordinary versatility, amazing durability, and low cost, polymeric materials (plastics) have become an indispensable part of our lives. With the advent of synthetic polymer chemistry during the past century, plastics have been utilized for an impressively wide range of applications. These applications range from seemingly simple consumer products such as food packaging and water bottles to more specialized technologies such as biomedical devices and electronics, and the global consumption of plastics was estimated to be approximately 300 million tons in 2013.[1] The societal benefits provided by synthetic polymers are undeniable and the modern society is built on these technologies and advancements.

However, the current chemical industry relies on fossil fuels and plastics are mainly produced from non-renewable feedstocks. In addition to their non-renewability, environmental challenges with the manufacturing and disposal processes of plastics is a cause for concern. The recycling of petroleum-derived polymers has been minimal, and their disposal can add to the uncontrolled release of carbon dioxide into the atmosphere, which in the long term is believed to induce global warming of our planet.[2] To ensure that polymers can continue their vital role in our lives, bio-sourced feedstocks have recently gained significant attention as alternatives to conventional petroleum-derived raw materials for plastics. In addition to renewability of these resources, our planet produces approximately 1.8×10^{11} tons of biomass annually,[3] providing an abundant and inexpensive green feedstock (compare to total production of petroleum in 2010 at 3.9×10^{9} tons[4]).

1.1.1 Carbohydrate-sourced Feedstocks

Although renewable polymers currently hold only a small share of the plastics market, environmental concerns associated with the manufacturing and disposal of petroleum-based materials have driven academic and industrial research, as well as governmental policies, to further explore utilization of biomass for commercial applications.[5] Carbohydrates, including small sugar molecules and their natural polymers, such as starch and cellulose, account for approximately three quarters of the total biomass and play a major role in the chemical industry.[3] Carbohydrates are excellent candidates as bio-based feedstocks for development of sustainable and renewable polymers. In addition to their abundancy, sugars are attractive because of their high heteroatom content, rigidity, non-toxicity, and stereochemistry, providing ability to impart unique properties that are not typically offered by petroleum-derived counterparts.[6] Polylactide (PLA) is currently one of the most successful examples for developing a sustainable polymer from biomass. PLA is produced from lactic acid, which is a fermentation product of sugars. Some physical properties of PLA are comparable to polystyrene and it has already been utilized in applications such as fibers, biomaterials, packaging, and single-use items.[7]

The commercial success of biomass-derived polymers, such as PLA, shows the promise for developing further sustainable polymeric materials from sugars. The research described in this thesis is mainly focused on incorporation of sugar-derived monomeric units into polymeric systems to produce renewable materials. This work employs glucose, an abundant and inexpensive sugar, and isosorbide, a product of hydrogenation of glucose to sorbitol and subsequent double dehydration. Both structures are shown in Figure (1.1).

These sugar-derived monomers are utilized to impart glassy segments to thermoplastic elastomers.

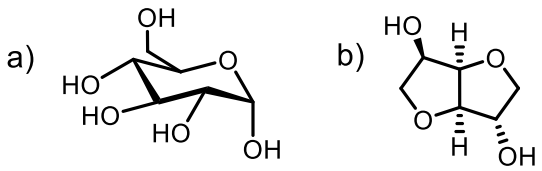

Figure 1.1 a) α-d- glucose. b) 1,4:3,6-dianhydro-d-glucidol (isosorbide)

1.2 Block Copolymer Self-assembly

Polymers derived from more than one monomeric unit are known as copolymers (heteropolymer). Based on the arrangement of these units, copolymers are classified in different groups: statistical copolymers, block copolymers, alternating copolymers, etc. If the copolymer is comprised of two or more covalently linked homopolymer subunits, it is called a block copolymer. Similar to separation phenomenon in a mixture of oil and water, polymers with different chemical make-up ordinarily tend to macrophase separate.[8] This macrophase separation in blends minimizes the free energy. Due to the incompatibility between the blocks, block copolymers with immiscible blocks also tend to phase separate. However, in a block copolymer, since the incompatible segments are bound together by covalent linkages, macro-phase separation is not feasible. Therefore, to minimize the free energy, block copolymers segregate into nanometer-sized structures.[9] The self-assembly behavior of block copolymers into spatially periodic composition patterns in bulk state is described by the term microphase separation.[10]

In general, interactions between chemically similar segments are more favorable compared to the interactions between the distinct portions, which renders the separated

form enthalpically more favorable compared to the mixed state. Due to thermodynamic forces driving the separation, which are required to keep two incompatible portions apart, block copolymers are forced to adapt fewer configurations, compared to their free, randomly coiled forms. Since the polymer chains can freely adapt more configurations in the mixed state, mixing is favored entropically. Although mixing is entropically favorable, the entropy gain is usually small.[9] If specific favorable interactions such as hydrogen bonding are not present between the polymer chains, this trivial entropy gain is not enough to overcome the unfavorable enthalpy of mixing.[10] Thus, even small differences in chemical make-up between the blocks favor phase separation leading to ordered morphologies.[10]

The Flory−Huggins interaction parameter (χ), which quantifies the thermodynamic interactions between two incompatible blocks, alongside the total degree of polymerization (N) and composition (relative ratio of the blocks, f) determine the ordered/disordered state and morphology of the polymer in equilibrium.[10] Bringing two chemically incompatible chains next to each other results in an enthalpic penalty. This energy cost is described by χ which for monomers A and B equals to:[11]

$$\chi_{AB} = \frac{Z}{kT}\left[\epsilon_{AB} - \frac{1}{2}(\epsilon_{AA} + \epsilon_{BB})\right]$$

where Z accounts for the number of the nearest monomers to a copolymer cell in Flory-Huggins theory, k is the Boltzmann constant, T is the temperature, and ϵ_{AB} describes interaction energy between A and B monomers. For an incompatible pair of A and B, χ_{AB} has a positive value. In contrast, negative values for χ_{AB} are indicative of miscibility and describe favorable mixing between A and B. The χ parameter is also temperature

dependent, and increasing temperature generally lowers the free energy penalty of mixing. On the other hand, the favorable entropy gain for the mixed state scales with N^{-1}. As a result, the product of $N\chi$ determines ordered or disordered state of the polymer. For $N\chi$ values smaller than 10.5, known as the location of order-disorder transition (ODT), the block copolymer remains in a disordered form because of the dominant entropic penalty of segregation. For higher $N\chi$ values, the block copolymer chains self-assemble into an ordered morphology.[10]

Morphology of the resulting ordered state is highly dependent on the composition.[9-10] The relationship between phase behavior and composition of block copolymers is described by phase diagrams. Phase behavior of linear block copolymers are the most studied among all different types of copolymer architectures. Phase diagrams resulting from self-consistent field theory (SCFT) studies of AB diblock and ABA triblock copolymers are shown in Figure 1.2.

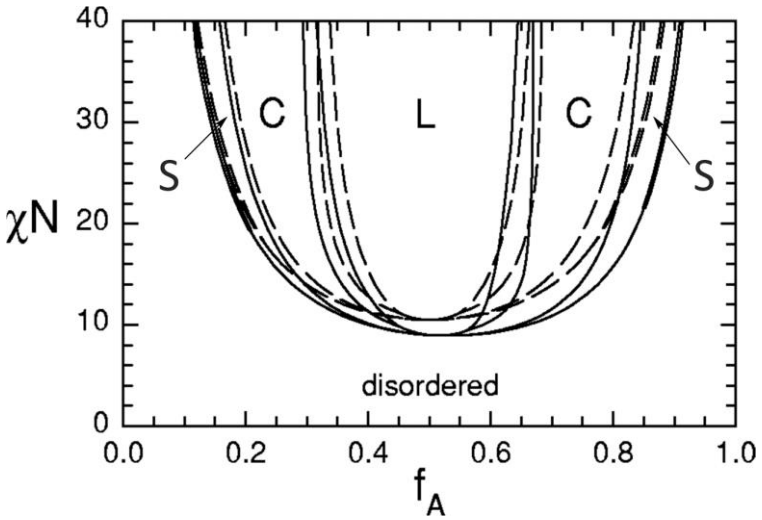

Figure 1.2. AB diblock copolymer phase diagram (dashed curves) overlaid on ABA triblock copolymer phase diagram (solid curves): Lamellar (L), Cylindrical (C), Spherical (S). Adapted from Matsen and Thompson.[12]

Since the temperature and the monomer selection for the distinct blocks determine the interaction parameter (χ), and the degree of polymerization (N) and composition (f) are controllable by synthetic methods, polymeric systems can be designed to phase-separate to desired morphologies. This extraordinary feature allows for utilization of block copolymers for a wide variety of applications.

1.3 Thermoplastic Elastomers

While the physical properties of a polymeric material are dictated by its chemical structure, the range of properties and performance for a polymer can be expanded by incorporation of a second monomer, comonomer, into its architecture. Recent advancements in synthetic techniques have allowed for engineering of polymeric materials with desired characteristics. ABA-type triblock copolymers are one of the very useful examples of this structural tuning and are commercially used as thermoplastic elastomers (TPE).[13] If the A and B units have the characteristics required for phase-separation, i.e. they are immiscible and the polymers are long enough, the disparate blocks of the copolymer tend to self-assemble into microstructures, with B segments forming physical cross-links between the A domains (Figure 1.3). ABA triblock copolymers for TPEs are designed to have a soft middle segment (B) with two glassy endblocks (A). Upon phase separation, the rubbery units bridge between the hard domains and form a physically cross-linked network. Physical cross-linking creates a resistance to flow in the material and the polymer exhibits elastomeric properties at room temperature.[14] Unlike their chemically cross-linked counterparts, i.e. thermosets, TPEs can be melted and reprocessed at elevated

temperatures. From the environmental standpoint, TPEs' reprocessability makes them an attractive class of polymeric materials. Although these materials can be recycled, only a small percentage of them, similar to other thermoplastics, are recovered for reuse. Thermoplastics suffer from minimal recycling rates mainly due to lack of education (both in end-consumers and trash disposal facilities, especially in underdeveloped areas of the world) and recycling cost and efficiency for the manufacturers (in most cases, recycling has almost similar cost to producing virgin materials, while the former gives a lower value product at times).[15]

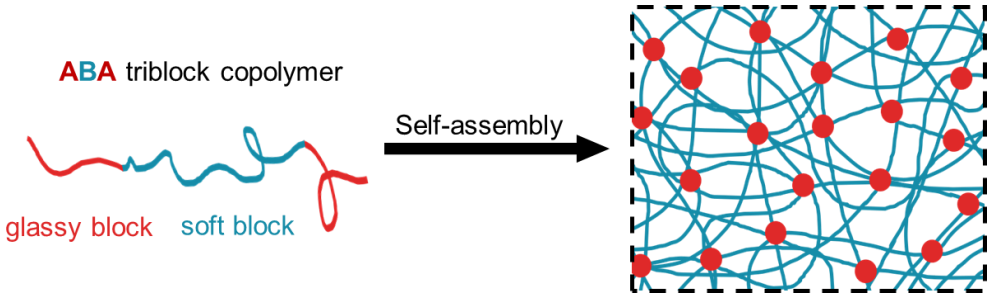

Figure 1.3. Schematic representation of physical cross-linking in ABA-type triblock copolymers.

Pressure sensitive adhesives (PSAs) are a useful type of TPEs that are commercially utilized for a wide variety of applications. A PSA is an adhesive that bonds to the substrate when pressure is applied. In general, PSA properties are defined by three main characteristics; peel adhesion, tack, and shear strength. Peel adhesion is a measure of the force required to peel off the adhesive from a substrate at 180°. Tack tests measure the instantaneous bonding between the adhesive and a substrate when they are brought into contact, without applying any force. Lastly, shear strength is a measure of the adhesive's resistance to flow under an applied pressure.[16] Additionally, the shear test can be conducted

under a temperature ramp to measure the limiting temperature above which the adhesive fails to resist the loaded pressure, shear adhesion failure temperature (SAFT). Depending on the desired end application, various ranges of the abovementioned characteristics may be favorable.

1.4 Nanoparticle Fabrication

The term "nanotechnology" is generally defined by the design and exploitation of materials and structures with dimensions in the nanometer range. A variety of research areas are involved with the nanotechnology principles, ranging from the fabrication of nanomachines, to the application of nanolithography, to the development of nanoparticles.[17] Since the nanoscale sizes are between molecular size and microscale range, the nanoparticle fabrication methods are divided into two main categories: “top–down” and “bottom–up” approaches according to the processes involved in creating nanoscale sizes. In a top–down method, the desired dimensions are achieved by reducing the larger dimensions in a mechanically controlled manner. On the other hand, a bottom-up approach corresponds to building up the constituents in their molecular sizes into more complex nanoscale assemblies.[18]

1.4.1 Polymeric Nanoparticle Fabrication

In this section, some of the methods for the preparation of polymeric nanoparticles are briefly described. These methods include: solvent displacement, dialysis, supercritical fluid technology, photolithography, and imprint lithography techniques.

1.4.1.1 Solvent Displacement

In the nanoparticle preparation via solvent displacement, two phases are used. These two can be both organic or aqueous phases, or one phase of each can be used but to phases should be immiscible. The important feature of this method, which needs to be taken into consideration when choosing the solvents, is that one phase should be a solvent for both the polymer and the drug and the other one should be a nonsolvent. To produce nanoparticles, the solvent phase containing the polymer and the drug is added to the nonsolvent phase, which is supplemented with one or more naturally occurring or synthetic surfactants as stabilizing agent(s). Since the solvents are immiscible, mixing the two phases results in dispersions of the solvent phase droplets, which contain the polymer and the drug, in the nonsolvent solution. Evaporation of the solvent results in the nanoparticles dispersion in the nonsolvent phase.[19]

1.4.1.2 Dialysis

The dialysis method uses an organic phase which is a solvent for the polymer. The other solvent is a nonsolvent for the polymer but miscible with the organic solvent. A dialysis membrane with a specific molecular cut-off is filled with the organic phase, containing the polymer, and placed in a large volume of the nonsolvent.[20,21] Due to the exchange of both solvents through the dialysis membrane, the concentration of the nonsolvent starts to increase inside of the dialysis bag; consequently, the polymer starts to precipitate and form the nanoparticles. Alternatively, a supercritical fluid such as carbon dioxide can be utilized to avoid toxic effects of organic solvents.[22]

In general, the aforementioned methods provide a low concentration of the nanoparticles, typically 50 mg polymer in 20-50 ml of the solvent. These concentrations are enough for physiochemical characterizations; however, performing cell cultures and animal studies require higher concentrations and the nanoparticles need to be concentrated. Techniques that are used for concentrating, such as ultracentrifugation, can change the characteristics of the prepared nanoparticles, and the concentration process is usually time-consuming and burdensome. These methods are able to fabricate spherical nanoparticles but usually do not have enough control on the size resulting in a wide distribution of nanoparticles, especially after concentrating.[19] On the other hand, lithographic and imprinting methods are able to produce nanoparticles with controlled sizes in various shapes.

1.4.1.3 Photolithography

Photolithography utilizes advances in the semiconductor industry in nanoparticle fabrication.[22] Approximately monodisperse nanoparticles with defined shapes can be achieved; these particles are known as litho-particles. The shape is defined by a mask with any arbitrarily designed pattern. In order to illustrate the ability of this method in the fabrication of particles with versatile shapes, Mason et al. produced all 26 letters of the English alphabet.[22] Litho-particles' fabrication process includes four major steps.[22] First, a sacrificial layer is spin-coated on a silicon wafer. Then, a second layer of the material of interest is formed on top of the sacrificial layer. The second layer usually is composed of a photoresist and the particle height is determined by the thickness of this layer. Third, UV

light exposure of the photoresist layer through a designed mask with the desired pattern results in the desired pattern of the photoresist on the sacrificial layer. Fourth, an organic solvent is used to wash away the unexposed parts of the photoresist. In the final step, the sacrificial layer is dissolved and nanoparticles are released.

There are several advantages for this process, including the excellent shape and size controllability. Also, with an ability to reach the fabrication capacity of 10^8 particles/min, it can be a high throughput process.[23] However, due to the practical and instrumental limitations, this technique is limited to thicknesses greater than 100 nm[23] and lateral dimensions greater than 800 nm.[24] Another major issue of photolithography is the requirement of a UV-sensitive material, thus dramatically restricting the range of particles achievable. Although it can be used for photopolymerizable materials, it is optimal for photoresists.[22] These issues with direct lithography have led to the development of imprinting techniques, where only the initial master template needs to be formed via lithography.

1.4.1.4 Imprint Lithography Methods

In order to replicate the shape of an original template, soft lithography methods use a master template to fabricate an elastomeric mold.[22] A cross-linked poly (dimethyl siloxane) (PDMS) elastomer is the traditional mold material for soft lithography. Nanoparticle fabrication via traditional soft lithography methods has been a challenge because of the formation of flash layer.[25] A flash layer is a residual layer of the molded materials which connects the prospective particles and prevents the formation of single

nanoparticles. Particle Replication in Non-wetting Templates (PRINT)[26] is a modified imprinting technique that utilizes cross-linked fluoropolymers (perfluoropolyether, PFPE) as the mold material to resolve this issue. Because of their lower surface energy, using PFPE avoids formation of the interconnecting flash layers.[26] Additionally, because of the Teflon-like characteristics of PFPE, the resultant particles can be easily collected from the mold.[26]

Optimized surface, size, and shape along with biocompatibility are essential prerequisites for an ideal nanotherapeutic.[22,26] Because of its ability to fabricate nearly monodisperse particles in the range of 10 nm-200 μm,[22] high precision and versatility on the shape of particles, and scalability, PRINT technology is known as one of the best methods for nanoparticle fabrication among the aforementioned methods. However, the high cost of the fluorinated matrices is one of the biggest drawbacks of the PRINT technology. In addition, PRINT process employs several steps with particular requirements depending on the characteristics of the material of interest. Each of these requirements could result in a potential challenge which influences its applicability in different chemistries (for instance, lamination conditions, adhesive layer, selective solvent for the adhesive layer, purification method which can be extremely challenging, etc.). Moreover, due to their mechanical features, top-down methods generally result in particles with imperfect surfaces.[19] This is one of the most important drawbacks for all of the top-down nanoparticle fabrication methods. At nanoscales, due to the high ratio of the surface to the volume, an imperfect and defected surface can significantly influence properties of the nanoparticles. In a bottom-up approach, particles are formed in their thermodynamically

most stable equilibrium state. In other words, atoms and molecules arrange accordingly to minimize the free energy. This stable chemical structure of the nanoparticles fabricated by bottom-up approach results in homogeneous surfaces with minimum defects.[27]

1.5 Thesis Outline

Considering the imperative role plastics play in the modern era and the crucial need for reducing our dependence on fossil fuel feedstock, polymeric materials derived from biomass were developed. Chapter 2 describes development of sugar-derived block copolymers to produce functional thermoplastic elastomers. The fundamental phase separation phenomenon in block copolymers is utilized in thermoplastic elastomers to create reprocessable and recyclable materials. Chapter 3 discusses further structural and chemical modifications on the sugar-based block copolymers to improve the performance of these materials as thermoplastic elastomers, and more specifically as pressure sensitive adhesives. Finally, a novel polymeric nanoparticle fabrication method for applications in the emerging field of nanomedicine is described in Chapter 4. Block copolymers self-assembly was utilized in a new top-down approach to fabrication of polymeric nanoparticles. Advantages of top-down and bottom-up approaches were combined for controlled fabrication of nanocylinders in their thermodynamically stable state.

1.6 References

1. Elias, H.-G.; Mülhaupt, R., Ullmann's Encyclopedia of Industrial Chemistry (Plastics, General Survey, 2. Production of Polymers and Plastics). Wiley-VCH Verlag GmbH & Co. KGaA: Weinheim, Germany, 2015; Vol. 38.

2. Xiong, M.; Schneiderman, D. K.; Bates, F. S.; Hillmyer, M. A.; Zhang, K., Scalable production of mechanically tunable block polymers from sugar. Proceedings of the National Academy of Sciences 2014, 111 (23), 8357-8362.

3. Lichtenthaler, F. W., Ullmann's Encyclopedia of Industrial Chemistry (Carbohydrates as Organic Raw Materials). Wiley-VCH Verlag GmbH & Co. KGaA: Weinheim, Germany, 2010; Vol. 6.

4. Kola, R.; Elsner, O. v.; Riepe, W.; Reuter, K., Ullmann's Encyclopedia of Industrial Chemistry (Raw Materials and Energy). Wiley-VCH Verlag GmbH & Co. KGaA: Weinheim, Germany, 2000.

5. Mekonnen, T.; Mussone, P.; Khalil, H.; Bressler, D., Progress in bio-based plastics and plasticizing modifications. Journal of Materials Chemistry A 2013, 1 (43), 13379-13398.

6. Fenouillot, F.; Rousseau, A.; Colomines, G.; Saint-Loup, R.; Pascault, J. P., Polymers from renewable 1,4:3,6-dianhydrohexitols (isosorbide, isomannide and isoidide): A review. Progress in Polymer Science 2010, 35 (5), 578-622.

7. Natureworks Product and Applications http://www.natureworksllc.com/Product-and-Applications. (accessed November 29).

8. Matsen, M. W.; Bates, F. S., Unifying weak- and strong-segregation block copolymer theories. Macromolecules 1996, 29 (4), 1091-1098.

9. Bates, F. S., Polymer-polymer phase behavior. Science 1991, 251 (4996), 898-905.
10. Bates, F. S.; Fredrickson, G. H., Block copolymers—designer soft materials. Physics Today 1999, 52 (2), 32.

11. Zalusky, A. S. Nanoporous material from ordered polylactide containing block copolymer template. University of Minnesota, Minneapolis, 2003.

12. Matsen, M. W.; Thompson, R. B., Equilibrium behavior of symmetric ABA triblock copolymer melts. The Journal of Chemical Physics 1999, 111 (15), 7139-7146.

13. Holden, G.; Quirk, R. P.; Kricheldorf, H. R., Thermoplastic Elastomers. 3rd ed.; Hanser Gardner Publications: Cincinnati, 2004.

14. Shin, J.; Kim, Y.-W.; Kim, G.-J., Sustainable Block Copolymer-based Thermoplastic Elastomers. Applied Chemical Engineering 2014, 25 (2), 121-133.

15. Kinnaman, T. C., The Economics of Municipal Solid Waste Management. Waste Management 2009, 2615-2617.

16. Shin, J.; Martello, M. T.; Shrestha, M.; Wissinger, J. E.; Tolman, W. B.; Hillmyer, M. A., Pressure-Sensitive Adhesives from Renewable Triblock Copolymers. *Macromolecules* **2011,** *44*, 87-94.

17. Euliss, L. E.; DuPont, J. A.; Gratton, S.; DeSimone, J., Imparting size, shape, and composition control of materials for nanomedicine. Chemical Society reviews 2006, 35 (11), 1095-104.

18. Biswas, A.; Bayer, I. S.; Biris, A. S.; Wang, T.; Dervishi, E.; Faupel, F., Advances in top-down and bottom-up surface nanofabrication: techniques, applications & future prospects. Advances in colloid and interface science 2012, 170 (1-2), 2-27.

19. Devadasu, V. R.; Bhardwaj, V.; Kumar, M. N., Can controversial nanotechnology promise drug delivery? Chemical reviews 2012, 113 (3), 1686–1735.

20. Lee, J. Y.; Cho, E. C.; Cho, K., Incorporation and release behavior of hydrophobic drug in functionalized poly(D,L-lactide)-block-poly(ethylene oxide) micelles. Journal of Controlled Release 2004, 94 (2-3), 323-335.

21. Akagi, T.; Kaneko, T.; Kida, T.; Akashi, M., Preparation and characterization of biodegradable nanoparticles based on poly(gamma-glutamic acid) with L-phenylalanine as a protein carrier. Journal of Controlled Release 2005, 108 (2-3), 226-236.

22. Merkel, T. J.; Herlihy, K. P.; Nunes, J.; Orgel, R. M.; Rolland, J. P.; DeSimone, J. M., Scalable, shape-specific, top-down fabrication methods for the synthesis of engineered colloidal particles. Langmuir 2010, 26 (16), 13086-13096.

23. Hernandez, C. J.; Mason, T. G., Colloidal alphabet soup: monodisperse dispersions of shape-designed LithoParticles. Journal of Physical Chemistry C 2007, 111 (12), 4477-4480.
24. Badaire, S.; Cottin-Bizonne, C.; Woody, J. W.; Yang, A.; Stroock, A. D., Shape selectivity in the assembly of lithographically designed colloidal particles. Journal of the American Chemical Society 2007, 129 (1), 40-41.

25. Dumond, J.; Low, H. Y., Residual layer self-removal in imprint lithography. Advanced Materials 2008, 20 (7), 1291-1297.

26. Canelas, D. A.; Herlihy, K. P.; DeSimone, J. M., Top-down particle fabrication: control of size and shape for diagnostic imaging and drug delivery. Wiley Interdisciplinary Reviews-Nanomedicine and Nanobiotechnology 2009, 1 (4), 391-404.

27. Varadan, V. K.; Chen, L.; Xie, J., Nanomedicine: design and applications of magnetic nanomaterials, nanosensors and nanosystems. Wiley: Chichester, 2008.

Chapter 2

Sustainable Glucose-based Block Copolymers with Elastomeric and Adhesive Behavior*

* Reproduced in part with permission from Nasiri, M.; Reineke, T. M**.** *Polym. Chem*.**, 2016**,*7*, 5233-5240. DOI: 10.1039/C6PY00700G

2.1 Introduction

Thermoplastic elastomers (TPEs) are of high utility and interest for a wide variety of applications, ranging from adhesives and electronics to clothing and automotive parts due to their highly processable structures.[1] With the ability to fine-tune the chemical TPE architecture and properties, triblock copolymers with an ABA architecture can be designed to comprise of a soft/rubbery middle segment (B) with two hard/glassy blocks at the ends (A). By selecting immiscible A and B blocks, the soft/rubber B segments will form intermolecular physical cross-links between the A segments.[2] Self-assembly of the glassy endblocks into microstructures at ambient temperatures, with the rubbery blocks bridging between the hard domains, creates a superior resistance to flow, resulting in a material with elastomeric properties.[1] Variations in the block lengths and component ratios allows for preparation of elastomeric materials with different nanopatterns (spheres, cylinders, etc.)[3] and the molecular compositions can be tuned to achieve the desired properties for any specific applications.

Currently, the most common and widely used ABA triblock copolymers for TPE applications are styrene-based copolymers, such as poly(styrene)-*b*-poly(butadiene)-*b*-poly(styrene) (SBS) and poly(styrene)-*b*-poly(isoprene)-*b*-poly(styrene) (SIS).[1] Although, these styrene-based materials possess valuable and functional properties for their intended applications, they are derived from nonrenewable feedstocks. Yet, the manufacturing and disposal of these petroleum-based materials (particularly, styrene) has a clear negative environmental impact,[4] which affirms the need for developing TPEs from more sustainable and plant-based feedstock sources.[5-11]

To date, sustainable TPE research has primarily focused on lactide and lactone derivatives.[1] For example, Qian[12] and Cohn[13] have used poly(lactide) (PLA) as the glassy component in tri- and multiblock copolymers, also consisting of rubbery poly(ethylene glycol) blocks, to create thermoplastic elastomers. PLA has been used in association with poly(isoprene) segments, a traditional soft segment, to prepare elastomeric materials,[14-15] and Lebarbe et al. have reported ABA triblock copolymers of PLA with poly(ricinoleic acid).[16] Additionally, α-methylene-γ-butyrolactone (MBL) has been copolymerized with *n*-butyl acrylate (nBA) to prepare ABA triblock copolymers for TPE applications.[17] Moreover, Gallagher et al. have used an acetylated methacrylic isosorbide (AMI) as a glassy sustainable monomer, to synthesize a series of well-defined di- and triblock copolymers utilizing nBA as the soft segment; this work has enabled development of new elastic and adhesive materials.[18-19] In another effort to create biorenewable thermoplastic elastomers, Robertson and coworkers have developed ABA linear triblock copolymers with fatty acid-derived midblock and salicylic acid-derived endblocks.[20] Also, Bolton et al. reported using α-methyl-p-methylstyrene and myrcene in their triblock system to create sustainable TPEs.[21]

Researchers have also sought alternative rubbery blocks from sustainable feedstocks.[22-29] For example, ABA triblock copolymers of menthide and lactide monomers have been created via sequential ring-opening polymerizations to produce renewable and hydrolytically degradable pressure sensitive adhesives (PSAs).[2] Wang et al. have utilized soybean oil derived monomers in their triblock copolymers to incorporate sustainable soft segments to styrene-based TPEs.[29-30] Shin and coworkers copolymerized ε-decalactone

with L-lactide to produce renewable triblock thermoplastic elastomers.[31] Additionally, copolymers of ε-caprolactone and ε-decalactone were used as the midblock for ABA triblocks with PLA endblocks.[32] Block polymers have also been created from substituted δ-valerolactone monomers and studied in detail for their structure activity relationships for sustainable material design.[33] Moreover, block copolymers from menthide and tulipalin A (α-methylene-γ-butyrolactone) have been examined for thermoplastic elastomer applications.[34] Ding et al. recently reported the preparation of poly(γ-methyl-α-methylene-γ-butyrolactone)-*b*-poly-(menthide)-*b*-poly(γ-methyl-α-methylene-γ-butyrolactone) ABA triblock copolymers that offer a significant enhancement in the adhesive properties compared to the previously reported sustainable elastomers.[35] Despite the enormous research efforts to create sustainable elastomeric materials, creating these materials to exhibit comparable properties to commercial petroleum-derived structures, at a reasonable cost, remains a great challenge.

Herein, we report a new family of thermoplastic elastomers based on the direct functionalization of glucose, an abundant and low cost sugar. The glucose-based monomer, glucose-6-acrylate-1,2,3,4-tetraacetate (GATA), was created to impart a sustainable glassy segment into block copolymers that have been copolymerized with rubbery *n*-butyl acrylate (nBA). Reversible Addition–Fragmentation Chain Transfer (RAFT) polymerization of the GATA monomer, in conjunction with its copolymerization with nBA, allowed preparation of fine-tuned diblock and triblock copolymers. Controlled radical polymerization methods such as RAFT provide a powerful tool to target copolymers with tailored architecture, composition, and molar mass to examine structure-activity relationships to achieve

targeted properties. Furthermore, triblock copolymers with the desired ABA architecture were investigated for the fidelity of phase-separation in the bulk and were initially examined for their adhesion and mechanical properties. Although different modifications of glucose have previously been explored for various biomaterials applications[36-40], this study is the first to utilize GATA in TPE applications. Indeed, the new family of materials introduced here in provides a green feedstock for the development of sustainable elastomeric materials that can be utilized in a wide variety of applications.

2.2 Results and Discussion

2.2.1 Synthesis and Polymerization of the GATA Monomer

The synthesis of the sugar-based monomer, glucose-6-acrylate-1,2,3,4-tetraacetate (GATA), was inspired from previously reported procedures.[39, 41] The primary hydroxyl group on glucose was protected with a trityl group followed by full acetylation of the remaining hydroxyl groups. The trityl protecting group was then selectively removed using trifluoroacetic acid (TFA) (Figure 2.1). Lastly, the acrylate functionality was installed on the primary alcohol position via esterification with acryloyl chloride (Scheme 2.1) to yield glucose-6-acrylate-1,2,3,4-tetraacetate (Figure 2.2)

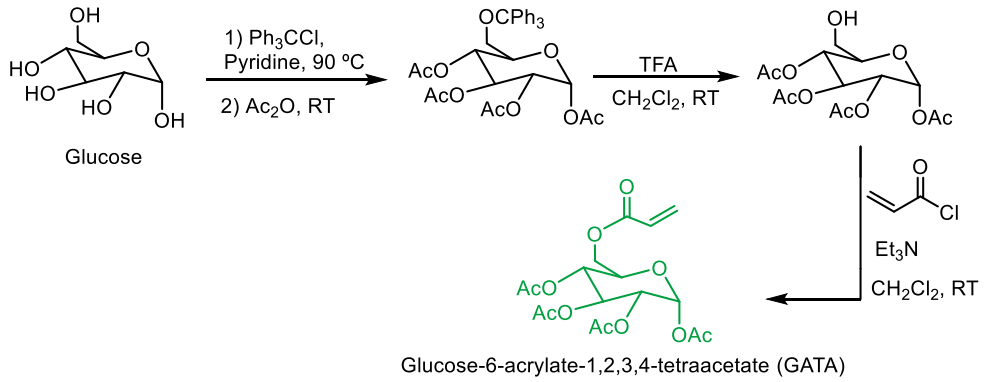

Scheme 2.1. Synthesis of glucose-6-acrylate-1,2,3,4-tetraacetate (GATA)

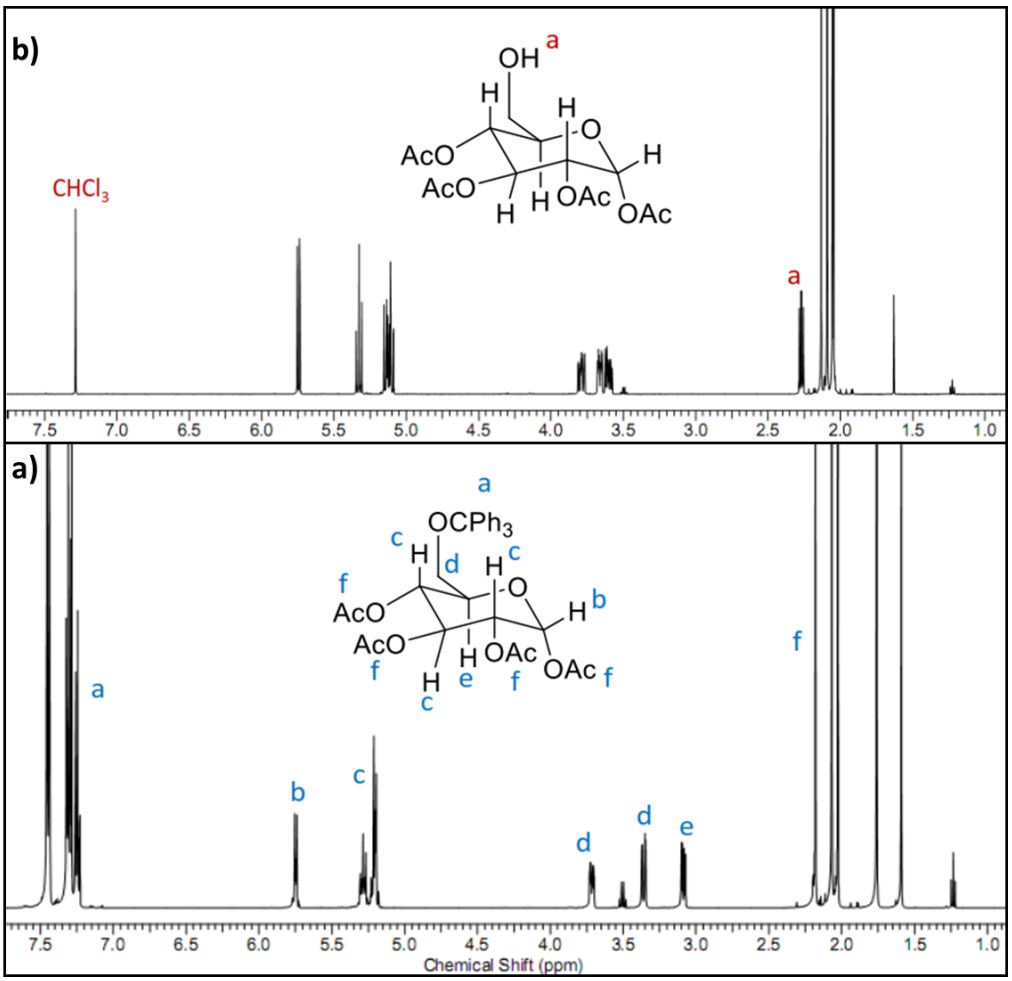

Figure 2.1. a) ^{1}H NMR spectrum of TGTA. b) ^{1}H NMR spectrum of GTA, 500 MHz, $CDCl_3$. Non-assigned peaks at 1.25, 1.65, and 3.5 ppm correspond to diethyl ether, water, and diethyl ether, respectively.

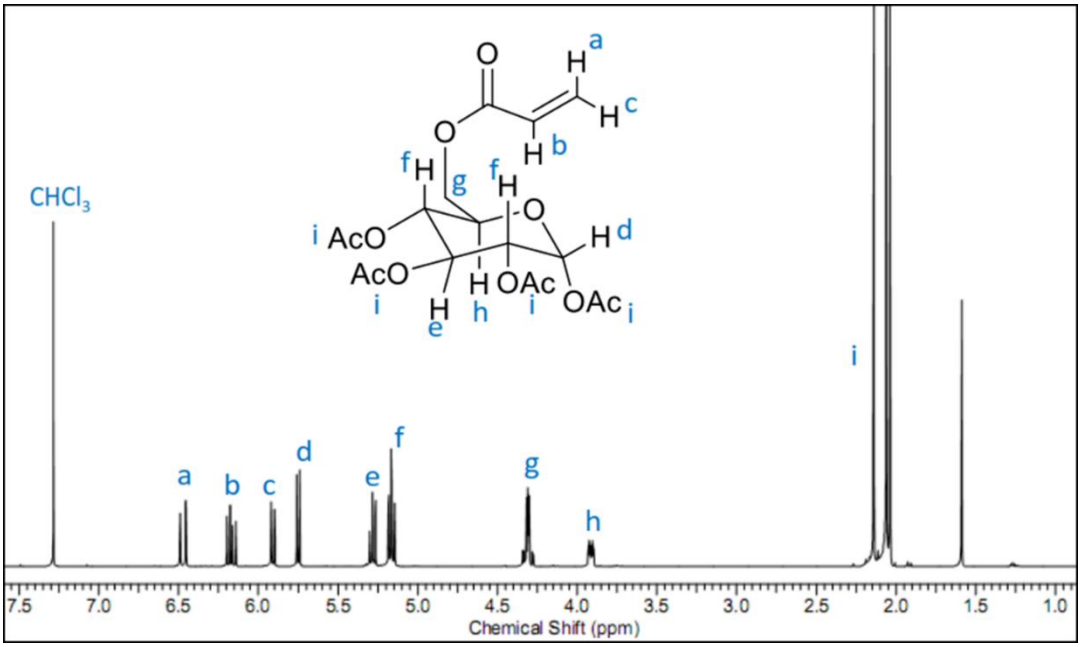

Figure 2.2. ^{1}H NMR spectrum of GATA, 500 MHz, $CDCl_3$. Non-assigned peak at 1.65 ppm corresponds to water.

2.2.2 RAFT Polymerization of GATA with *N*-butyl Acrylate

RAFT polymerization of the GATA monomer was employed to synthesize the glassy block. Using 4-cyano-4-[(ethylsulfanylthiocarbonyl)sulfanyl] pentanoic acid (CEP) as the chain transfer agent (CTA), the poly(GATA) macro-CTA was synthesized (Scheme 2.2, Table 2.1: denoted as P1 "polymer 1"). Subsequently, *n*-butyl acrylate (nBA) was sequentially added to the P1 macro-CTA to yield poly(glucose-6-acrylate-1,2,3,4-tetraacetate)-*b*-poly(*n*-butyl acrylate) (PGATA-*b*-PnBA) diblock copolymers with low molar mass distributions (Table 2.1, see the Supporting Figures, Figure 2.S1, for the size exclusion chromatography results). All diblock copolymers were created from the P1 macro-CTA.

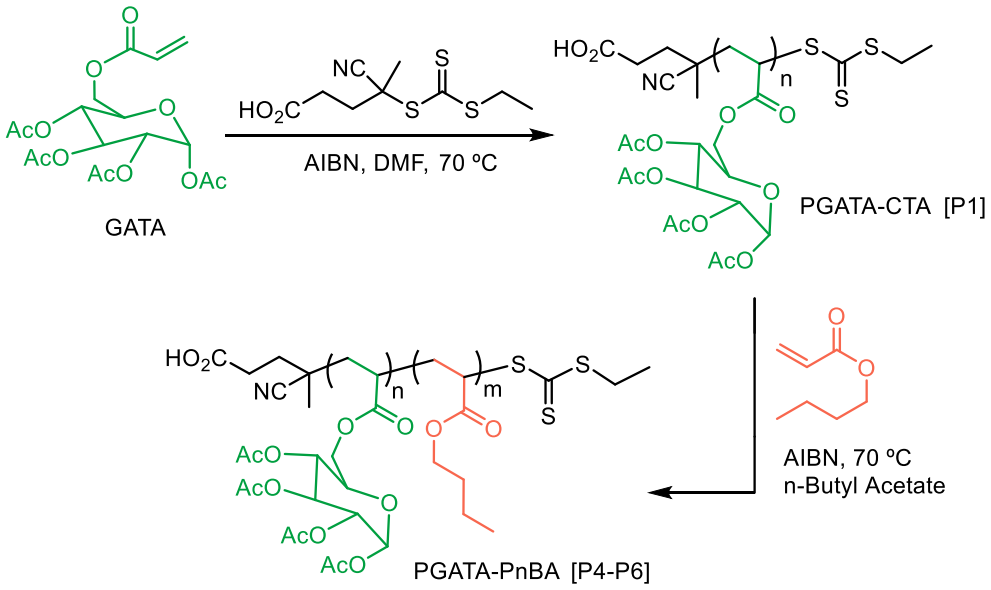

Scheme 2.2. Schematic synthesis of the PGATA macro-CTA followed by copolymerization with *n*-butyl acrylate (nBA).

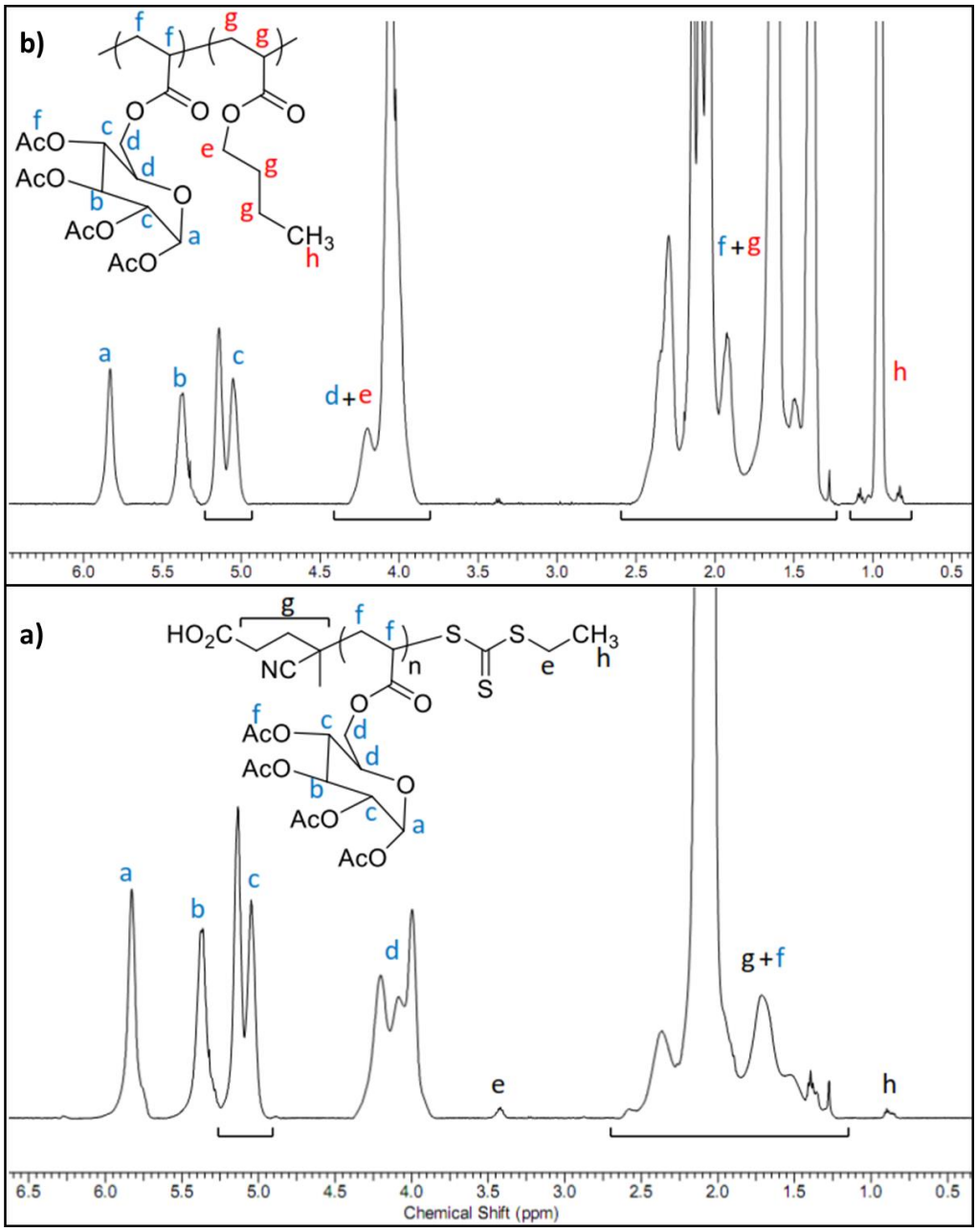

Figure 2.3. Representative ^{1}H NMR spectra of a) PGATA and b) PGATA-*b*-PnBA, 500 MHz, $CDCl_3$.

To examine the ability to target different block lengths with high control, a series of diblocks with various component ratios were synthesized (P4-P6, Table 2.1). These systems displayed thermal stability ($T_d \geq 275$ ºC). Additionally, in all cases, the diblocks

exhibited two well-separated glass transition temperatures (T_g), which are near the T_g values of the respective homopolymers (104 ºC and –50 ºC[42] for poly(GATA) and Poly(nBA), respectively), indicating microphase separation between the PGATA and PnBA domains. These results indicated that these segments were promising for further study by synthesizing ABA-type triblock copolymers, to enable physically cross-linked networks for TPE applications. Thus, we were inspired to proceed with the sequential polymerization to construct PGATA-*b*-PnBA-*b*-PGATA triblock copolymers with this same synthetic procedure. However, attempts to sequentially add a third block via RAFT polymerization on the PnBA end of the diblock macro-CTA were unsuccessful. To this end, we explored the use of a symmetric trithiocarbonate CTA to build the desired PGATA-*b*-PnBA-*b*-PGATA triblocks. As shown in Scheme 2.3, we employed S,S-dibenzyl trithiocarbonate (DTC) as the chain transfer agent for this two-step synthesis. P2 and P3 homopolymers were synthesized using DTC and were subsequently chain extended with *n*-butyl acrylate to yield the triblock copolymers listed in Table 2.1 (P7-P9). Similar to the diblock analogs, the triblock copolymers showed excellent thermal stability (with decomposition temperatures higher than 279 °C) along with two well-separated T_g values (∼ −45 °C and ∼ 105 °C for the PnBA and PGATA domains, respectively). Close inspection of the size exclusion chromatography (SEC) traces shows that there is a lower molar mass shoulder with the triblocks, which can be attributed to the dead chains from the macro-CTA synthesis (Figure 2.4).

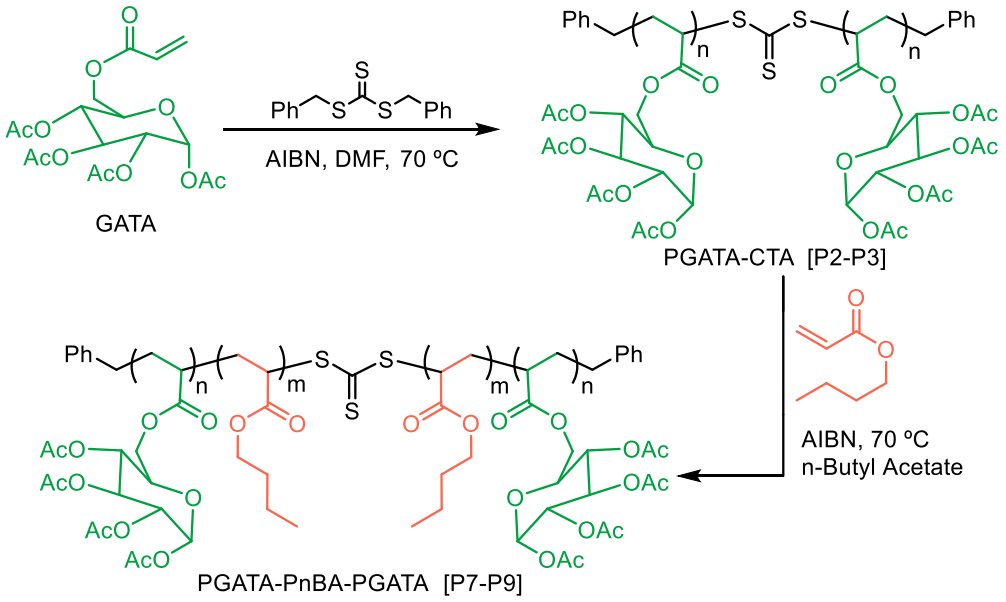

Scheme 2.3. Two-step synthesis of the PGATA-*b*-PnBA-*b*-PGATA triblock copolymers using a symmetric trithiocarbonate as the CTA.

Both the di- and triblock polymers presented in Table 1 were prepared in various GATA weight percentages and with low dispersities, which supports a successful utilization of the RAFT mechanism for copolymerization of GATA and nBA. Although this approach offers a simple two-step synthesis for the desired triblocks, the resulting copolymers carry a trithiocarbonate functionality within the midblock. This internal trithiocarbonate can impact the processability of the materials at high temperatures as this group is susceptible to degradation via high temperature or hydrolysis. Yet, this simple preparation method offered a facile means to produce and study this family of triblock copolymers and evaluate their properties for further study.

Table 2.1. Data summary of the GATA homopolymers and the respective diblock and triblock copolymers of GATA and nBA.

Polymer	**Sample Code**	$\mathbf{M_n}$[a] (kDa, NMR)	$\mathbf{M_n}$[b] (kDa, SEC)	$Đ$[b]	**GATA wt%**(NMR)	T_d[c] (°C)	T_g[d] (°C)
PGATA	P1	21	19	1.17	100	283	104
	P2	22	25	1.17	100	278	104
	P3	21	23	1.09	100	275	100
PGATA-PnBA[e]	P4	40	53	1.12	52	275	–45, 103
	P5	86	96	1.20	24	279	–45, 105
	P6	106	130	1.20	20	280	–43, 92
PGATA-PnBA-PGATA[f]	P7	38	54	1.15	58	279	–45, 105
	P8	134	99	1.29	16	298	–44, 107
	P9	147	124	1.16	14	312	–43, 105

[a]Number average molar mass determined by ^{1}H NMR spectroscopy. [b]Number average molar mass and polydispersity determined by SEC-MALLS in THF at room temperature. [c]Decomposition temperature at 5% weight loss determined by thermal gravimetric analysis (TGA). [d]Glass transition temperature determined by differential scanning calorimetry (DSC). [e]All diblock copolymers were synthesized using P1 as the macro-CTA. [f]Corresponding macro-CTA for P7 was P2, and P3 was chain extended to achieve the other two triblock copolymers (P8 and P9).

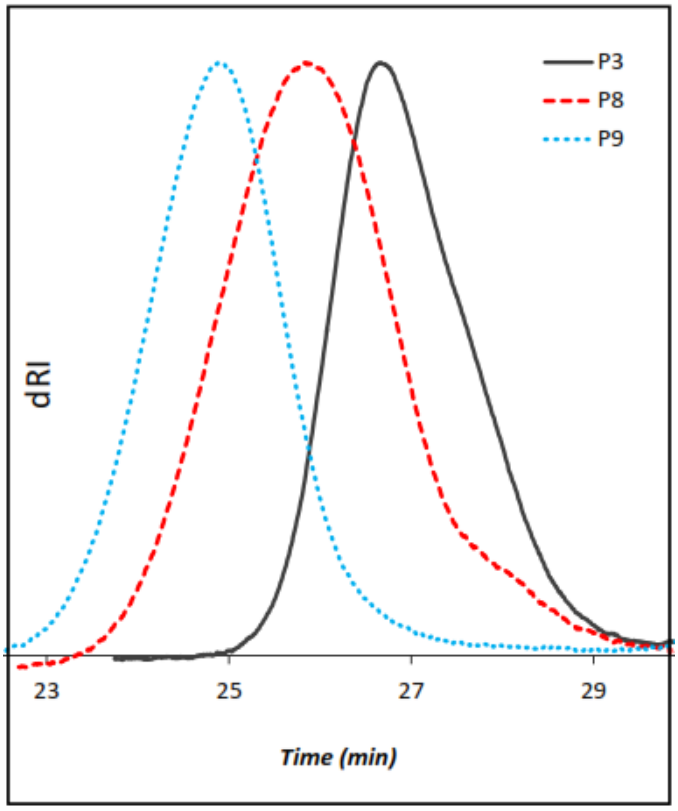

Figure 2.4. Representative SEC traces of the PGATA-*b*-PnBA-*b*-PGATA triblock copolymers (P8 and P9), using DTC as the CTA, and the corresponding macro-CTA, P3 (eluent: THF, at room temperature).

2.2.3 Physical Cross-linking in ABA Triblock Copolymers

The ABA architecture of these triblock copolymers, which are comprised of a rubbery and low T_g midblock (PnBA) and two hard and high T_g end-segments (PGATA), provides a template that can form a network via physical cross-linking between the two domains when phase-separated at room temperature. ABA-type copolymers are appealing for TPE applications and P9, as an illustrative example, was selected to be examined for its PSA properties. With 14% GATA, this triblock is a tacky material at room temperature and was tested for its peel adhesion. The force required to remove an adhesive from a

substrate is responsible for the peel strength.[2] For adhesion testing, solutions of 30 wt% of the polymers were uniformly spread on a polyethylene terephthalate (PETE) film. After complete evaporation of the solvent, the coated films were adhered onto a stainless steel plate and the peel resistance was measured by pulling the adhered films off the plate at an angle of 180º. Polymer P9 (PGATA-PnBA-PGATA: 11-125-11 kDa) exhibited a peel strength of 1.05 ± 0.12 Ncm^{-1} when the neat polymer was examined as an adhesive material. The peel adhesion was also tested with a mixture of the polymer and a tackifier. The use of a tackifier moderates the plateau modulus by diluting the entanglements in the midblock leading to more effective PSAs.[2, 43-44] Addition of a rosin ester tackifier, 30 mass percent of the polymer weight, boosted this value to 2.31 ± 0.14 Ncm^{-1}. As a comparison, paper tape, scotch tape, electrical tape, and Post-it® note commercial products offer peel adhesion values of 2.4, 1.9, 1.8, and 0.3 Ncm^{-1}, respectively, under similar experimental conditions.[2] The adhesion results were very promising and encouraged us to further improve the polymerizations to more efficiently increase the scalability and stability of this system.

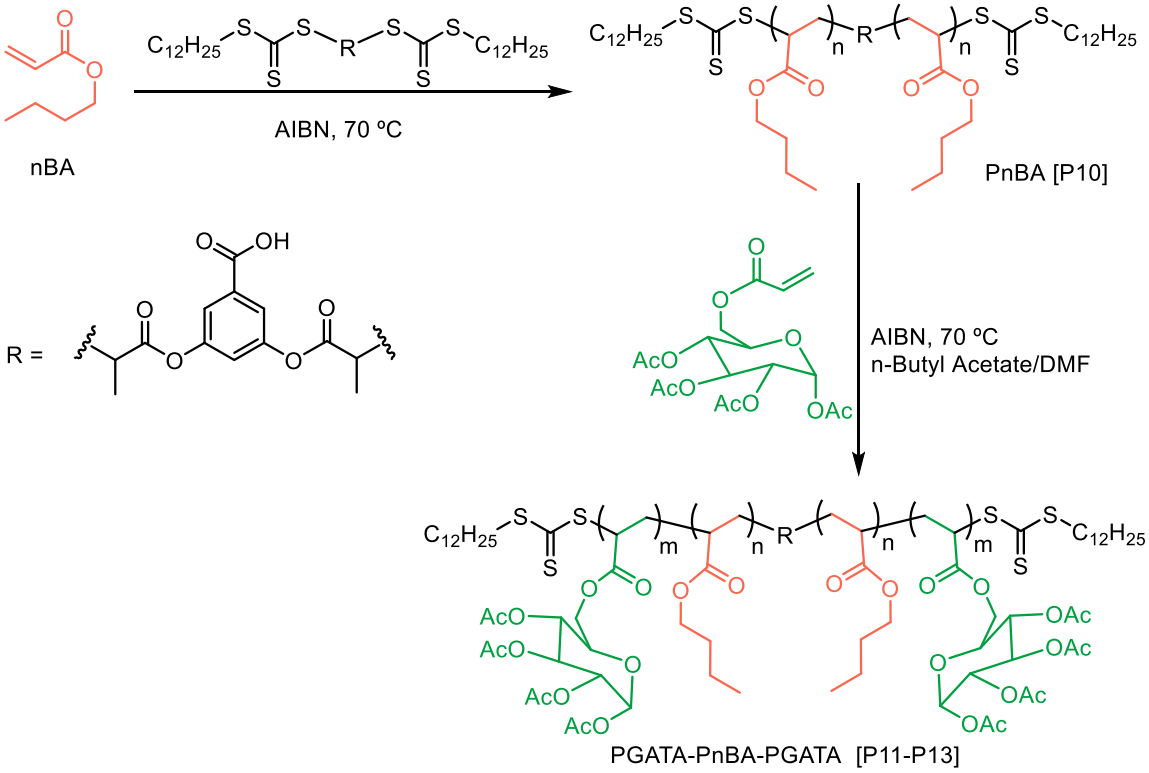

Scheme 2.4. Two-step synthesis of the PGATA-*b*-PnBA-*b*-PGATA triblocks using BTCBA as the chain transfer agent.

2.2.4 Improved RAFT Polymerization of ABA Triblock Copolymers

To improve the potential scalability, stability, and processability of the triblock TPEs, another polymerization pathway was explored (Scheme 2.4) that employed 3,5-Bis(2-dodecylthiocarbonothioylthio-1oxopropoxy)benzoic acid (BTCBA) as the CTA.[45] This bifunctional CTA leaves the cleavable trithiocarbonate groups on the ends of the polymer chains (Scheme 2.4), while maintaining a facile two-step synthesis to yield the desired triblocks. Final triblock copolymer structures were achieved with excellent control as low dispersities ($Đ \leq 1.08$) were obtained. Using BTCBA as the CTA demonstrated that this strategy offers an efficient and effective route for advanced development of these

materials. Figure 2.5 shows the clear shift to higher molar mass elution times with the increase in the GATA content. A summary of the characteristics for this new family of triblock copolymers is provided in Table 2.2.

Similar thermal stability to the previous analogous copolymers were observed (T_d ≥ 264 ºC). Triblocks with 12, 19 and 25% of GATA content were prepared in a controlled manner. The glass transition for the soft domains (PnBA block) was evidently observed in differential scanning calorimetry (DSC), however, a clear transition was not observed for the hard domains (GATA blocks) (representative DSC traces of the two triblock copolymer groups are shown in Supporting Figures, Figure 2.S2). One possible explanation for this lack of clear PGATA T_g in the DSC could be small heat change during the glass transitions for these polymers, attributed to their short PGATA segments (approximately 4, 6, and 9 kDa endblocks, compared to PGATA segments greater than 11 kDa for the previous di and triblocks). It should be noted that even the glass transitions observed for the previous triblocks, with endblocks ≥11 kDa, was a very small transition. Lack of a second glass transition could also be attributed to presence of the dodecyl alkyl chains on the hard ends of the triblock copolymers.

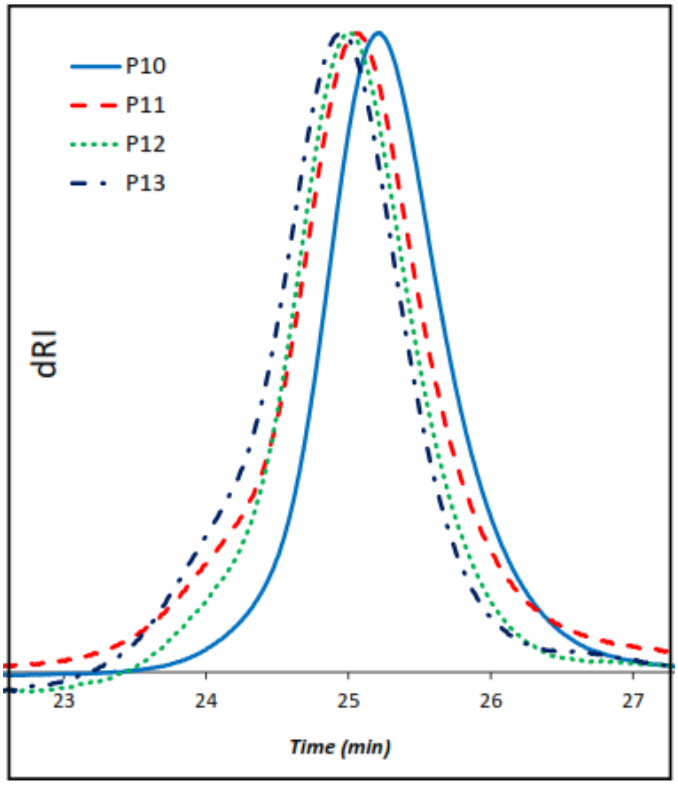

Figure 2.5. SEC traces of the PGATA-*b*-PnBA-*b*-PGATA triblock copolymers, synthesized with BTCBA as the CTA, and their corresponding macro-CTA (eluent: THF, at room temperature).

Table 2.2. Data summary of the *n*-butyl acrylate homopolymers and the respective triblock copolymers of GATA and nBA with BTCBA chain transfer agent.

Polymer	**Sample**	**M_n**[a] (kDa, NMR)	**M_n**[b] (kDa, SEC)	***Đ***[b]	**GATA wt%**(NMR)	T_d[c] (°C)	T_g[d] (°C)
PnBA	P10	56	56	1.04	–	276	–43
PGATA-	P11	64	61	1.06	12	268	–42
b-PnBA-	P12	69	67	1.07	19	287	–44
b-PGATA	P13	75	75	1.08	25	264	–43

[a]Number average molar mass determined by ^{1}H NMR spectroscopy. [b]Number average molar mass and polydispersity determined by SEC-MALLS in THF at room temperature. [c]Decomposition temperature at 5% weight loss determined by thermal gravimetric analysis (TGA). [d]Glass transition temperature determined by differential scanning calorimetry (DSC).

Small angle x-ray scattering (SAXS) was employed to further investigate the fidelity of phase-segregation in these triblock copolymer materials. After solvent casting, the polymer samples were annealed at 140 ºC for two hours for SAXS analysis. The SAXS profile for a bulk sample generated from P9 is shown in Figure 2.6(a). A strong principal reflection (q^*) indicates phase-separation between the two segments in this copolymer. Although the higher order reflections are not very well-defined, the peak position ratios of the observed broad features suggest a disorganized spherical morphology.[34, 46] SAXS analysis of P12 revealed an intense primary peak along with higher order broad reflections (Figure 2.6(b)). The relative peak positions (q/q^*) = √3 and √7 can be associated with a cylindrical structure.[17, 46-48] Principal reflections corresponding to phase-segregation were also observed for bulk samples generated from P11 and P13 (see Figure 2.S3 for the SAXS profiles).

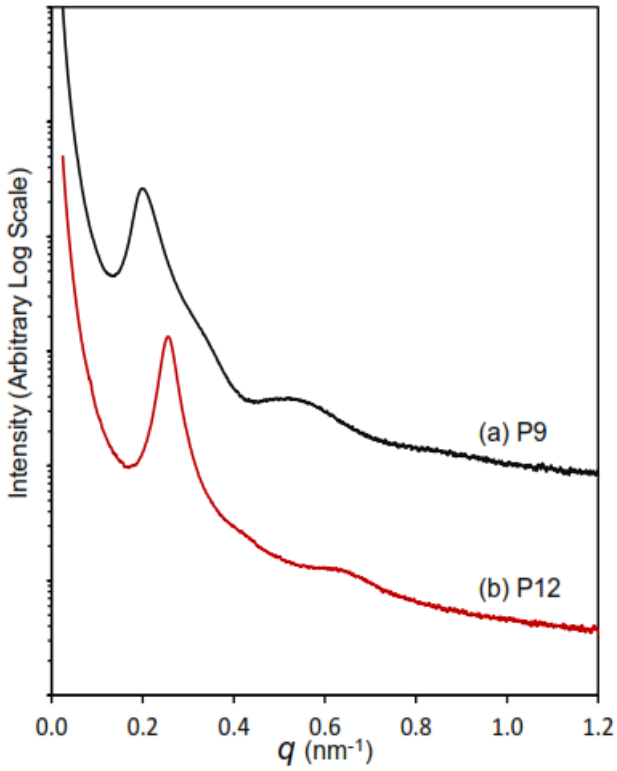

Figure 2.6. (a) Experimental 1D synchrotron SAXS profile of P9 (PGATA-PnBA-PGATA: 11-125-11 kDa) at 25 °C. The higher order reflections are approximately positioned at √2 and √7 relative to the principal peak. (b) Experimental 1D synchrotron SAXS profile of P12 (PGATA-PnBA-PGATA: 6-56-6 kDa) at 25 °C. The higher order reflections are approximately positioned at √3 and √7 relative the principal peak.

2.2.5 Adhesion and Mechanical Properties

After synthesizing polymers with the desired ABA architecture and confirming their phase-separation, we also conducted initial examinations of the TPE properties of these triblock copolymers. Samples with lower GATA content in the polymer series were evaluated for their adhesion properties in a similar manner as previously studied. As shown in Table 2.3, the peel adhesion significantly drops from P11 to P12 with an increase in GATA content (12 and 19 wt %, respectively). Addition of more GATA in P13 (25 wt %) resulted in a dry/rubbery material with nearly no tack. P11 and P9 and P11 exhibited

excellent adhesion properties (with peel adhesion of 2.31 and 2.01 Ncm^{-1}, respectively) that are comparable or superior to many commercial PSA products (such as scotch tape, electrical tape, paper tape, etc.).[2]

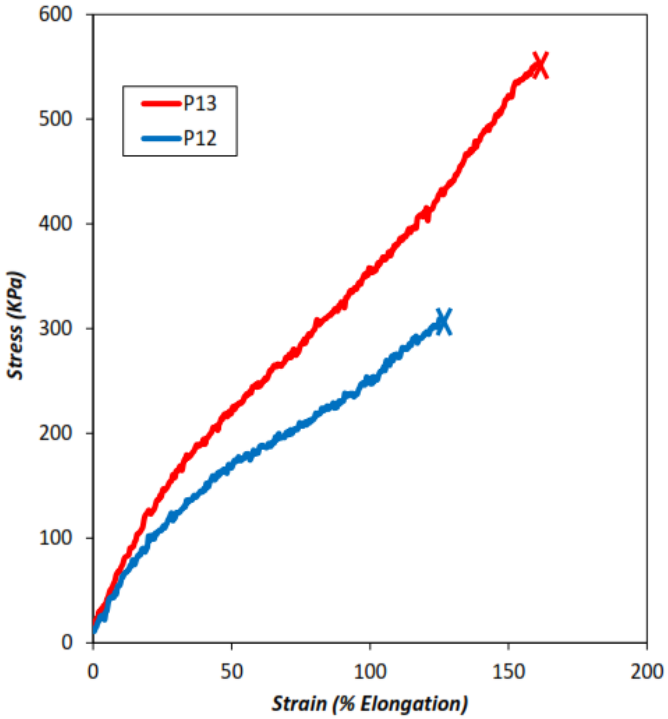

Figure 2.7. Stress−strain curves of P12 (PGATA-PnBA-PGATA: 6-56-6 kDa) and P9 (PGATA-PnBA-PGATA: 11-125-11 kDa). Experiments were conducted at room temperature at 5 mm/min; failure point marked with x. Five replicate tensile bars of each polymer sample were conducted.

The tensile properties of these triblocks were also investigated. Due to the high tack in P11 and P9 (12 and 14 wt % GATA, respectively) at ambient temperature, only samples of P12 and P13 were able to be prepared for tensile testing (Figure 2.7). As shown in Figure 2.7, at low strain, a linear response was observed in the stress-strain curves for both P12 and P13 triblocks, which represents a Young's modulus of 440 and 560 kPa, respectively

(Table 2.3). The stress at break and maximum elongation for these two triblocks (Table 2.3) are comparable to previously reported examples with similar nBA midblock length and very high T_g end blocks, such as PMBL.[17] However, the triblock copolymers used in this proof of concept study are comprised of mostly short block lengths; because elastomeric properties are tightly tied to polymer length and entanglements[2], this ABA copolymer system can significantly benefit from triblock copolymers with longer block segments. Indeed, exploring the role of longer block lengths on the bulk polymer morphology, such as the ability to form highly cross-linked networks, and/or incorporation of functional groups to promote non-covalent interactions within the soft network, (*i.e.*, hydrogen bonding)[49-50] to improve elastomeric properties, are certainly warranted and currently in progress.

Table 2.3. Tensile and peel tests summary.

Sample	**NMR M_n**[a] kDa (GATA wt%)	**SEC M_n**[b] kDa (GATA wt%)	**Peel Adhesion** (N/cm)	**E**[d] (kPa)	**σ**[e] (kPa)	**ε**[f] (% elongation)
P9	147 (14)	124 (18)	2.31 ± 0.14[c]	NA[g]	NA[g]	NA[g]
P11	64 (12)	61 (9)	2.01± 0.38[c]	NA[g]	NA[g]	NA[g]
P12	69 (19)	67 (16)	0.29 ± 0.05	440 ± 100	312 ± 10	123 ± 8
P13	75 (25)	75 (25)	NA[h]	560 ± 50	573 ± 48	171 ± 12

[a]Number average molar mass determined by ^{1}H NMR spectroscopy [b]Number average molar mass determined by SEC-MALLS in THF at room temperature. [c]This value is for the mixture of the polymer and 30 weight percent of a tackifier (see Supporting Information) and the peel adhesion for neat polymer was 1.05 ± 0.12 and 1.44 ± 0.31 for P9 and P11, respectively. [d]Young's modulus calculated at the first 5% elongation. [e]Average stress at break for 5 measurements. [f]Average maximum elongation. [g]The tensile properties were not measured due to high tack at room temperature. [h]Dry, non-tacky material not relevant for adhesion testing.

2.3 Conclusion

In summary, this study is the first to report the use of GATA, a glucose-based monomer, for the design of sustainable thermoplastic elastomers. Alternative polymerization pathways were explored and both diblock and triblock copolymers with narrow molar mass distributions were synthesized by RAFT polymerization. BTCBA, a bifunctional chain transfer agent, provided a simple and straightforward two-step synthesis for the desired ABA (PGATA-*b*-PnBA-*b*-PGATA) triblock copolymers. Phase-separation of the blocks was found by SAXS analysis and the triblock copolymers demonstrated moderate mechanical properties with excellent thermomechanical and adhesion properties. Indeed, the work herein demonstrates a new bio-based feedstock to produce greener elastomeric materials particularly for TPE applications. The role of block length and chemistry is currently being optimized to drive further improvements in the mechanical properties towards replacement of petroleum-derived elastomeric materials.

2.4 Materials and Methods

2.4.1 Materials

4-Cyano-4-[(ethylsulfanylthiocarbonyl)sulfanyl] pentanoic acid (CEP) was purchased from Strem Chemicals, Newburyport, MA and was used as received. The tackifier (Sylvalite RE-80HP) was purchased from Arizona Chemicals, Jacksonville, FL and was used as received. All other reagents used in this study were purchased from Sigma-Aldrich, St. Louis, MO and were used as received. Acryloyl chloride and *n*-butyl acrylate

(nBA) were passed through an activated alumina column to remove the inhibitors and stored at –20 °C for future use.

2.4.2 Characterization

All ^{1}H NMR spectra were recorded at room temperature on a Brüker Avance III 500 MHz Spectrometer in $CDCl_3$ as the solvent. Chemical shifts are reported relative to the Tetramethylsilane (TMS) internal standard peak at 0.00 ppm. Size-exclusion chromatography (SEC) was performed in THF using a Waters Styragel guard column and 3 Waters Styragel columns (HR6, HR4, and HR1) in series with separation ability of 100–10,000,000 g.mol^{-1}. The columns were contained in an Agilent 1260 Infinity liquid chromatograph equipped with a Wyatt Dawn Heleos II multiangle light scattering detector and a Wyatt Optilab T-rEX refractive index detector. The dn/dc values were calculated from the refractive index signal using a known sample concentration and assuming 100% mass recovery from the column and were used for molar mass calculations. Thermogravimetric analysis (TGA) was performed on a TA Instruments Q500 at a heating rate of 10 °C min^{-1}. Differential scanning calorimetry (DSC) measurements were carried out using a TA Instruments Discovery DSC under air. The glass transition temperature, T_g, values were determined on the second heating at a heating rate of 10 °C min^{-1}. Tensile testing was performed using a Shimadzu AGS-X tensile tester at room temperature on tensile bars that had gauge dimensions of approximately 10 mm×8 mm×0.2 mm. All samples were elongated at a speed of 5 mm per minute. Samples were annealed at 140 ºC for 1-2 hours before testing. Five replicate tensile bars of each polymer sample were

conducted. Small-angle X-ray scattering (SAXS) experiments were performed at the Sector 5-ID-D beamline of the Advanced Photon Source (APS) at Argonne National Laboratories, maintained by the Dow-Northwestern-Dupont Collaborative Access Team (DNDCAT), unless otherwise mentioned. The source produces X-rays with a 0.70 Å wavelength. The sample to detector distance was fixed at 7.491 m. Scattering intensity was monitored using a Mar 165 mm diameter CCD detector operating with a resolution of 2048 by 2048. The two dimensional scattering patterns were azimuthally integrated to afford one-dimensional profiles presented as spatial frequency (q) versus scattered intensity. Samples were annealed at 140 ºC for 2 hours before the SAXS experiments.

2.4.3 Sample Preparation for Adhesion Testing[2]

For adhesion testing, solutions of the polymers (or a mixture of the polymer and tackifier) in ethyl acetate (EtOAc) were cast on a polyethylene terephthalate (PETE) film. Rosin esters were used as the tackifier (Sylvalite RE-80HP) and the tackifier concentration was 30 weight percent of the total solid content, where appropriate. The concentration of polymer/tackifier solution was 30 weight percent. As a representative example, 200 mg of P9 was dissolved in 520 µl EtOAc (or when using a tackifier, 140 mg of P9 and 60.0 mg of the Rosin ester tackifier were dissolved in 520 µl EtOAc). Then, the solution was evenly spread on a PETE film using a standard laboratory drawdown rod (two centimeters in diameter). The film was dried at room temperature open to air in a chemical fume hood overnight. The resultant coated PETE film was cut into 2-cm wide strips for adhesion testing. The strips were approximately 5-cm long.

2.4.4 180° Peel Adhesion Testing

The peel strength of the polymers was measured using a Shimadzu AGS-X tensile tester at a peel rate of 305 mm per minute. Two centimeter-wide strips of the coated PETE films were placed on a clean stainless steel panel, as an adherend. To develop good contact between the adhesive and the steel plate, the coated film was gently pressed against the steel plate by manually rolling an electric tape roll on it. The strip was then peeled from the stainless steel panel. The reported average peel force and standard deviation values were acquired from at least five replicates.

2.4.5 Synthesis of the GATA Monomer

A modified version of previously reported procedures[39, 41] was followed. To a dried one liter round bottom flask, anhydrous D-(+)-glucose (30.0 g, 167 mmol), trityl chloride (50.0 g, 180 mmol), and anhydrous pyridine (125 ml) were added sequentially. The mixture was placed in a preheated, well-mixed oil bath at 90°C until everything was fully dissolved. Then, acetic anhydride (90 ml) was added in one portion and allowed to stir at room temperature with the removal of the oil bath for 16 h. Afterward, the solution was slowly poured into a mixture of 4 liters of ice water and 250 ml acetic acid and then vigorously stirred for 4 hours. The resultant white precipitate was filtered and washed with cold water and dried under fume hood overnight. The solid obtained was dispersed in 100 ml ethyl ether and stirred for 10 minutes. The solid obtained was then vacuum filtered to afford 6-trityl-d-glucose-1,2,3,4-tetraacetate (TGTA) (49.5 g, 50.2 % isolated yield). ^{1}H NMR ($CDCl_3$): δ 1.60-2.20 (m, 12H, CH_3-CO); 3.05 (dd, 1H); 3.33 (dd, 1H), 3.63-3.75 (m, 1H);

5.10-5.30 (m, 3H); 5.68-5.78 (m, 1H, O-CH-O-CO-CH_3); 7.15-7.50 (m, 15H) ppm (Figure S1a). Next, TGTA (25.0 g, 42.4 mmol), 2 ml water, and 40 ml dichloromethane were mixed in a 250 ml round bottom flask. 12.5 ml trifluroacetic acid was slowly added and the mixture stirred at room temperature for 10 minutes. The mixture was diluted with 100 ml dichloromethane and 100 ml water and transferred into a separatory funnel. Another wash with dichloromethane was performed with 200 ml dichloromethane. The organic wash solutions were combined and washed with a saturated solution of $NaHCO_3$ (250 ml) and then water (2 x 250 ml). The organic layers were then dried over magnesium sulfate and concentrated by rotary evaporation. The resulting viscous solution was dissolved in a minimum amount of anhydrous ether, and agitated with a glass rod to induce recrystallization, which was left in a refrigerator overnight. The resulting white crystals, D-glucose-1,2,3,4-tetraacetate (GTA, 10.8 g, 73.0% isolated yield) were vacuum filtered and dried at ambient conditions. ^{1}H NMR ($CDCl_3$): δ 2.00-2.12 (m, 12H, CH3-CO); 2.21 (dd, 1H, -CH_2-OH); 3.54-3.82 (m, 3H), 5.05-5.15 (m, 2H); 5.31 (t, 1H); 5.72 (d, 1H, O-CH-CH-OH) ppm (Figure S1b). Next, a solution of GTA (5.00 g, 14.4 mmol) and triethylamine (4.35 g, 43.1 mmol) in 20 ml dichloromethane was added dropwise to a stirred 0 °C solution of acryloyl chloride (3.60 g, 39.8 mmol) in 100 ml dichloromethane in a 250 ml round bottom flask. After 2 h, the mixture was allowed to warm to room temperature and was stirred for an additional 14 h. The solvent was then removed by evaporation. The remaining solid was dissolved in 10 ml dichloromethane and passed through a plug of silica gel using 500 ml of an ethyl acetate:hexanes (80:20) mixture. The solvent was removed to afford glucose-6-acrylate-1,2,3,4-tetraacetate (GATA, 5.15 g,

88.9% isolated yield). ^{1}H NMR ($CDCl_3$): δ 1.95-2.15 (m, 12H, CH_3-CO); 3.84-3.91 (m, 1H), 4.20-4.30 (m, 2H), 5.08-5.14 (m, 2H), 5.23 (t, 1H), 5.70 (d, 1H, O-CH-CH-OH), 5.86 (d, 1H), 6.12 (dd, 1H), 6.42 (d, 1H) ppm (Figure S2).

2.4.6 Synthesis of the Polymers

Poly(glucose-6-acrylate-1,2,3,4-tetraacetate) (PGATA). An illustrative example is provided. P1: To a 10 ml round-bottom flask equipped with a teflon stirring bar was added 4-cyano-4-(ethylsulfanylthiocarbonyl) sulfanylpentanoic acid (CEP) (29.0 mg, 0.110 mmol), AIBN (1.80 mg, 0.011 mmol), GATA (2.00 g, 4.98 mmol), and 3 ml of dimethylformamide (DMF). The flask was sealed and the mixture was degassed by purging with nitrogen at room temperature for 30 minutes. Subsequently, the reaction vessel was submerged into a thermostated oil bath at 70 °C for 13 hours. The polymerization was quenched by immediately placing the flask into liquid nitrogen and opening it to air. The reaction mixture was diluted by adding 2 ml of methylene chloride, and subsequently the polymer was precipitated in 100 ml of ice-cold methanol. The yellow solid was isolated via filtration and the resulting PGATA-CTA powder was dried under vacuum at 40 °C (1.70 g, 85.0% isolated yield). M_n= 21 kg.mol^{-1} (full conversion), $Đ$ =1.17. ^{1}HNMR ($CDCl_3$, 500 MHz): δ = 1.4-2.5 (br m, CH, CH_2, CH_3), 3.9-4.4 (br m, CH_2 and CH), 5-5.2 (br m, CH and CH), 5.3-5.5 (br m, CH), 5.7-5.9 (br m, CH) ppm.

Poly(glucose-6-acrylate-1,2,3,4-tetraacetate)-b-poly(n-butyl acrylate) (PGATA-b-PnBA). An illustrative example is provided. P5: To synthesize the PGATA-PnBA block copolymer, AIBN (0.660 mg, 0.004 mmol), the relevant macro-CTA (i.e. PGATA-CEP)

(P1) (300 mg, 0.014 mmol), nBA (1.50 ml, 10.4 mmol) and 5 ml of *n*-butyl acetate were mixed in a 10 ml round-bottom flask equipped with a teflon stirring bar. The flask was sealed and the mixture was degassed under inert nitrogen at room temperature for 30 minutes. Subsequently, the reaction vessel was submerged into a preheated, stirred oil bath maintained at 70 °C. After 14 hours, the reaction was quenched by immediately placing the flask into liquid nitrogen and opening it to air. CH_2Cl_2 (2 ml) was added to the mixture, and subsequently the polymer was precipitated in 150 ml of ice-cold methanol. The precipitates were isolated via gravity filtration and dried under vacuum at 40 °C (1.00 g, 82.8% isolated yield). M_n (PnBA)= 65 kg.mol^{-1} (68% conversion), $Đ$ =1.20. ^{1}HNMR ($CDCl_3$, 500 MHz): δ = 0.9-1.1 (m, CH_3- PnBA), 1.3-2.4 (br m, CH- PGATA and PnBA, CH_2- PGATA and PnBA, CH_3- PGATA, CH_2- PnBA, CH_2- PnBA), 3.9-4.4 (br m, CH_2– PGATA and PnBA, CH- PGATA), 5-5.2 (br m, CH- PGATA and CH- PGATA), 5.3-5.5 (br m, CH- PGATA), 5.7-5.9 (br m, CH- PGATA).

Poly(glucose-6-acrylate-1,2,3,4-tetraacetate)-b-poly(n-butyl acrylate)-trithiocarbonate-poly(n-butyl acrylate)-b-poly(glucose-6-acrylate-1,2,3,4-tetraacetate) (PGATA-b-PnBA-trithiocarbonate-PnBA-b-PGATA). An illustrative example is provided. P9: to synthesize the triblock copolymers that carry the trithiocarbonate functionality within the midblock, AIBN (0.500 mg, 0.003 mmol), the relevant macro-CTA (i.e. PGATA-DTC macro-CTA) (P3) (150 mg, 0.007 mmol), nBA (1.25 ml, 8.69 mmol) and 6 ml of *n*-butyl acetate were mixed in a 10 ml round-bottom flask equipped with a teflon stirring bar. The flask was sealed and the mixture was degassed under inert nitrogen at room temperature for 45 minutes. Subsequently, the reaction vessel was submerged into a

preheated, stirred oil bath maintained at 80 °C. After 52 hours, the reaction was quenched by immediately placing the flask into liquid nitrogen and opening it to air. CH_2Cl_2 (2 ml) was added to the mixture, and subsequently the polymer was precipitated in 200 ml of ice-cold methanol. The precipitates were isolated via gravity filtration and dried under vacuum at 40 °C (750 mg, 73.0% isolated yield). M_n (PnBA)= 126 kg.mol^{-1} (79% conversion), $Đ$ =1.16. ^{1}HNMR ($CDCl_3$, 500 MHz): δ = 0.9-1.1 (m, CH_3- PnBA), 1.3-2.4 (br m, CH- PGATA and PnBA, CH_2- PGATA and PnBA, CH_3- PGATA, CH_2- PnBA, CH_2- PnBA), 3.9-4.4 (br m, CH_2– PGATA and PnBA, CH- PGATA), 5-5.2 (br m, CH- PGATA and CH- PGATA), 5.3-5.5 (br m, CH- PGATA), 5.7-5.9 (br m, CH- PGATA).

Poly(n-butyl acrylate) (PnBA). The synthesis of *n*-butyl acrylate macro-CTA was performed in bulk. AIBN (3.50 mg, 0.021 mmol), 3,5-bis(2-dodecylthiocarbonothioylthio-1-oxopropoxy)benzoic acid (BTCBA) (100 mg, 0.122 mmol), and *n*-butyl acrylate (9.80 ml, 68.1 mmol) were mixed in a 25 ml round-bottom flask equipped with a teflon stirring bar. The flask was sealed and the mixture was degassed under inert nitrogen at room temperature for 45 minutes. Subsequently, the reaction vessel was submerged into a preheated, stirring oil bath maintained at 70 °C. After 1.5 hours, the reaction was quenched by immediately placing the flask into liquid nitrogen and opening it to air. 10 ml of CH_2Cl_2 was added to the mixture, and subsequently the polymer was precipitated in 400 ml of ice-cold methanol and was left in the freezer for two hours. The precipitates were isolated by decanting off the supernatant fluid. The procedure was repeated three times and precipitates were dried under vacuum at 40 °C (4.15 g, 61.2% isolated yield). M_n (PnBA)= 56 kg.mol^{-}

[1] (78% conversion), $Đ$ =1.04. ^{1}HNMR ($CDCl_3$, 500 MHz): δ = 0.9-1.1 (m, CH_3), 1.2-2 (br m, CH_2, CH_2, CH_2), 2.2-2.4 (br m, CH), 3.9-4.1 (br m, CH_2).

Poly(glucose-6-acrylate-1,2,3,4-tetraacetate)-b-poly(n-butyl acrylate)-b-poly(glucose-6-acrylate-1,2,3,4-tetraacetate) (PGATA-b-PnBA-b-PGATA). An illustrative example is provided. P12: to synthesize triblock copolymers with the bifunctional CTA, AIBN (0.600 mg, 0.004 mmol), the relevant macro-CTA (i.e. PnBA-BTCBA macro-CTA) (1.00 g, 0.018 mmol), GATA (600 mg, 1.49 mmol), 4 ml of *n*-butyl acetate, and one ml of dimethylformamide were mixed in a 10 ml round-bottom flask equipped with a teflon stirring bar. The flask was sealed and the mixture was degassed under inert nitrogen at room temperature for 45 minutes. Subsequently, the reaction vessel was submerged into a preheated, stirred oil bath maintained at 70 °C. After 43 hours, the reaction was quenched by immediately placing the flask into liquid nitrogen and opening it to air. CH_2Cl_2 (2 ml) was added to the mixture, and subsequently the polymer was precipitated in 300 ml of ice-cold methanol. The precipitates were isolated via gravity filtration and dried under vacuum at 40 °C (1.10 g, 89.1% isolated yield). M_n (PGATA) = 13 kg.mol^{-1} (39% conversion), $Đ$ =1.07. ^{1}H NMR ($CDCl_3$, 500 MHz): δ = 0.9-1.1 (m, CH_3- PnBA), 1.3-2.4 (br m, CH- PGATA and PnBA, CH_2- PGATA and PnBA, CH_3- PGATA, CH_2- PnBA, CH_2- PnBA), 3.9-4.4 (br m, CH_2– PGATA and PnBA, CH- PGATA), 5-5.2 (br m, CH- PGATA and CH- PGATA), 5.3-5.5 (br m, CH- PGATA), 5.7-5.9 (br m, CH- PGATA).

2.5 Supplementary Figures

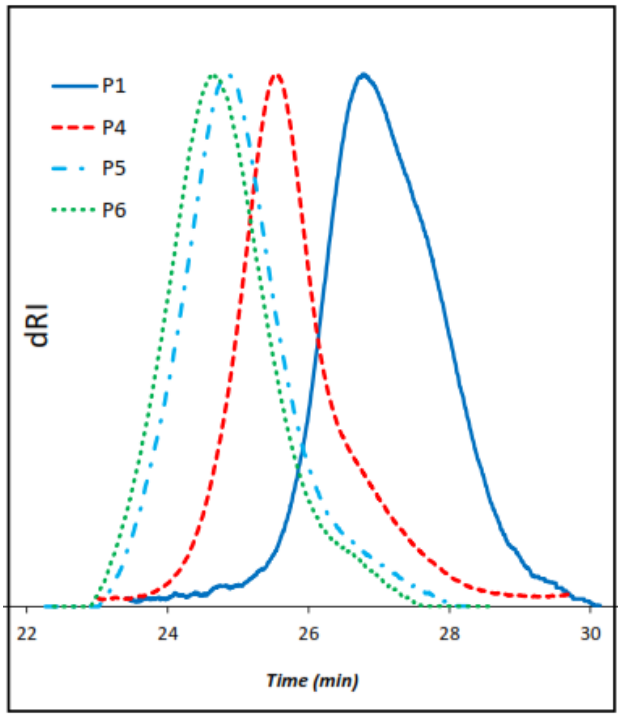

Figure 2.S1. SEC traces of the PGATA-*b*-PnBA diblock copolymers [P4-P6] and the corresponding maco-CTA [P1] (eluent: THF, at room temperature).

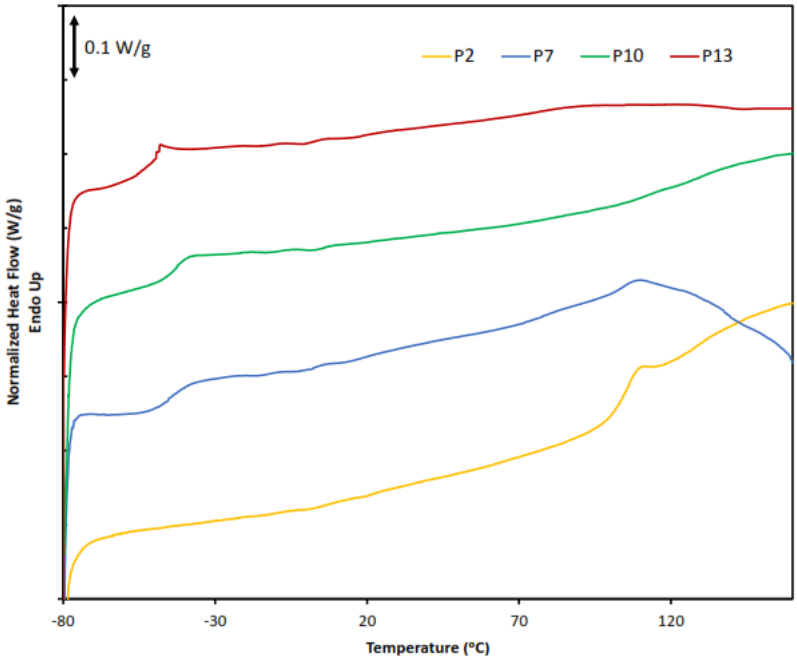

Figure 2.S2. Representative DSC traces of the two groups of the triblock copolymers: P7 (PGATA-PnBA-PGATA: 12-29-12 kDa) and P13 (PGATA-PnBA-PGATA: 9-56-9 kDa), and their corresponding macro-CTAs, P2 and P10, respectively.

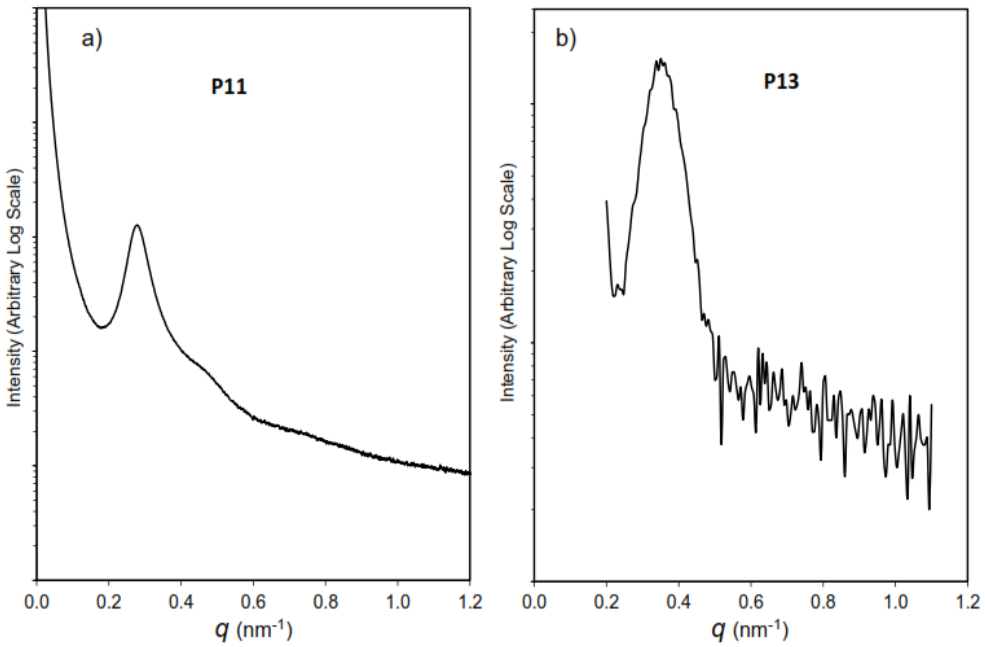

Figure 2.S3. Experimental 1D SAXS profile of a) P11 (PGATA-PnBA-PGATA: 4-56-4 kDa) and b) P13 (PGATA-PnBA-PGATA: 9-56-9 kDa) at 25 °C. b) P13 SAXS data was acquired using a home-built instrument. The sample to detector distance was 2.15 meters and the beam source produces X-rays with 1.54 Å wavelengths.

2.6 References

1. Shin, J.; Kim, Y.-W.; Kim, G.-J., Sustainable Block Copolymer-based Thermoplastic Elastomers. *Applied Chemical Engineering* **2014,** *25*, 121-133.

2. Shin, J.; Martello, M. T.; Shrestha, M.; Wissinger, J. E.; Tolman, W. B.; Hillmyer, M. A., Pressure-Sensitive Adhesives from Renewable Triblock Copolymers. *Macromolecules* **2011,** *44*, 87-94.

3. Bates, F. S.; Fredrickson, G. H., Block Copolymers-Design Soft Materials. *Physics Today* **1999,** *52*, 32-38.

4. Li, H. X.; Getzinger, G. J.; Ferguson, P. L.; Orihuela, B.; Zhu, M.; Rittschof, D., Effects of Toxic Leachate from Commercial Plastics on Larval Survival and Settlement of the Barnacle Amphibalanus amphitrite. *Environmental science & technology* **2016,** *50*, 924-31.

5. Miller, S. A., Sustainable Polymers: Opportunities for the Next Decade. *ACS Macro Letters* **2013,** *2*, 550-554.

6. Saito, T.; Brown, R. H.; Hunt, M. A.; Pickel, D. L.; Pickel, J. M.; Messman, J. M.; Baker, F. S.; Keller, M.; Naskar, A. K., Turning renewable resources into value-added polymer: development of lignin-based thermoplastic. *Green Chemistry* **2012,** *14*, 3295.

7. Gandini, A., The irruption of polymers from renewable resources on the scene of macromolecular science and technology. *Green Chemistry* **2011,** *13*, 1061.

8. Liu, Y.; Yao, K.; Chen, X.; Wang, J.; Wang, Z.; Ploehn, H. J.; Wang, C.; Chu, F.; Tang, C., Sustainable thermoplastic elastomers derived from renewable cellulose, rosin and fatty acids. *Polymer Chemistry* **2014,** *5*, 3170.

9. Wang, Z.; Yuan, L.; Jiang, F.; Zhang, Y.; Wang, Z.; Tang, C., Bioinspired High Resilient Elastomers to Mimic Resilin. *ACS Macro Letters* **2016,** *5*, 220-223.

10. Mauck, S. C.; Wang, S.; Ding, W.; Rohde, B. J.; Fortune, C. K.; Yang, G.; Ahn, S.-K.; Robertson, M. L., Biorenewable Tough Blends of Polylactide and Acrylated Epoxidized Soybean Oil Compatibilized by a Polylactide Star Polymer. *Macromolecules* **2016,** *49*, 1605-1615.

11. Miller, S. A., <Sustainable polymers replacing polymers derived.pdf>. *Polymer Chemistry* **2014,** *5*, 3117-3118.

12. Haitao, Q.; Jianzhong, B.; Shenguo, W., Synthesis, characterization and degradation of ABA block copolymer of l-lactide and ε-caprolactone. *Polymer Degradation and Stability* **2000,** *68*, 423-429.

13. Cohn, D.; Hotovely-Salomon, A., Biodegradable multiblock PEO/PLA thermoplastic elastomers: molecular design and properties. *Polymer* **2005,** *46*, 2068-2075.

14. Frick, E. M.; Hillmyer, M. A., Synthesis and characterization of polylactide-block-polyisoprene-block-polylactide triblock copolymers: new thermoplastic elastomers containing biodegradable segments. *Macromolecular Rapid Communications* **2000,** *21*, 1317-1322.

15. Frick, E. M.; Zalusky, A. S.; Hillmye, M. A., Characterization of Polylactide-b-polyisoprene-b-polylactide Thermoplastic Elastomers. *Biomacromolecules* **2002,** *4*, 216-223.

16. Lebarbé, T.; Ibarboure, E.; Gadenne, B.; Alfos, C.; Cramail, H., Fully bio-based poly(l-lactide)-b-poly(ricinoleic acid)-b-poly(l-lactide) triblock copolyesters: investigation of solid-state morphology and thermo-mechanical properties. *Polymer Chemistry* **2013,** *4*, 3357.

17. Mosnáček, J.; Yoon, J. A.; Juhari, A.; Koynov, K.; Matyjaszewski, K., Synthesis, morphology and mechanical properties of linear triblock copolymers based on poly(α-methylene-γ-butyrolactone). *Polymer* **2009,** *50*, 2087-2094.

18. Gallagher, J. J.; Hillmyer, M. A.; Reineke, T. M., Isosorbide-based Polymethacrylates. *ACS Sustainable Chemistry & Engineering* **2015,** *3*, 662-667.

19. Gallagher, J. J.; Hillmyer, M. A.; Reineke, T. M., Acrylic Triblock Copolymers Incorporating Isosorbide for Pressure Sensitive Adhesives. *ACS Sustainable Chemistry & Engineering* **2016,** *4*, 3379-3387.

20. Wang, S.; Ding, W.; Yang, G.; Robertson, M. L., Biorenewable Thermoplastic Elastomeric Triblock Copolymers Containing Salicylic Acid-Derived End-Blocks and a Fatty Acid-Derived Midblock. *Macromolecular Chemistry and Physics* **2016,** *217*, 292-303.

21. Bolton, J. M.; Hillmyer, M. A.; Hoye, T. R., Sustainable Thermoplastic Elastomers from Terpene-Derived Monomers. *ACS Macro Letters* **2014,** *3*, 717-720.

22. Martello, M. T.; Schneiderman, D. K.; Hillmyer, M. A., Synthesis and Melt Processing of Sustainable Poly(ε-decalactone)-block-Poly(lactide) Multiblock Thermoplastic Elastomers. *ACS Sustainable Chemistry & Engineering* **2014,** *2*, 2519-2526.

23. Maisonneuve, L.; Lebarbé, T.; Grau, E.; Cramail, H., Structure–properties relationship of fatty acid-based thermoplastics as synthetic polymer mimics. *Polymer Chemistry* **2013,** *4*, 5472.

24. Satoh, K.; Sugiyama, H.; Kamigaito, M., Biomass-derived heat-resistant alicyclic hydrocarbon polymers: poly(terpenes) and their hydrogenated derivatives. *Green Chemistry* **2006,** *8*, 878.

25. Satoh, K.; Matsuda, M.; Nagai, K.; Kamigaito, M., AAB-Sequence Living Radical Chain Copolymerization of Naturally Occurring Limonene with Maleimide: An End-to-End Sequence-Regulated Copolymer. *Journal of the American Chemical Society* **2010,** *132*, 10003-10005.

26. Matsuda, M.; Satoh, K.; Kamigaito, M., Periodically Functionalized and Grafted Copolymers via 1:2-Sequence-Regulated Radical Copolymerization of Naturally Occurring Functional Limonene and Maleimide Derivatives. *Macromolecules* **2013,** *46*, 5473-5482.

27. Shearouse, W. C.; Lillie, L. M.; Reineke, T. M.; Tolman, W. B., Sustainable Polyesters Derived from Glucose and Castor Oil: Building Block Structure Impacts Properties. *ACS Macro Letters* **2015,** *4*, 284-288.

28. Wang, S.; Vajjala Kesava, S.; Gomez, E. D.; Robertson, M. L., Sustainable Thermoplastic Elastomers Derived from Fatty Acids. *Macromolecules* **2013,** *46*, 7202-7212.

29. Wang, Z.; Yuan, L.; Trenor, N. M.; Vlaminck, L.; Billiet, S.; Sarkar, A.; Du Prez, F. E.; Stefik, M.; Tang, C., Sustainable thermoplastic elastomers derived from plant oil and their "click-coupling" via TAD chemistry. *Green Chem.* **2015,** *17*, 3806-3818.

30. Yuan, L.; Wang, Z.; Trenor, N. M.; Tang, C., Robust Amidation Transformation of Plant Oils into Fatty Derivatives for Sustainable Monomers and Polymers. *Macromolecules* **2015,** *48*, 1320-1328.

31. Lee, S.; Lee, K.; Kim, Y.-W.; Shin, J., Preparation and Characterization of a Renewable Pressure-Sensitive Adhesive System Derived from ε-Decalactone,l-Lactide, Epoxidized Soybean Oil, and Rosin Ester. *ACS Sustainable Chemistry & Engineering* **2015,** *3*, 2309-2320.

32. Schneiderman, D. K.; Hill, E. M.; Martello, M. T.; Hillmyer, M. A., Poly(lactide)-block-poly(ε-caprolactone-co-ε-decalactone)-block-poly(lactide) copolymer elastomers. *Polym. Chem.* **2015,** *6*, 3641-3651.

33. Schneiderman, D. K.; Hillmyer, M. A., Aliphatic Polyester Block Polymer Design. *Macromolecules* **2016,** *49*, 2419-2428.

34. Shin, J.; Lee, Y.; Tolman, W. B.; Hillmyer, M. A., Thermoplastic elastomers derived from menthide and tulipalin A. *Biomacromolecules* **2012,** *13*, 3833-40.

35. Ding, K.; John, A.; Shin, J.; Lee, Y.; Quinn, T.; Tolman, W. B.; Hillmyer, M. A., High-Performance Pressure-Sensitive Adhesives from Renewable Triblock Copolymers. *Biomacromolecules* **2015,** *16*, 2537-9.

36. Lee, C.-C.; Liu, Y.; Reineke, T. M., Glucose-Based Poly(ester amines): Synthesis, Degradation, and Biological Delivery. *ACS Macro Letters* **2012,** *1*, 1388-1392.

37. Wu, Y.; Wang, M.; Sprouse, D.; Smith, A. E.; Reineke, T. M., Glucose-containing diblock polycations exhibit molecular weight, charge, and cell-type dependence for pDNA delivery. *Biomacromolecules* **2014,** *15*, 1716-26.

38. Yin, L.; Dalsin, M. C.; Sizovs, A.; Reineke, T. M.; Hillmyer, M. A., Glucose-Functionalized, Serum-Stable Polymeric Micelles from the Combination of Anionic and RAFT Polymerizations. *Macromolecules* **2012,** *45*, 4322-4332.

39. Ting, J. M.; Navale, T. S.; Bates, F. S.; Reineke, T. M., Design of Tunable Multicomponent Polymers as Modular Vehicles To Solubilize Highly Lipophilic Drugs. *Macromolecules* **2014,** *47*, 6554-6565.

40. Shi, H.; Liu, L.; Wang, X.; Li, J., Glycopolymer–peptide bioconjugates with antioxidant activity via RAFT polymerization. *Polymer Chemistry* **2012,** *3*, 1182.

41. Mahkam, M., New pH-Sensitive Glycopolymers for Colon-Specific Drug Delivery. *Drug Delivery* **2007,** *14*, 147-153.

42. J, B.; E, I.; E, G.; A, A.; D, B., *Polymer Handbook*. 4th ed.; Wiley: New York, 1999; Vol. 49.

43. Hiemenz, P. C.; Lodge, T. P., *Polymer Chemistry*. CRC Press: Boca Raton, FL, 2007.

44. Nakamura, Y.; Sakai, Y.; Adachi, M.; Fujii, S.; Sasaki, M.; Urahama, Y., Effects of Compatibility of Acrylic Block Copolymer and Tackifier on Phase Structure and Peel Adhesion of Their Blend. *Journal of Adhesion Science and Technology* **2008,** *22*, 1313-1331.

45. Malic, N.; Evans, R. A., Synthesis of Carboxylic Acid and Ester Mid-Functionalized Polymers using RAFT Polymerization and ATRP. *Australian Journal of Chemistry* **2006,** *59*, 763–771.

46. Li, Y.; Peng, B.; Chen, Y., Encapsulation properties of reverse-amphiphilic core/shell polymeric nanoobjects with different shapes. *Journal of Materials Chemistry B* **2013,** *1*, 5694.

47. Nasiri, M.; Bertrand, A.; Reineke, T. M.; Hillmyer, M. A., Polymeric nanocylinders by combining block copolymer self-assembly and nanoskiving. *ACS Appl Mater Interfaces* **2014,** *6*, 16283-8.

48. Zhang, J.; Sides, S.; Bates, F. S., Ordering of Sphere Forming SISO Tetrablock Terpolymers on a Simple Hexagonal Lattice. *Macromolecules* **2012,** *45*, 256-265.

49. Hayashi, M.; Matsushima, S.; Noro, A.; Matsushita, Y., Mechanical Property Enhancement of ABA Block Copolymer-Based Elastomers by Incorporating Transient Cross-Links into Soft Middle Block. *Macromolecules* **2015,** *48*, 421-431.

50. Hayashi, M.; Noro, A.; Matsushita, Y., Highly Extensible Supramolecular Elastomers with Large Stress Generation Capability Originating from Multiple Hydrogen Bonds on the Long Soft Network Strands. *Macromol Rapid Commun* **2016,** *37*, 678-84.

Chapter 3

Enhanced Mechanical and Adhesion Properties in Sustainable Triblock Copolymers via Non-covalent Interactions*

* Submitted to *Macromolecules*

3.1 Introduction

The versatility of synthetic polymer chemistry has allowed for the design of functional block copolymers to construct thermoplastic elastomers (TPEs) that address the recyclability challenges of thermosetting materials. TPEs are comprised of ABA-type triblock copolymers and their exceptional thermomechanical properties are due to their phase-separated morphology, which results in glassy domains dispersed in a continuous flexible network. This physically cross-linked network of rubbery polymer chains mimics the chemical cross-linking of vulcanized rubber while maintaining the reprocessability of thermoplastics. Various block copolymer architectures along with their adhesive and viscoelastic properties have been extensively studied as TPEs.[1-6] Due to their appealing features, TPEs have been widely utilized in various industries.[7-9] Their composition and architecture can be tuned for a broad range of applications such as pressure sensitive adhesives, medical devices, coatings, and automotive parts.[7] However, commercial TPEs typically employ polystyrene as the glassy end block and polybutadiene or polyisoprene are used as the rubbery midblock. The environmental concerns associated with the use of these petroleum-based building blocks have led to significant research efforts towards the design of sustainable block copolymers.

Researchers have paid tremendous attention to fashioning alternatives from bio-based feedstocks for the outer (A) and/or inner (B) blocks. For example, efforts toward substituting styrene-based polymers in daily-use commodity products with poly(lactide) (PLA) have been examined by the incorporation of PLA as the glassy component in TPEs.[10] Previous work on sustainable TPEs has provided many examples of PLA

incorporation as the hard end blocks in ABA triblock copolymers.[11-24] For example, PLA has been copolymerized with various lactones,[11-16] cyclooctadiene and cyclooctene ketone,[17] menthide,[18-20] ethylene glycol,[21] propylene glycol,[22] isoprene,[23] and ricinoleic acid.[24] Although PLA has been shown to provide a useful glassy component for TPEs, it has inherent drawbacks (*e.g.* low glass transition temperature), which limits its utility in TPEs. Thus, the scientific community has sought to develop sustainable thermoplastic elastomers that can benefit from glassy domains with higher glass transition temperatures, allowing for a wider range of applications. Accordingly, alternative biomass derivatives including natural polymers such as lignin and cellulose[25-28] as well as rosin acid- and terpene-derived monomers[29-35] have been explored. Our group has also previously reported using acrylic derivatives of acetylated glucose and isosorbide as the glassy end blocks in triblock copolymers.[36-37] The previous studies showed that these sustainable building blocks provide excellent candidates for the glassy domain of an ABA triblock copolymer TPE.

Herein, properties and performance of triblock copolymers derived from both sustainable monomers, acetylated glucose and isosorbide, are further explored. Two sustainable and glassy monomers, acetylated acrylic isosorbide (AAI) and glucose acrylate tetraacetate (GATA), were copolymerized with *n*-butyl acrylate (nBA) as the rubbery midblock to generate high molar mass ABA triblock copolymers (*i.e.* 100-150 kDa). Their adhesion and mechanical properties were evaluated. Comprehensive adhesion testing– including peel adhesion, loop tack, steady shear, and shear failure temperature tests– revealed that the isosorbide-based copolymer possesses properties comparable or superior

to many of the commercially used pressure sensitive adhesives. Polymers with greater ratios of the glassy components were also prepared and examined for their mechanical performance. We incorporated hydrogen bonding within the GATA end blocks of the glucose-derived triblock copolymer by selective deacetylation of the anomeric hydroxyl groups in order to probe the effect of non-covalent interactions on the mechanical properties. Hydrogen bonding and other non-covalent interactions have been shown to play a significant role in various chemistries such as development of organic super acids and bases,[38-40] catalysis,[41] drug excipients,[42-43] and polymer-polymer interactions.[44-48] Herein, we show that enhancing intermolecular interactions within the glassy domains promoted stronger physical cross-links and improved the mechanical performance.

3.2 Results and Discussion

3.2.1 Synthesis of GATA and AAI Monomers

We utilized two different derivatives of glucose to impart sustainable glassy components into our triblock copolymers. Glucose acrylate tetraacetate (GATA) was obtained via direct modification of glucose. The GATA monomer was prepared following our previously reported procedure, in which we selectively protect the primary hydroxyl group followed by acetylation of the remaining hydroxyl groups, and subsequently the protecting group is lifted and the acrylate functionality is installed on the primary alcohol, to yield glucose-6-acrylate-1,2,3,4-tetraacetate (GATA; Scheme 3.S1).[36] The final monomer structure was confirmed by ^{1}H NMR spectroscopy (Figure 3.S1). Additionally, a widely used glucose derivative, isosorbide, was modified to prepare a sustainable acrylic monomer. Due to recent

advancements in the industrial conversion of sorbitol to isosorbide, this bio-based molecule is easily accessible and can be obtained at low cost. Following a previously described procedure by our group,[37] isosorbide was selectively mono-acetylated and an acrylate was subsequently installed at the second hydroxyl group to yield acetylated acrylic isosorbide (AAI; Scheme 3.S2). Figure 3.S2 shows that AAI was successfully synthesized and purified. Due to their rigid cyclic structures, both GATA and AAI monomers exhibit high glass transition temperatures (T_g) when polymerized and can serve as the glassy component in thermoplastic elastomers.[36-37]

3.2.2 RAFT Polymerization

Controlled radical copolymerization of GATA and AAI monomers with *n*-butyl acylate (nBA) was previously introduced by our group.[36-37] Employing reversible addition–fragmentation chain transfer (RAFT) polymerization and utilizing a bifunctional chain transfer agent (CTA), we were able to synthesize well-controlled triblock copolymers of GATA/AAI with nBA in a two-step reaction. 3,5-bis(2-dodecylthiocarbonothioylthio-1-oxopropoxy) benzoic acid (BTCBA) was used as the CTA; Scheme 3.1 shows the synthetic procedure used to prepare ABA-type triblock copolymers for this study. The synthesized polymers were characterized by ^{1}H NMR spectroscopy and size exclusion chromatography (SEC) (representative NMR spectra and SEC traces are shown in Figure 3.S3-3.S6). The work described here provides a deeper understanding of characteristic properties of our formerly developed platform for utilizing sugar-based polymers as thermoplastic elastomers. Structural modifications via non-covalent interactions, such as chain

entanglements and hydrogen bonding, were also explored to enhance the performance of these materials for desired applications.

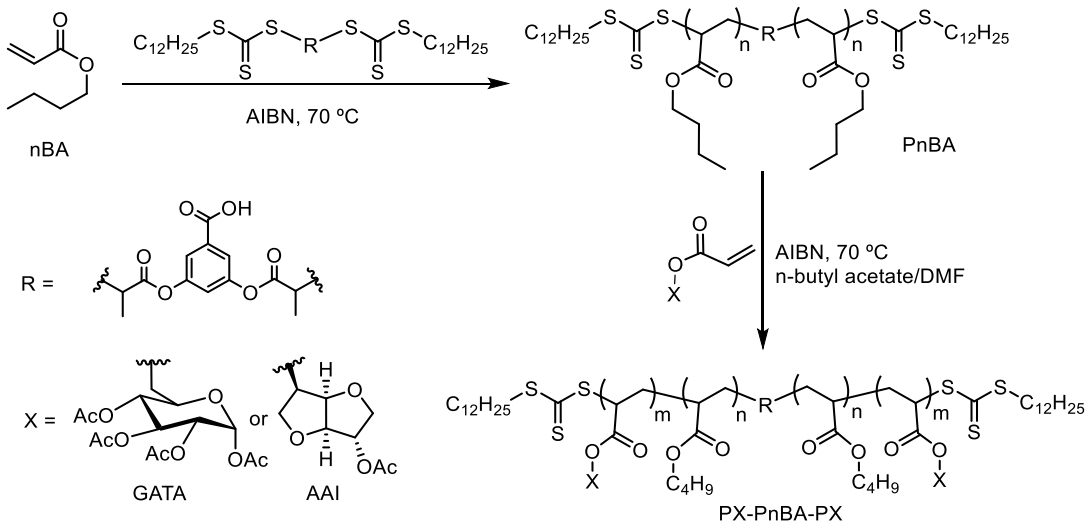

Scheme 3.1. Synthesis of PX-PnBA-PX triblock copolymers (where X is GATA or AAI).

3.2.3 Pressure Sensitive Adhesives Application

N-butyl acrylate has a relatively large entanglement molecular weight (28 kDa)[49] and can serve as a tacky component in a pressure sensitive adhesive.[7] In previous work, we demonstrated that PGATA-PnBA-PGATA triblock copolymers have excellent peel adhesion characteristics and exhibit peel adhesion values comparable to several commercial products.[36] In this study, we report the synthesis and characterization of triblock copolymers with longer block lengths to benefit from higher degree of entanglements between the polymer chains and more robust networks.[49-50] Following the schematic presented in Scheme 3.1, ABA triblock copolymers of GATA and AAI (as the A end blocks) with nBA (as the B midblock) were synthesized. The molar masses of the

polymers were measured by size exclusion chromatography (SEC) and their thermal properties were analyzed by differential scanning calorimetry (DSC) and thermal gravimetric analysis (TGA) (the thermal decomposition profiles are shown in Figure 3.S7). Table 3.1 shows a summary of the characterization data for the synthesized macro-CTAs and their respective triblock copolymers.

While observation of two well-separated glass transition temperatures near the T_g values of the respective homopolymers verifies phase segregation of the polymers, small angle X-ray scattering (SAXS) can be employed to confirm the phase-segregated network.[51] SAXS analysis of bulk samples generated from the synthesized triblock copolymers (P2 and P3 in Table 3.1) revealed distinct principal reflections, suggesting phase segregation (Figure 3.S8). Due to broad higher-order reflections, it is difficult to definitively assign a morphology; however, based on the estimated volume fractions of the glassy blocks (Table 3.1), a spherical morphology is expected. Although an increased number of entanglements can limit the adhesive performance of the neat polymer, it allows for a larger window for dilution of the entanglements via addition of a tackifier, and the properties can be tuned for a wider range of applications. Addition of a tackifier to the polymers lowers the modulus of the material and allows for stronger pressure sensitive adhesive properties. Sylvalite™ 80HP rosin ester is a renewable resin produced by Arizona Chemicals (Jacksonville, FL) and was utilized as the tackifier in this study (T_g = 32 ℃ and miscible with the PnBA midblock). DSC measurements showed that addition of the tackifier increases the glass transition of the PnBA midblock, relative to that of the pure polymer (the midblock T_g changed from –48 ℃ to –26 ℃ and from –45 ℃ to –27 ℃ for P2

and P3, respectively) (Figure 3.S9). Triblock copolymers P2 and P3 were mixed with 40 wt% of the rosin ester tackifier and a comprehensive study of the adhesion properties of these samples was conducted via peel adhesion, loop tack, shear adhesion temperature failure, and static shear tests.

Table 3.1. Molecular and thermal characteristics of PnBA macro-CTAs and their respective PGATA and PAAI triblock copolymers.

Polymer	**Sample Code** [a]	M_n [b] **(kDa)**	$Đ$ [b]	**Hard Block** [c] (wt%)	**DP** [d]	T_d [e] (°C)	T_g [f] (°C)
PnBA	P1	90	1.04	-	700	330	–47
PGATA-PnBA-PGATA	P2	100	1.14	10	12-700-12	307	–48, 98
PAAI-PnBA-PAAI	P3	102	1.19	12	25-700-25	314	–45, 78
PnBA	P4	110	1.05	-	860	290	–59
PGATA-PnBA-PGATA	P5	146	1.24	25	45-860-45	295	–46, 123
PAAI-PnBA-PAAI	P6	152	1.44	28	87-700-87	317	–46, 96

[a]P1 was chain extended to produce P2 and P3, and P5 and P6 were produced from P4 [b]Number average molar mass and polydispersity determined by SEC-MALLS in THF at room temperature. [c]GATA and AAI content determined by ^{1}H NMR spectroscopy; volume fractions are estimated to be the same as the weight fractions (where ρ = 1.08 g mL^{-1} for PnBA homopolymers and ρ = 1.05 g mL^{-1} for PGATA and PAAI homopolymers, which is estimated from chemically similar poly(2-tetrahydropyranyl acrylate)).[52] [d]Average degree of polymerization for each block. [e]Decomposition temperature at 5% weight loss determined by thermal gravimetric analysis (TGA). [f]Glass transition temperature determined by differential scanning calorimetry (DSC).

Adhesive strength can be measured using various methods depending on the desired end application. Peel testing is appropriate when there is flexibility in the joint layer and corresponds to the force required to remove the adhesive from a substrate. 180 degree peel strength can be achieved by pulling the adhesive film, flexible backing film that is coated with the adhesive, against a supporting plate. A similar test for PSAs is the loop tack method, if the adhesives form a bond of measurable strength rapidly upon contact with another surface, and it provides a quantitative measure of tackiness of the adhesive. Loop

tack is a measure of the instantaneous bonding between the substrate and the adhesive at the interface, without being pressed or rolled, and corresponds to the force required to lift off the adhesive from the substrate immediately after they have been brought into contact. Static shear strength is another important characteristic of a PSA and represents the internal resistance of the adhesive to flow under a constant static force. Shear resistance is quantified by applying a given force parallel to the substrate and surface of the tape and monitoring the time before the adhesive fails. An additional test for shear resistance is the shear adhesion failure temperature (SAFT) test, which measures the heat-fail temperature in shear strength of a pressure sensitive adhesive. Samples are assembled as in the shear test and the only difference is that the temperature is increased at a defined rate, and the temperature at which the adhesive layer fails is noted as the shear adhesion failure temperature (SAFT). The SAFT provides a limiting temperature above which the adhesive fails to resist the loaded shear force.

Comprehensive adhesion testing results for the synthesized isosorbide- and glucose-based triblock copolymers are summarized in Table 3.2. The standard methods from the American Society for Testing and Materials (ASTM) were used and the evaluations were conducted in an industrial setting by Adherent Laboratories Inc. (Saint Paul, MN). Excellent peel and loop tack adhesion values were observed for both P2 and P3. While the glucose-based polymer (P2) exhibited moderate shear resistance (failure after 844 minutes), the isosorbide-based polymer (P3) demonstrated outstanding shear strength, with no failure up to 100 hours (the test was manually terminated after 6000 minutes). The lower shear resistance observed for P2 could be attributed to weaker physical

cross-linking within its network. Despite two clear T_g values in DSC, which are similar to those of homopolymers of GATA[36] and nBA (Table 3.1), and clear ordering in SAXS analysis (Figure 3.S8), which suggest phase segregation is present, it appears that the intermolecular interactions in glassy domains of P2 are weaker than P3, resulting in the lower shear resistance observed. SAFT measurements are consistent with the static shear results and failure temperatures of 42 °C and 60 °C were observed for P2 and P3, respectively. In general, the adhesive performance is dependent on the thickness of the adhesive material.[53] For consistency, the measurements were conducted using the industry standard for adhesive layers (25 gsm). Figure 3.1 compares the adhesive properties of our polymers, P2 and P3 blended with 40% rosin ester tackifier, to those of commonly used commercial products as reported by Lee *et al.*;[13] as evidenced, these sustainable polymers have comparable or superior performance to a variety of commercial products. Thus, the thickness of the adhesive layer, as well as the ratio of polymer to tackifier, can be easily tuned to achieve the desired properties.

Table 3.2. Summary of adhesion properties of PGATA-PnBA-PGATA (P2) and PAAI-PnBA-PAAI (P3) copolymers.

Polymer	P2[a]	P3[a]
M_n (kDa)	5-90-5	6-90-6
Peel Adhesion[b] (N/cm)	8.22 ± 0.35	8.74 ± 0.35
Loop Tack[c] (N/cm^2)	4.34 ± 0.69	2.96 ± 0.14
Shear[d] (min)	844 ± 228	>6000
SAFT[e] (°C)	42	60

[a]The polymer is blended with 40 wt% of a rosin ester resin as tackifier. [b]180° peel adhesion to a stainless-steel plate, test method: PSTC: 101, cohesive failure was observed. [c]Loop tack to a stainless-steel plate, test method: ASTM: D6195. [d]Static shear strength using 1 in × 1 in films and 500 gram load, test method: PSTC: 107. [e]Shear adhesion failure temperature using 1 in × 1 in films and 500 gram load, test method: ASTM-D4498.

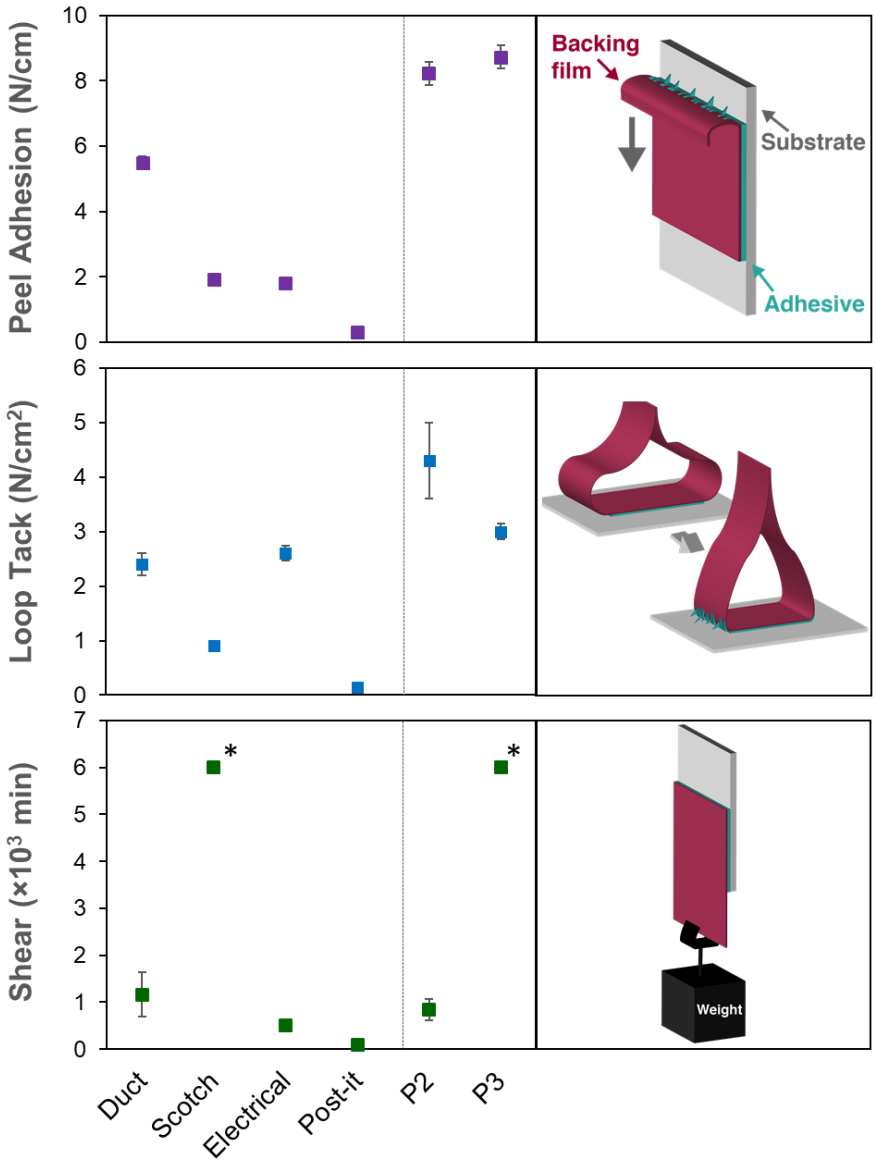

Figure 3.1. Adhesive properties of P2 and P3 polymers, blended with 40 wt% tackifier, compared to commercial products as reported by Lee et al.[13] (the corresponding values are listed in Table 3.2 and Table 3.S1). * The adhesive did not fail after 100 hours and the test was terminated.

3.2.4 Mechanical Properties of Thermoplastic Elastomers

To demonstrate the versatility of these materials, triblock copolymers with larger amounts of the glassy components were also prepared (Table 3.1) and examined for their

mechanical properties. Successful synthesis of the triblock copolymers was confirmed with SEC (Figure 3.S10) and the ratio of the glassy/soft components was calculated from ^{1}H NMR spectra. To avoid any structural changes at higher temperatures for these triblock copolymers, the trithiocarbonate CTA groups were removed by aminolysis and the ends of the polymer chains were capped with methyl acrylate via Michael addition (Scheme 3.S3).[54] The tensile behavior of P5 and P6 was investigated and the results are shown in Figure 3.2 and summarized in Table 3.3. As expected from the shear adhesion testing, the GATA-based polymer (P5) produces relatively weak material with ductile behavior. Again, this may be attributed to weaker intermolecular interactions in the glassy domains, and thus weaker physical cross-links, resulting in a softer material with a lower modulus. However, the AAI-based polymer (P6) results in a tough elastomeric material, with high ultimate tensile strength and high strain at break. It should be noted that the high molecular weight shoulder present in P6 (Figure 3.S10) may contribute to its mechanical performance. A high molecular weight shoulder in radical polymerization could be attributed to chain coupling at high conversion, potentially resulting in multiblock copolymers, which may contribute to the increased modulus.

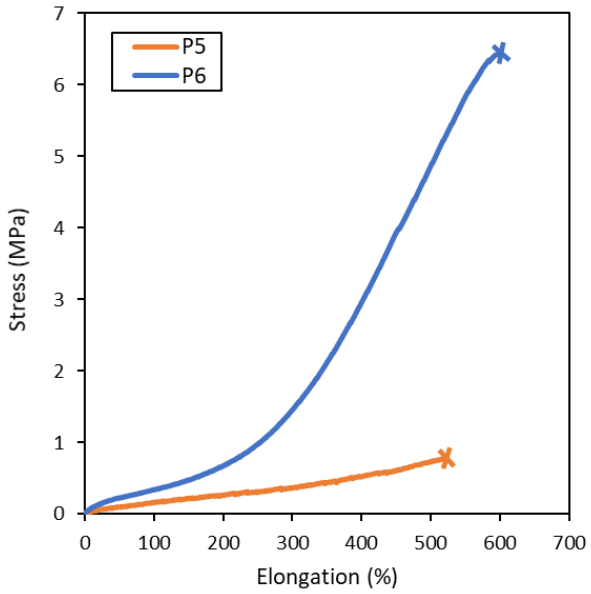

Figure 3.2. Uniaxial stress−strain curves for P5 (PGATA-PnBA-PGATA: 18-110-18 kDa) and P6 (PAAI-PnBA-PAAI: 21-110-21 kDa). Experiments were conducted at room temperature at 5 mm min^{-1}; failure point marked with ×. Five replicate tensile bars of each polymer sample were conducted.

Table 3.3. Tensile properties of P5 and P6 triblock copolymers.

Polymer		P5	P6
M_n (kDa)		18-110-18	21-110-21
Hard Block (wt%)		25	28
E[a] (kPa)		640 ± 106	773 ± 70
σ[b] (MPa)		0.81 ± 0.05	6.47 ± 0.46
ε[c] (% elongation)		476 ± 35	620 ± 76
Hysteresis[d] (%)	C1	22.1	18.3
	C2-10	2.56 ± 1.93	1.88 ± 1.74

Average values for five replicate tensile bars extended at 5 mm min^{-1} are reported. [a]Young's modulus calculated based on the first 5% strain. [b]Stress at break. [c]Elongation at break. [d]Hysteresis loss under cyclic loading and unloading for the first cycle (C1) and the average of the subsequent cycles (C2-C10) conducted at 60% of maximum elongation.

To gain a deeper insight into the mechanical performance of these polymers, oscillatory shear rheometry was employed. Monitoring the modulus as a function of temperature revealed wide rubbery plateaus for both of the polymers, confirming a physically cross-linked network. Temperature dependence of the loss and storage moduli for P5 (PGATA-PnBA-PGATA: 18-110-18 kDa) and P6 (PAAI-PnBA-PAAI: 21-110-21 kDa) are presented in Figures 3.3 and 3.4, respectively. The T_g values for the hard blocks of both P5 and P6 are evident at 142 ºC and 105 ºC, respectively. The rubbery plateaus appear to be combination of two succeeding sub-plateaus, which can be interpreted as the presence of two entanglement mechanisms: presumably, one for the chain entanglements within the midblock and another for the physical cross-link points throughout the network. Figure 3.3 also reveals that glucose-based polymer (P5) has a stronger temperature-dependent modulus compared to the isosorbide-based analogue (P6). Additionally, the order-disorder transition temperatures appear to be relatively high for both P5 and P6; however, it is worth noting that the polymers become soft and may be melt-processed above approximately 160 ºC. Overall, observation of weak shear strength and low moduli for the GATA-based triblock copolymers encouraged us to modify the structure of the GATA blocks to promote stronger intermolecular interactions within the glassy domains, thus stronger physical cross-links, to ultimately enhance mechanical performance. The next section describes our approach and summarizes the results.

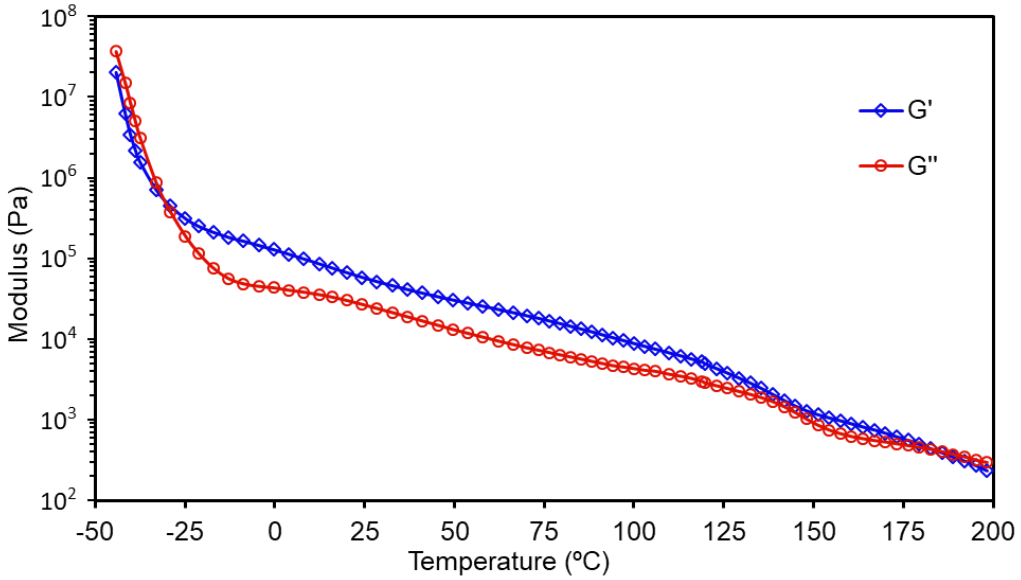

Figure 3.3. Temperature dependence of the loss and storage moduli in P5 (PGATA-PnBA-PGATA: 18-110-18 kDa). The temperature ramp was conducted at 5% strain and 10 °C min^{-1}.

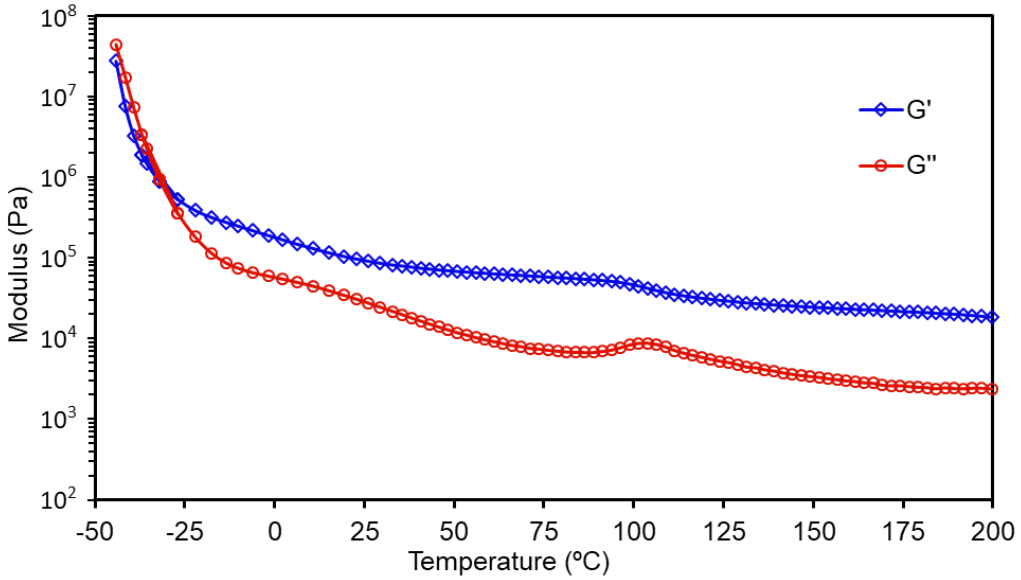

Figure 3.4. Temperature dependence of the loss and storage moduli in P6 (PAAI-PnBA-PAAI: 21-110-21 kDa). The temperature ramp was conducted at 5% strain and 10 °C min^{-1}.

3.2.5 Hydrogen-bonded Segregates

Self-complementary hydrogen bonding between polymer chains has been utilized to incorporate transient networking within the rubbery network of TPEs.[46] Here, we introduced hydrogen bonding between the GATA units to improve the strength of phase segregation in the glassy domains of GATA-based polymers. To avoid any significant alterations in the glassy properties of the GATA blocks, such as high T_g, the structural modification of GATA units must be conducted in a controlled manner. The anomeric hydroxyl group can be selectively deacetylated,[55] leaving the other ester functionalities in the polymer intact. The reaction was carried out in a mixture of butyl acetate and DMF and hydrazine acetate was used as the selective deprotecting reagent (Scheme 3.2). SEC showed that the polymer structure remains intact after the reaction (Figure 3.5) and ^{1}H NMR spectroscopy confirmed successful deacetylation of the anomeric hydroxyl group by monitoring the chemical shift for the anomeric proton (which shifts to lower frequencies upon deacetylation). Figure 3.6 shows the NMR spectra for P5 (before deprotection) and P7 (after deprotection); the peak corresponding to the anomeric proton (5.82 ppm) shifts upfield after deacetylation, overlapping with other glucose backbone peaks, which undergo smaller changes in their electronic environment upon deprotection of the anomeric hydroxyl group. Since the peak corresponding to the anomeric proton almost completely shifts upfield (Figure 3.6, inset), and only a miniscule number of the anomeric hydroxyl groups appear to remain acetylated, the conversion for the deacetylation reaction was estimated to be near completion (*ca.* 20-25% total deacetylation of the GATA blocks).

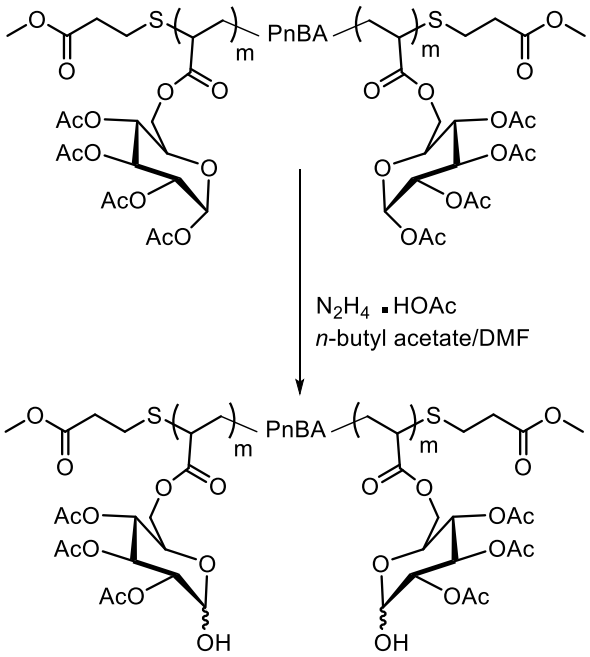

Scheme 3.2. Selective deprotection of the anomeric hydroxyl groups of GATA units on P5 to generate P7.

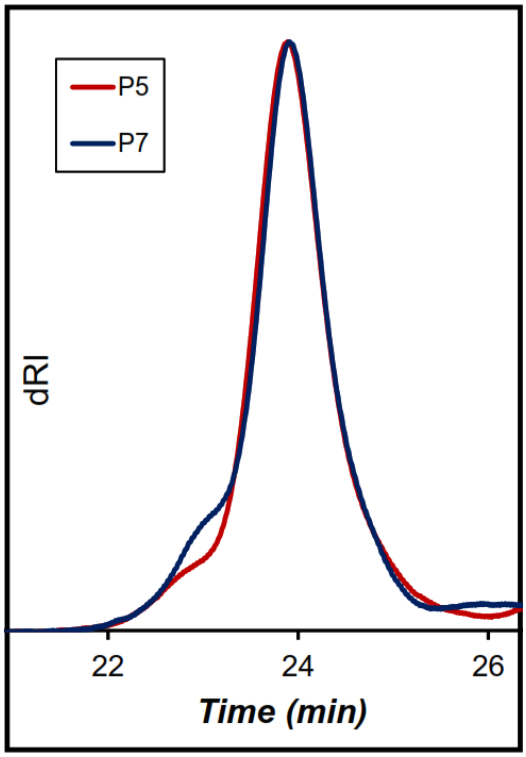

Figure 3.5. SEC traces of P5 (PGATA-PnBA-PGATA: 18-110-18 kDa) before deacetylation and after deacetylation (P7).

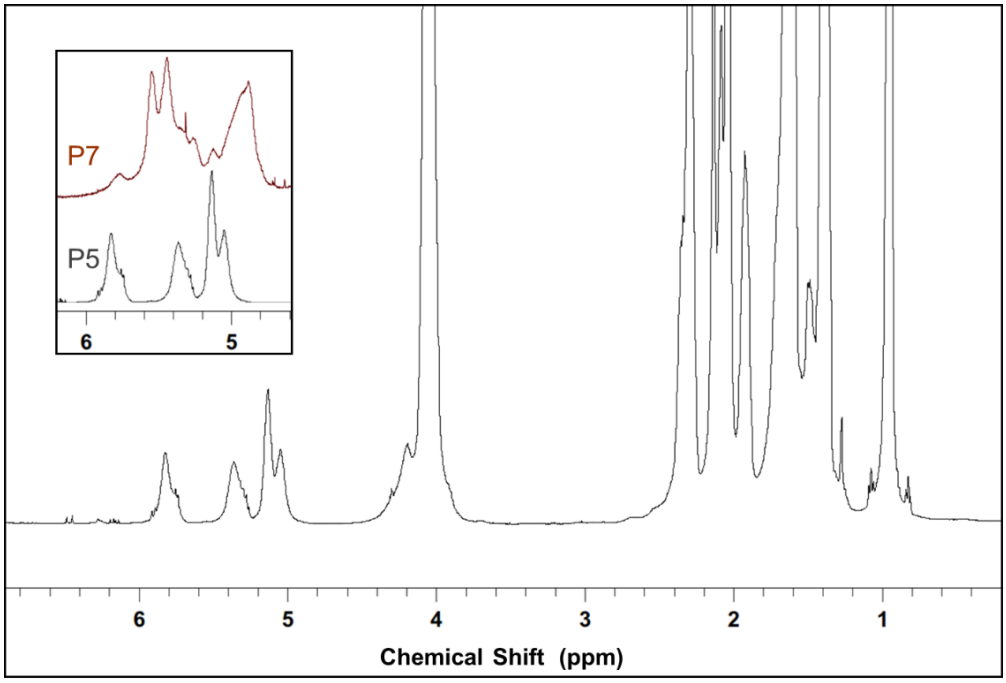

Figure 3.6. ^{1}H NMR spectrum (500 MHz, $CDCl_3$) for P5. The inset compares peak positions for before (P5) and after (P7) selective deacetylation.

Tensile testing revealed significant enhancement in mechanical properties of the GATA polymers after deprotection. Figure 3.7 compares the tensile behavior of P5 with its partially deacetylated derivative (P7) and the results are tabulated in Table 3.4. Upon partial deacetylation, an 80% increase in the ultimate tensile strength was observed as compared to P5. This may be attributable to complementary hydrogen bonding, due to presence of free hydroxyl groups within the glassy domains, which can ultimately result in stronger physical cross-links and reduce chain-pullouts under an applied stress. Similar SAXS patterns were observed for the triblock copolymers before (P5) and after (P7) deprotection (Figure 3.S11). Moreover, the broad stretch near 3500-3100 cm^{-1} in the FT–IR spectrum of P7 is indicative of hydrogen-bonded hydroxyl groups (Figure 3.S12). It

should be noted that the low intensity for this feature is likely due to the small number of hydroxyl groups, which comprise a very small portion of the polymer molecules.

Oscillatory shear rheometry was also employed to investigate the viscoelastic properties of the GATA-based triblock copolymers upon deacetylation (P7) (Figure 3.8). Clearly the T_g for P5 near 142 ºC is no longer observed for P7; however, a transition seems to be beginning around 180 ºC. Moreover, rheology suggests a strengthened physical cross-linking in P7 compared to P5. Although the difference in the modulus is not very distinct, which could be due to differences in sample preparation and sample geometry during the measurements, P7 clearly retains its structure at higher temperatures by demonstrating a greater storage modulus than the loss modulus at least up to 200 ºC (the test was stopped at 200 ºC to avoid potential thermal degradation). This may be inferred as a result of strengthened glassy domains aided by hydrogen bonding.

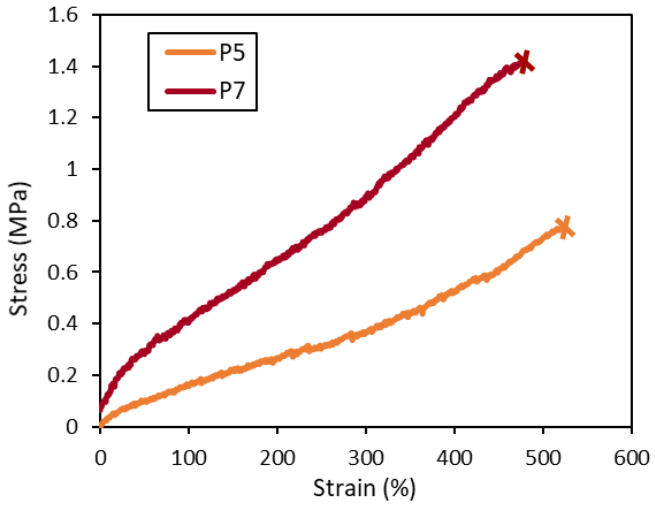

Figure 3.7. Tensile properties before (P5) and after (P7) partial removal of the anomeric acetyl protecting groups in GATA blocks. Experiments were conducted at room temperature at 5 mm min^{-1}; failure point marked with ×. Three replicate tensile bars of each polymer sample were conducted.

Table 3.4. Summary of the tensile properties before (P5) and after (P7) the selective deacetylation.

Polymer	P5	P7
E[a] (kPa)	640 ± 106	805 ± 123
σ[b] (MPa)	0.81 ± 0.05	1.46 ± 0.12
ε[c] (% elongation)	476 ± 35	459 ± 30

Average values for three replicate tensile bars extended at 5 mm min^{-1} are reported. [a]Young's modulus calculated based on the first 5% strain. [b]Stress at break. [c]Elongation at break.

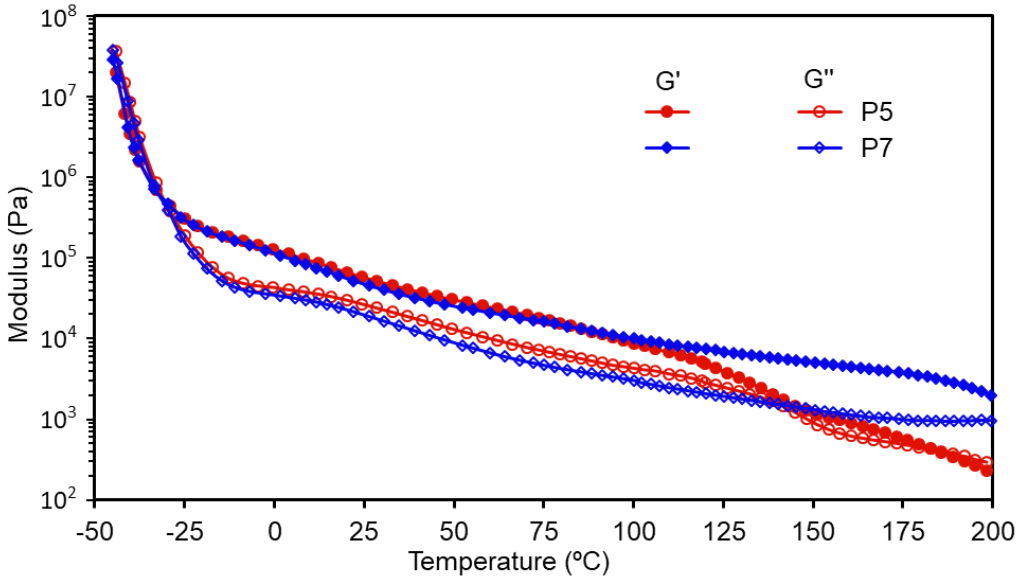

Figure 3.8. Temperature dependence of the loss and storage moduli for P5 (red) and P7 (blue). The temperature ramp was conducted at 5% strain and 10 °C min^{-1}.

3.3 Conclusion

In summary, we demonstrated that incorporation of high T_g glucose- and isosorbide-derived components in ABA triblock copolymers results in sustainable alternatives to commodity TPEs. PGATA and PAAI end blocks were chain-extended from

a PnBA midblock via RAFT polymerization. High molar mass ABA triblock copolymers were prepared to benefit from a larger number of trapped entanglements in the rubbery midblock. A comprehensive evaluation of the adhesion properties of these triblock copolymers was conducted and the polymers were found to perform comparable or superior to many commercial pressure sensitive adhesives (with peel adhesions greater than 8.22 N cm^{-1}). Moreover, these sustainable alternatives have the potential to be tuned for a wide range of applications by modifying the adhesive layer thickness and polymer to tackifier ratio. While AAI-based polymers exhibited stronger shear resistance compared to the GATA-based analogue, no shear failure up to 100 h compared to failure after 14 h, respectively, loop tack tests revealed a higher instantaneous bonding tendency for the GATA-based polymers, 4.34 N cm^{-2}. Mechanical properties of the polymers were evaluated with uniaxial tensile testing and oscillatory shear rheometry. PAAI-PnBA-PAAI was found to be a tough elastomer with high ultimate tensile strength and elongation at break (σ = 6.5 MPa and ε = 620%, respectively). On the other hand, moderate mechanical features were observed for PGATA-PnBA-PGATA (σ = 0.8 MPa and ε = 476%). Thus, hydrogen bonding was introduced into the glassy domain of PGATA-PnBA-PGATA via selective deprotection of the anomeric hydroxyl group of the GATA units. Presence of free hydroxyl groups increase the intermolecular interactions within the glassy domains and promote stronger physical cross-links and ultimately improve the shear strength, exhibited by an 80% increase in the ultimate tensile strength upon the selective deacetylation. This study demonstrates enhancement of properties in sugar-derived triblock copolymers via utilization of non-covalent interactions such as chain entanglements and self-

complementary hydrogen bonding. Marked improvements in the adhesion and mechanical properties of these materials as a result of such non-covalent interactions allows for improved design of sustainable, sugar-derived polymers as high performance TPEs.

3.4 Materials and Methods

3.4.1 Materials

The tackifier (Sylvalite^{TM} RE-80HP) was received as a gift from Arizona Chemicals (Jacksonville, FL) and was used as received. All other reagents used in this study were purchased from Sigma-Aldrich (St. Louis, MO) and were used as received. Acryloyl chloride and n-butyl acrylate (n-BA) were passed through an activated alumina column to remove the inhibitors and stored at –20 °C for future use.

3.4.2 Characterization

All ^{1}H NMR spectra were recorded at room temperature on a Brüker Avance III 500 MHz Spectrometer in $CDCl_3$ as the solvent. Chemical shifts are reported relative to the tetramethylsilane (TMS) internal standard peak at 0.00 ppm. Size-exclusion chromatography (SEC) was performed in THF using a Waters Styragel guard column and 3 Waters Styragel columns (HR6, HR4, and HR1) in series with separation ability of 100–10,000,000 g.mol^{-1}. The columns were contained in an Agilent 1260 Infinity liquid chromatograph equipped with a Wyatt Dawn Heleos II multiangle light scattering detector and a Wyatt Optilab T-rEX refractive index detector. The dn/dc values were calculated from the refractive index signal using a known sample concentration and assuming 100%

mass recovery from the column and were used for molar mass calculations. A Bruker Alpha Platinum ATR spectrometer was used to acquire the FT–IR spectra at 2 cm^{-1} resolution. Thermal gravimetric analysis (TGA) was performed on a TA Instruments Q500 at a heating rate of 10 °C min^{-1}. Differential scanning calorimetry (DSC) measurements were carried out using a TA Instruments Discovery DSC under air. The glass transition temperature, T_g, values were determined on the second heating at a heating rate of 20 °C min^{-1}. Small-angle X-ray scattering (SAXS) experiments were performed at the Sector 5-ID-D beamline of the Advanced Photon Source (APS) at Argonne National Laboratories, maintained by the Dow-Northwestern-Dupont Collaborative Access Team (DNDCAT). The source produces X-rays with a 0.70 Å wavelength. The sample to detector distance was fixed at 7.491 m. Scattering intensity was monitored using a Mar 165 mm diameter CCD detector operating with a resolution of 2048 by 2048. The two dimensional scattering patterns were azimuthally integrated to afford one-dimensional profiles presented as spatial frequency (q) versus scattered intensity. Samples were annealed at 150 ºC for 1 hour prior to the SAXS experiments.

3.4.3 Monomer and Polymer Syntheses

Synthesis of glucose-6-acrylate-1,2,3,4-tetraacetate (GATA). Anhydrous D-(+)-glucose (30.0 g, 167 mmol), trityl chloride (50.0 g, 180 mmol), and anhydrous pyridine (125 ml) were sequentially added to a 1000 ml round bottom flask and the mixture was placed in a preheated oil bath at 90 °C until all components were fully dissolved. Then, acetic anhydride (90 ml) was added and allowed to stir at room temperature for 20 h.

Afterward, the solution was slowly poured into a mixture of 6 liters of ice water and 250 ml acetic acid and then vigorously stirred for 4 h. The resultant white precipitate was filtered and washed with cold water and air dried for 24 h. The solid obtained was dispersed in 150 ml ethyl ether, stirred for 10 minutes, and vacuum filtered to afford 6-trityl-d-glucose-1,2,3,4-tetraacetate (TGTA) (52.0 g, 52.7 % isolated yield). Next, TGTA (25.0 g, 42.4 mmol), 3 ml water, and 50 ml dichloromethane were mixed in a 250 ml round bottom flask. 13 ml trifluroacetic acid was slowly added and the mixture was stirred at room temperature for 15 minutes. The mixture was diluted with 200 ml dichloromethane and 200 ml water and transferred into a separatory funnel. The wash with dichloromethane was repeated with another 200 ml dichloromethane. The organic washes were combined and washed with a saturated solution of $NaHCO_3$ (250 ml) followed by two washes with water (2 x 250 ml). The organic solution was then dried over magnesium sulfate and concentrated by rotary evaporation. The resulting viscous solution was dissolved in a minimum amount of anhydrous diethyl ether at 40 ºC, and agitated with a spatula to induce recrystallization, which was left in a refrigerator for two days. The resulting crystals were vacuum filtered, washed with cold diethyl ether, and air dried to afford D-glucose-1,2,3,4-tetraacetate (GTA, 11.0 g, 74.4% isolated yield). Finally, a solution of GTA (10.0 g, 28.7 mmol) and triethylamine (9.00 g, 89.2 mmol) in 30 ml dichloromethane was added dropwise to a stirred 0 °C solution of acryloyl chloride (7.50 g, 82.9 mmol) in 200 ml dichloromethane in a 500 ml round bottom flask. After 2 h, the mixture was allowed to warm to room temperature and was stirred for an additional 16 h. The solvent was then removed by rotary evaporation and the remaining solid was dissolved in 20 ml dichloromethane and passed

through a plug of silica gel using 1500 ml of an ethyl acetate:hexanes (80:20) mixture. The solvent was removed to afford glucose-6-acrylate-1,2,3,4-tetraacetate (GATA, 9.00 g, 78.0% isolated yield). ^{1}H NMR ($CDCl_3$): δ 1.95-2.15 (m, 12H, CH_3-CO); 3.84-3.91 (m, 1H), 4.20-4.30 (m, 2H), 5.08-5.14 (m, 2H), 5.23 (t, 1H), 5.70 (d, 1H, O-CH-CH-OH), 5.86 (d, 1H), 6.12 (dd, 1H), 6.42 (d, 1H) ppm (Figure 3.S1).

Synthesis of exo-acetyl-endo-acryl isosorbide (AAI). Isosorbide (20.0 g, 137 mmol) and acetic anhydride (13.0 ml, 137 mmol) were dissolved in acetonitrile (200 ml) with stirring. The flask was then submerged in an ice bath and cooled to 0 ºC. $Sc(OTf)_3$ (34.5 mg, 0.05 mol%) was dissolved in a minimal amount of acetonitrile and added to the stirring solution at 0 ºC. After 20 min, the solution was concentrated by rotary evaporation. Toluene (25 ml) was added to the concentrate and rotovapped two times to facilitate the removal of acetic acid. The crude mixture was subjected to column chromatography on silica gel (CH_2Cl_2 → 1:1 CH_2Cl_2:EtOAc) to isolate a mixture of *endo*- and *exo*-acetyl isosorbide (AI) as a clear, viscous liquid (8.31 g, 32.2%). *Note*: Further purification was performed to isolate exo-AI for this study; however, the mixture of isomers can be used with no significant differences in polymer properties. AI (1.00 g, 5.31 mmol), trimethylamine (0.81 ml, 5.81 mmol), and DCM (10.6 ml) were added to a 50-ml round bottom flask with stirring. The flask was submerged in an ice bath and acryloyl chloride (0.45 ml, 5.57 mmol) was added dropwise via addition funnel. The reaction was allowed to warm slowly to room temperature and after 18 h, the trimethylamine salts were removed by filtration. The filtrate was passed through a plug of silica and then basic alumina successively (*ca.* 10 g each; diethyl ether eluent). The solvent was concentrated, dissolved in a minimal amount of

diethyl ether, and crystallization was aided by the addition of pentane to afford *exo*-acetyl-*endo*-acryl isosorbide (AAI, 1.01 g, 78.6%).^{1}H NMR ($CDCl_3$): δ 6.46 (dd, *J* = 17.3, 1.5 Hz, 1H), 6.17 (dd, *J* = 17.3, 10.5 Hz, 1H), 5.89 (dd, *J* = 10.4, 1.5 Hz, 1H), 5.23 (q, *J* = 5.4 Hz, 1H), 5.19 (d, *J* = 2.6 Hz, 1H), 4.87 (t, *J* = 5.0 Hz, 1H), 4.50 (d, *J* = 4.5 Hz, 1H), 4.00-3.95 (m, 3H), 3.85 (dd, *J* = 9.8, 5.3 Hz, 1H), 2.07 (s, 3H) (Figure 3.S3).

Synthesis of poly(n-butyl acrylate)(CTA-PnBA-CTA). P1 is described as an illustrative example. AIBN (5.70 mg, 0.035 mmol), 3,5-bis(2-dodecylthiocarbonothioylthio-1-oxopropoxy)benzoic acid (BTCBA) (150 mg, 0.183 mmol), and n-butyl acrylate (40.0 ml, 278 mmol) were mixed in a 50 ml round bottom flask equipped with a teflon stirring bar. The flask was sealed and degassed under inert nitrogen at room temperature for 1 h. Subsequently, the reaction vessel was submerged into a preheated oil bath maintained at 70 °C. The reaction was quenched by immediately placing the flask into liquid nitrogen and opening it to air after 75 minutes. CH_2Cl_2 (10 ml) was added to the mixture, and subsequently the polymer was precipitated in 600 ml of ice-cold methanol and was left in the freezer for two hours. The precipitates were isolated by decanting off the supernatant fluid. The procedure was repeated two times and precipitates were dried under vacuum at 40 °C (11.1 g, 67.1% isolated yield). M_n (PnBA)= 90 kg.mol^{-1} (46.3% conversion), $Đ$ =1.04.

Synthesis of poly(glucose-6-acrylate-1,2,3,4-tetraacetate)-poly(n-butyl acrylate)-poly(glucose-6-acrylate-1,2,3,4-tetraacetate)(PGATA-PnBA-PGATA). P2 is described as an illustrative example. AIBN (2.05 mg, 0.012 mmol), PnBA macro-CTA (P1, 3.04 g, 0.034 mmol), GATA (393 mg, 0.98 mmol), 8 ml of n-butyl acetate, and 3 ml of

dimethylformamide were mixed in a 25 ml round bottom flask equipped with a teflon stirring bar. The flask was sealed and the mixture was degassed under inert nitrogen at room temperature for 60 minutes. Subsequently, the reaction vessel was submerged into a preheated, vigorously stirred oil bath maintained at 70 °C. After 38 hours, the reaction was quenched by immediately placing the flask into liquid nitrogen and opening it to air. CH_2Cl_2 (5 ml) was added to the mixture, and subsequently the polymer was precipitated in 400 ml of ice-cold methanol. The precipitates were isolated by decanting off the supernatant fluid. The procedure was repeated one more time and precipitates were dried under vacuum at 40 °C (2.95 g, 87.3% isolated yield). M_n (PGATA) = 10 kg.mol^{-1} (86% conversion), $Đ$ =1.14.

Synthesis of poly(exo-acetyl acrylate isosorbide)-poly(n-butyl acrylate)-poly(exo-acetyl acrylate isosorbide)(PAAI-PnBA-PAAI). P3 is described as an illustrative example. CTA-PnBA-CTA (P1, 3.01 g, 0.033 mmol), AAI (390 mg, 1.61 mmol), AIBN (2.00 mg, 0.012 mmol), 8 ml of *n*-butyl acetate, and 3 ml of dimethylformamide were mixed in a 25 ml round bottom flask equipped with a teflon stirring bar. The flask was degassed with nitrogen for 60 minutes and placed in a preheated oil bath at 70 °C and vigorously stirred for 27 h. Then, the reaction was immediately immersed in liquid nitrogen and exposed to air. The polymer was isolated by precipitating into 400 ml ice-cold methanol and pouring off the supernatant. The polymer was re-dissolved and re-precipitated one more time and dried under vacuum at 40 °C (3.00 g, 88.2% isolated yield). M_n (PAAI) = 12 kg.mol^{-1} (full conversion), $Đ$ =1.19.

CTA Removal. The trithiocarbonate end groups of triblock copolymers were removed by aminolysis and Michael addition. P6 is described as an illustrative example. PAAI-PnBA-PAAI (2.20 g, 0.014 mmol), n-propylamine (86.3 mg, 1.46 mmol), and tris(2-carboxyethyl)phosphine hydrochloride (10 mg, 0.035 mmol) were dissolved in THF (20 mL) in a 25 ml round bottom flask. The reaction mixture was stirred for 1.5 h at room temperature under a nitrogen atmosphere and methyl acrylate (382 mg, 4.45 mmol) was added to the reaction mixture and stirred at room temperature for 100 h. The solvent was removed using a rotary vacuum evaporator and the remaining sold was dissolved in 10 ml CH_2Cl_2 and precipitated in 400 ml ice-cold methanol. The precipitates were dried under vacuum at 40 °C.

Selective Deacetylation. The 1-*O*-acetyl group of GATA units were removed by treatment of the PGATA-PnBA-PGATA triblock copolymer (P5) with hydrazinium acetate at room temperature. In a 25 ml flask, P5 (658 mg, 0.0045 mmol) was dissolved in 3.5 ml dimethylformamide and 3.5 ml *n*-butyl acetate. In a separate vial, hydrazine acetate (29 mg, 0.31 mmol) was dissolved in 4 ml dimethylformamide at 40 °C. Then, the hydrazine acetate solution was added to the reaction flask and the mixture was stirred at room temperature. After 5.5 h, the mixture was transferred into a separatory funnel, diluted with 20 ml ethyl acetate and 20 ml dichloromethane, and washed with two portions brine solution (2 x 50 ml). The organic layers were dried over magnesium sulfate and concentrated by rotary evaporation. The remaining solid was dried under vacuum oven at 40 °C to afford partially deprotected PGATA-PnBA-PGATA triblock copolymer (P7).

3.4.4 Adhesion Properties Testing

The pressure sensitive adhesive evaluations were conducted by the Adherent Laboratories (Saint Paul, MN). Rosin esters were used as the tackifier (Sylvalite^{TM} RE-80HP) and the tackifier concentration was 40 weight percent of the total solid content. The blends of the polymer and tackifier were dissolved in toluene to produce 50% solids content solution and then the solution was casted onto a 2 mm polyester film using a baker draw down bar. The bar was set to target a coat weight of 25 gsm. The film was allowed to air-dry overnight before the performance evaluation was conducted. The resultant coated film was cut into one-inch wide strips for adhesion testing. The standard test methods employed for peel adhesion, loop tack, shear strength, and shear adhesion failure temperature (SAFT) testing were PSTC: 101, ASTM: D6195, PSTC: 107, and ASTM-D4498, respectively. The reported average adhesion values and standard deviations were acquired from 3-5 replicates. The static shear strength and SAFT tests (PSTC: 107 and ASTM-D4498, respectively) were conducted using a 500 g weight. Cohesive failure was observed for peel adhesion testing from a steel plate.

3.4.5 Mechanical Properties Testing

The polymers were dissolved in minimum amount of ethyl acetate and casted on a Teflon sheet and were left to dry under a fume hood overnight. Tensile testing on the dog-bone-shape films was performed using a Shimadzu AGS-X tensile tester at room temperature on tensile bars that had gauge dimensions of approximately 10 mm×3 mm×0.5 mm. All samples were elongated at a speed of 5 mm per minute. 3-5 replicate tensile bars

of each polymer sample were conducted. Rotational rheometry was performed on a TA Instruments ARES rheometer under N_2. Approximately 50 mg of the polymer film was placed between 8 mm parallel plates and heated to 160 °C. Dynamic temperature sweeps were performed at 5% strain and at heating rate of 10 °C min^{-1}.

3.5 Supplementary Figures and Tables

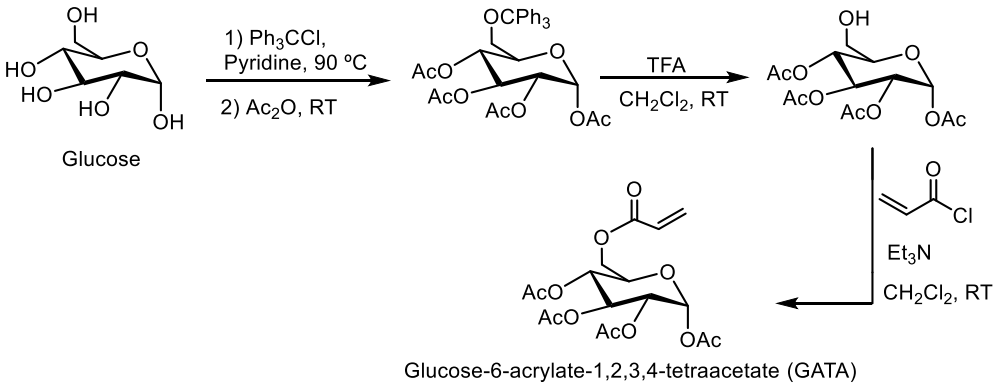

Scheme 3.S1. Synthesis of the GATA monomer.[36]

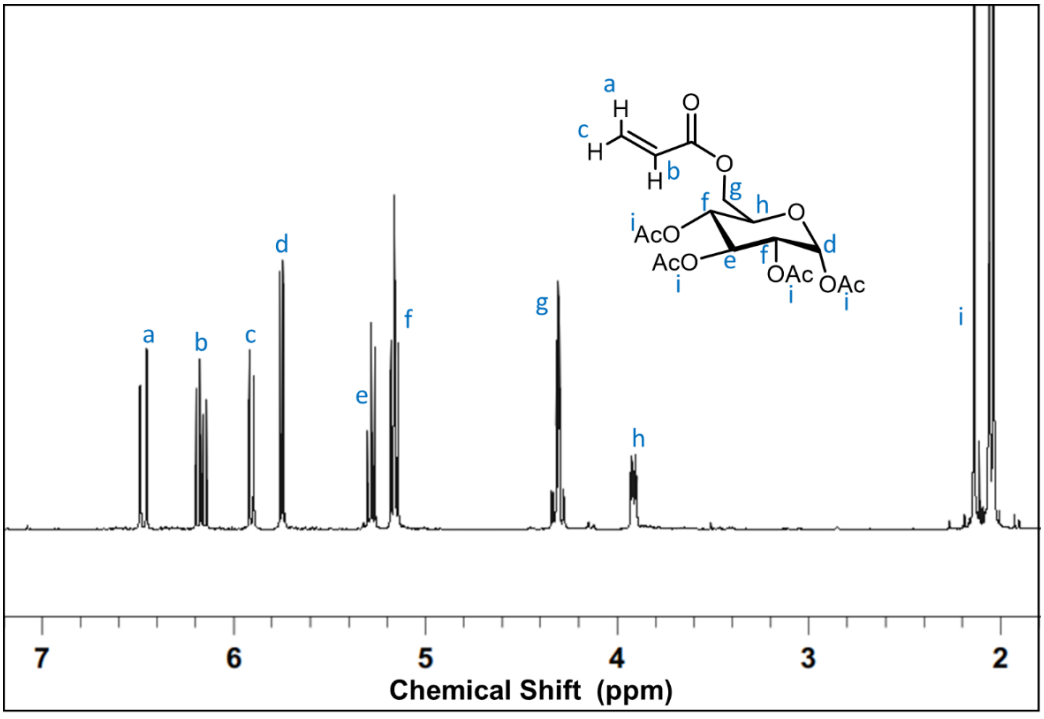

Figure 3.S1. ^{1}H NMR spectrum of GATA. 500 MHz, $CDCl_3$.

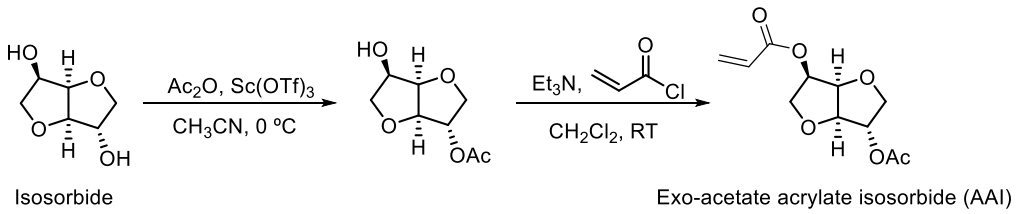

Scheme 3.S2. Schematic synthesis of the AAI monomer.[37]

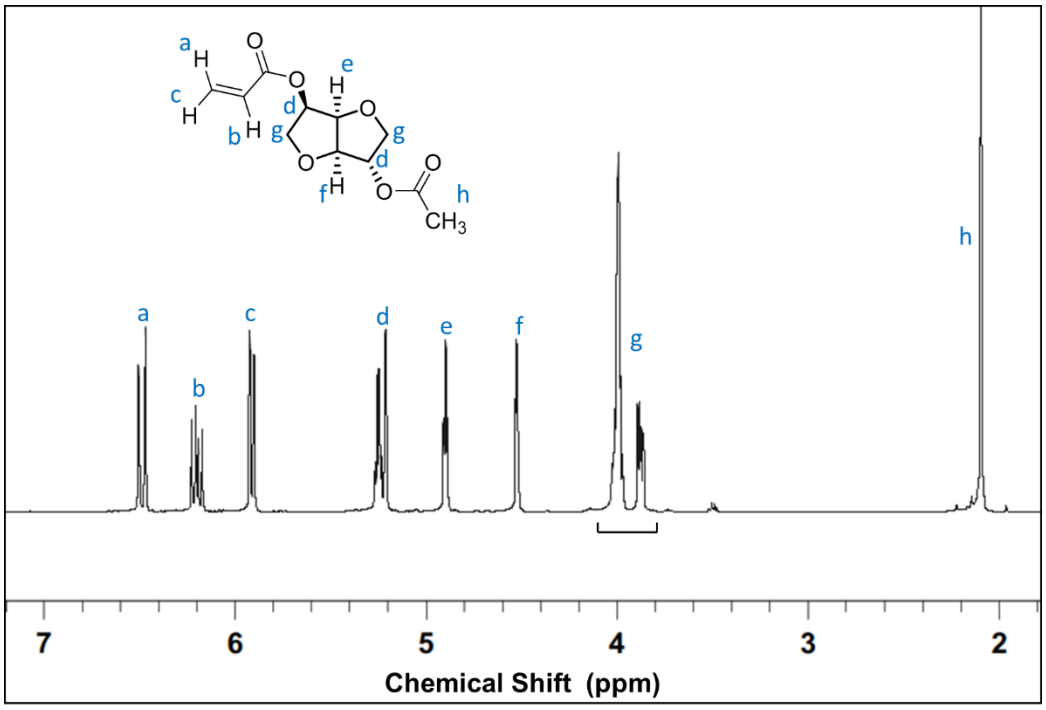

Figure 3.S2. ^{1}H NMR spectrum of AAI. 500 MHz, $CDCl_3$. Non-assigned peak at 3.55 ppm corresponds to residual ethyl acetate.

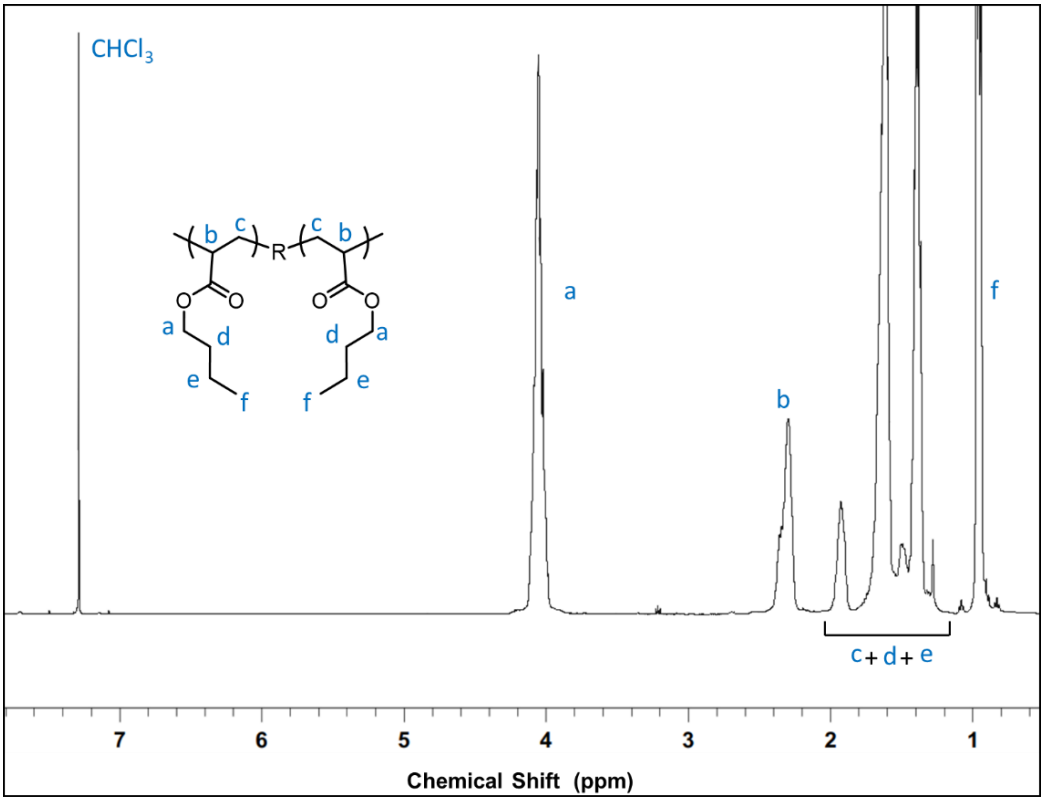

Figure 3.S3. Representative ^{1}H NMR spectra of a PnBA macro-CTA. 500 MHz, $CDCl_3$. A generic polymer structure is illustrated and the end groups are not shown.

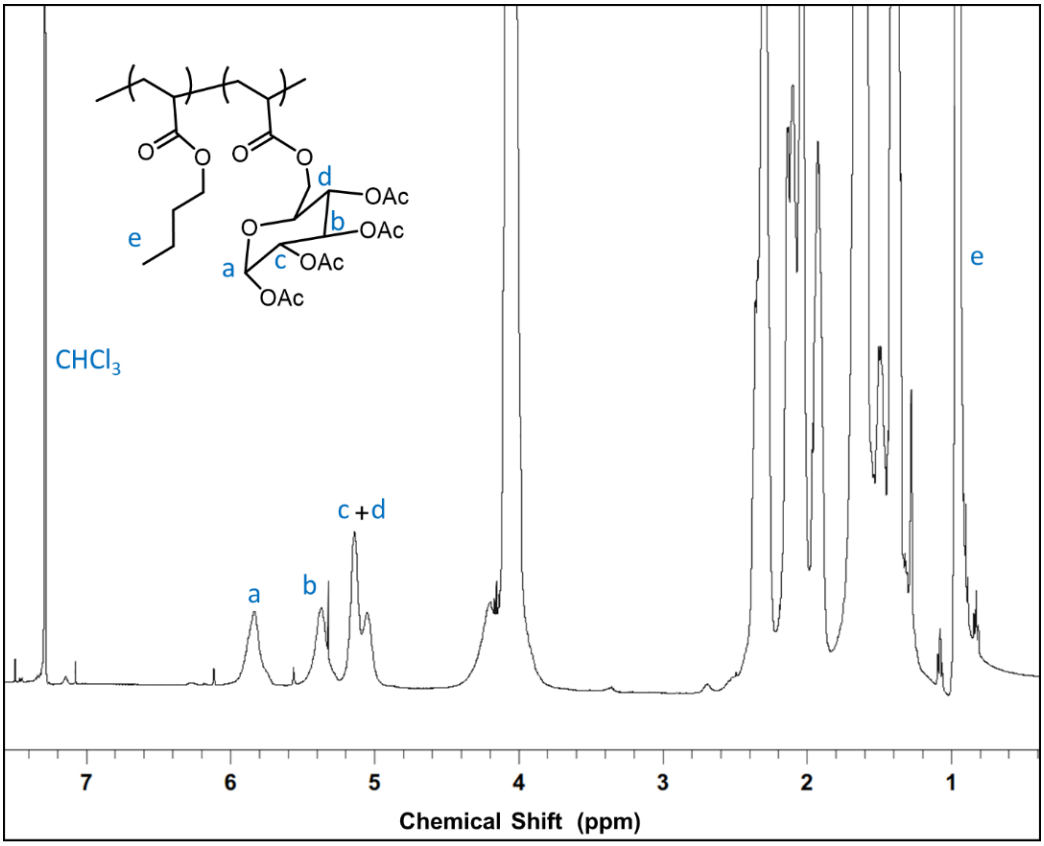

Figure 3.S4. Representative ^{1}H NMR spectra of a PGATA-PnBA-PGATA triblock copolymer. 500 MHz, $CDCl_3$. Due to its symmetrical structure, only one side of the polymer structure is illustrated.

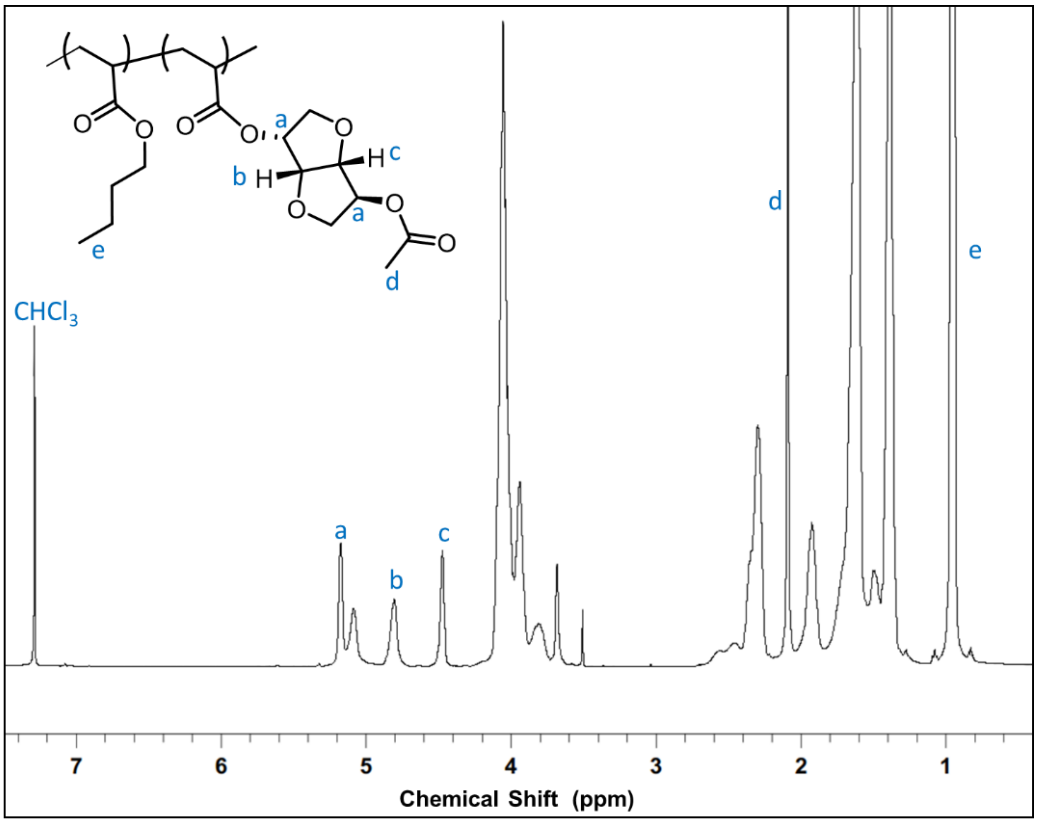

Figure 3.S5. Representative ^{1}H NMR spectra of a PAAI-PnBA-PAAI triblock copolymer. 500 MHz, $CDCl_3$. Due to its symmetrical structure, only one side of the polymer structure is illustrated.

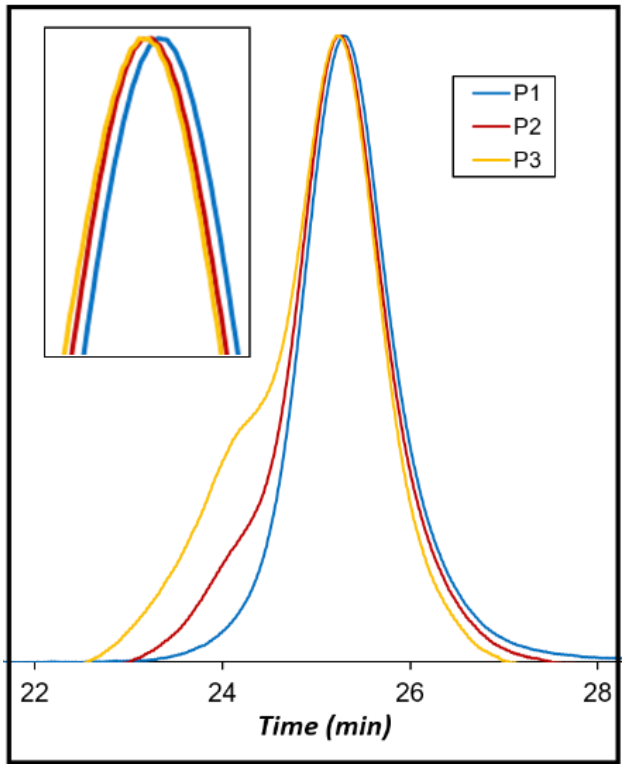

Figure 3.S6. SEC traces of the P2 [PGATA-PnBA-PGATA: 5-90-5 kDa] and P3 [PAAI-PnBA-PAAI: 6-90-6 kDa] triblock copolymers and their respective PnBA maco-CTA [P1] (eluent: THF, at room temperature).

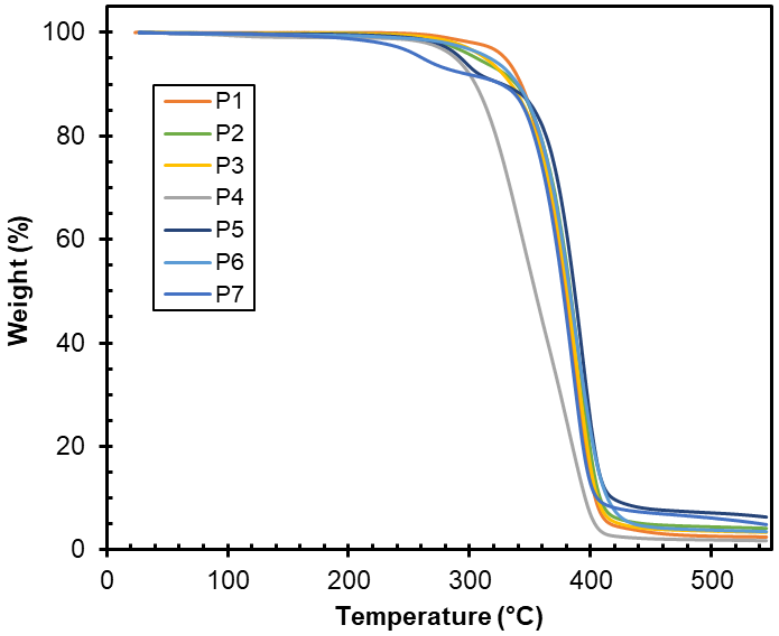

Figure 3.S7. TGA profiles of the polymers used in this study.

Table 3.S2. Adhesion values for commercial products adapted from Lee, et al.[13]

Polymer	Duct tape (25 mm-wide)	Scotch® tape (18 mm-wide)	Electrical tape (18 mm-wide)	Post-it® Note (10 mm-wide)
Peel Adhesion (N/cm)	5.53 ± 0.19	1.90 ± 0.05	1.37 ± 0.12	< 0.045
Loop Tack (N/cm^2)	2.41 ± 0.20	0.91 ± 0.05	2.58 ± 0.14	0.14 ± 0.02
Shear (min)	1172 ± 477	>6000	503 ± 29	< 0.5

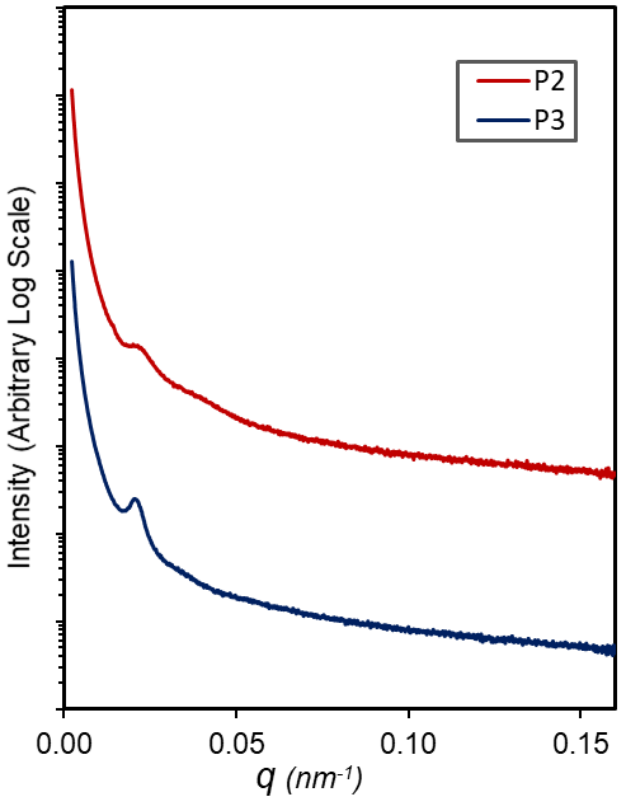

Figure 3.S8. Experimental 1D SAXS profile of P2 (PGATA-PnBA-PGATA: 5-90-5 kDa) and P3 (PAAI-PnBA-PAAI: 6-90-6 kDa) at 25 °C.

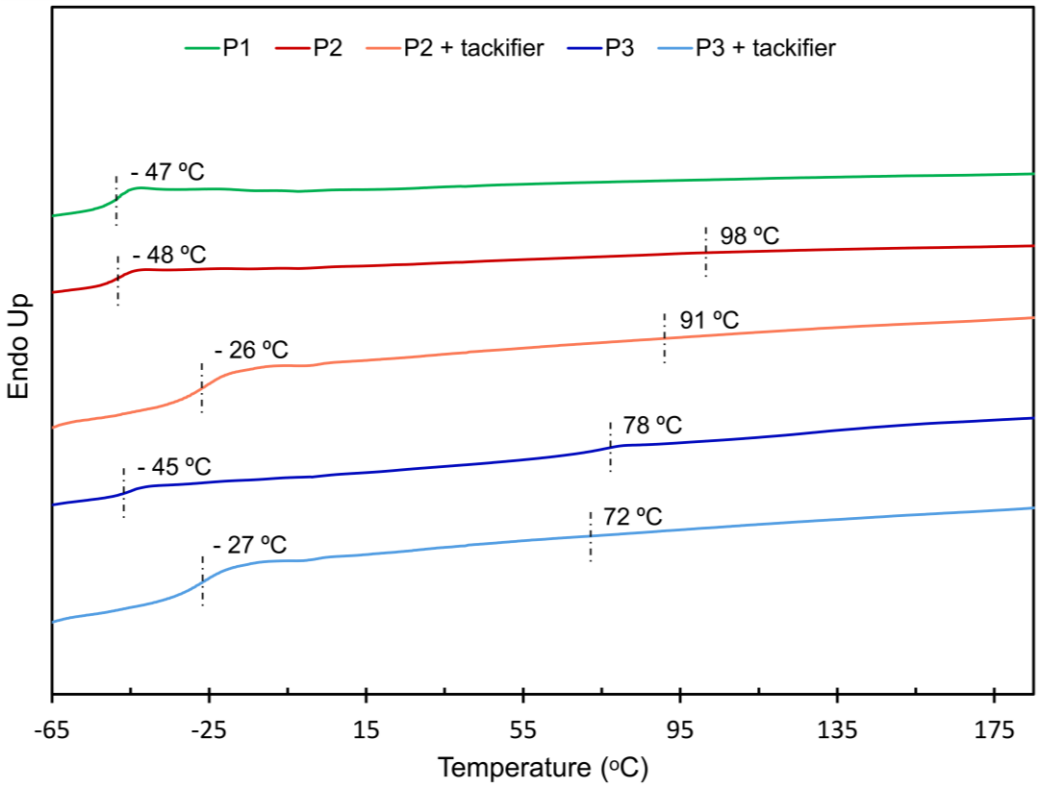

Figure 3.S9. DSC traces of the P2 (PGATA-PnBA-PGATA: 5-90-5 kDa) and P3 (PAAI-PnBA-PAAI: 6-90-6 kDa) triblock copolymers, their respective macro-CTA (P1), and their blend with 40 wt% of a rosin ester resin tackifier.

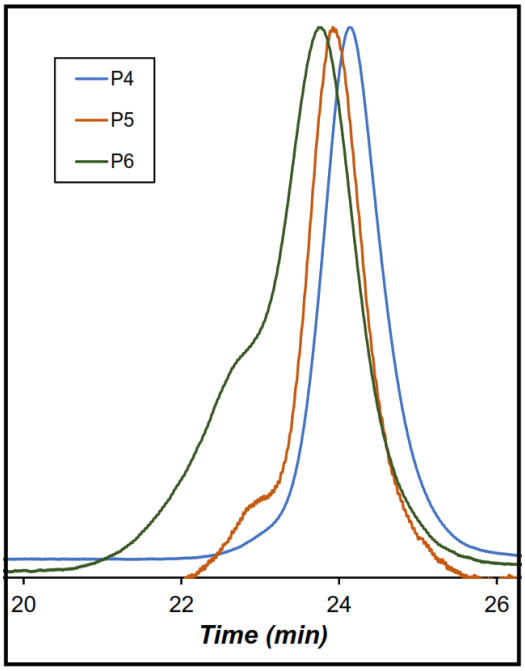

Figure 3.S10. SEC traces of the P5 [PGATA-PnBA-PGATA: 18-110-18 kDa] and P6 [PAAI-PnBA-PAAI: 21-110-21 kDa] triblock copolymers and their respective PnBA maco-CTA [P4] (eluent: THF, at room temperature).

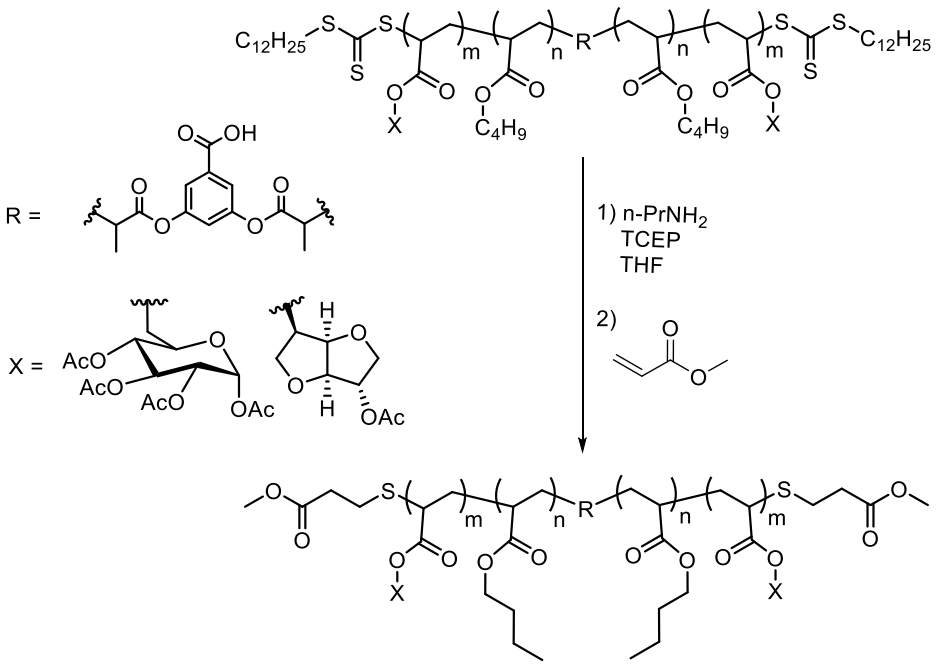

Scheme 3.S3. Schematic illustration of removal of the CTA end groups.[54]

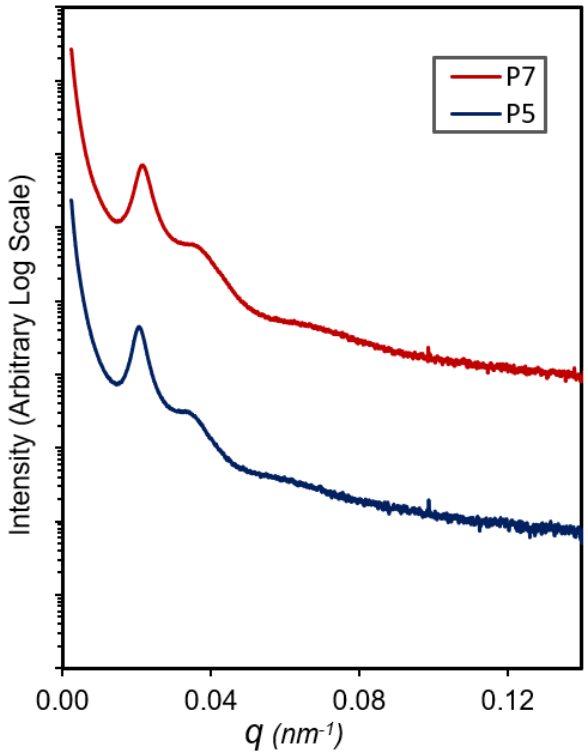

Figure 3.S11. Experimental 1D SAXS profile of before (P5) and after (P7) partial removal of the anomeric acetyl protecting groups in GATA blocks.

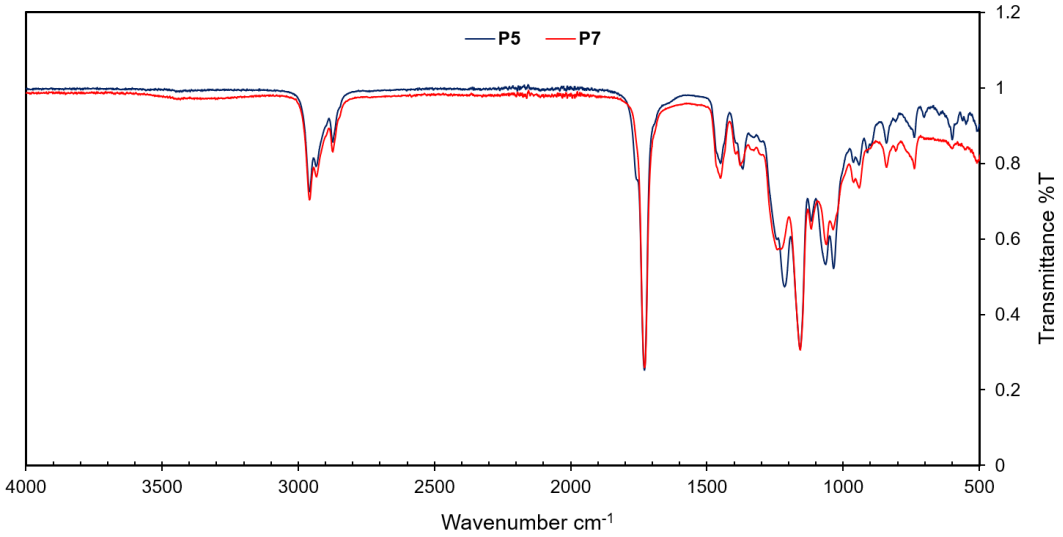

Figure 3.S12. FT–IR spectra before (P5) and after (P7) partial removal of the anomeric acetyl protecting groups in GATA blocks.

3.6 References

1. Nakajima, N.; Babrowicz, R.; Harrell, E. R., Rheology, composition, and peel-mechanism of block copolymer–tackifier-based pressure sensitive adhesives. *Journal of Applied Polymer Science* **1992,** *44*, 1437-1456.

2. Gibert, F. X.; Marin, G.; Derail, C.; Allal, A.; Lechat, J., Rheological properties of hot melt pressure-sensitive adhesives based on styrene--isoprene copolymers. Part 1: A rheological model for [sis-si] formulations. *The Journal of Adhesion* **2003,** *79*, 825-852.

3. Derail, C.; Cazenave, M. N.; Gibert, F. X.; Marin, G.; Kappes, N.; Lechat, J., Rheological Properties of Hot-melt Pressure-sensitive Adhesive (HMPSAS) Based on Styrene–Isoprene Copolymers. Part 2: Innovative Molecular Design from Predictive Formulation. *The Journal of Adhesion* **2004,** *80*, 1131-1151.

4. Daoulas, K. C.; Theodorou, D. N.; Roos, A.; Creton, C., Experimental and Self-Consistent-Field Theoretical Study of Styrene Block Copolymer Self-Adhesive Materials. *Macromolecules* **2004,** *37*, 5093-5109.

5. Jeusette, M.; Leclère, P.; Lazzaroni, R.; Simal, F.; Vaneecke, J.; Lardot, T.; Roose, P., New "All-Acrylate" Block Copolymers: Synthesis and Influence of the Architecture on the Morphology and the Mechanical Properties. *Macromolecules* **2007,** *40*, 1055-1065.

6. Creton, C.; Hu, G.; Deplace, F.; Morgret, L.; Shull, K. R., Large-Strain Mechanical Behavior of Model Block Copolymer Adhesives. *Macromolecules* **2009,** *42*, 7605-7615.

7. Holden, G.; Quirk, R. P.; Kricheldorf, H. R., *Thermoplastic Elastomers*. 3rd ed.; Hanser Gardner Publications: Cincinnati, 2004.

8. Shin, J.; Kim, Y.-W.; Kim, G.-J., Sustainable Block Copolymer-based Thermoplastic Elastomers. *Applied Chemistry for Engineering* **2014,** *25*, 121-133.

9. Tang, B.; Schneiderman, D. K.; Zare Bidoky, F.; Frisbie, C. D.; Lodge, T. P., Printable, Degradable, and Biocompatible Ion Gels from a Renewable ABA Triblock Polyester and a Low Toxicity Ionic Liquid. *ACS Macro Letters* **2017,** *6*, 1083-1088.

10. Watts, A.; Kurokawa, N.; Hillmyer, M. A., Strong, Resilient, and Sustainable Aliphatic Polyester Thermoplastic Elastomers. *Biomacromolecules* **2017,** *18*, 1845-1854.

11. Haitao, Q.; Jianzhong, B.; Shenguo, W., Synthesis, characterization and degradation of ABA block copolymer of l-lactide and ε-caprolactone. *Polymer Degradation and Stability* **2000,** *68*, 423-429.

12. Lee, S.; Lee, K.; Jang, J.; Choung, J. S.; Choi, W. J.; Kim, G.-J.; Kim, Y.-W.; Shin, J., Sustainable poly(ε-decalactone)−poly(l-lactide) multiarm star copolymer architectures for thermoplastic elastomers with fixed molar mass and block ratio. *Polymer* **2017,** *112*, 306-317.

13. Lee, S.; Lee, K.; Kim, Y.-W.; Shin, J., Preparation and Characterization of a Renewable Pressure-Sensitive Adhesive System Derived from ε-Decalactone,l-Lactide, Epoxidized Soybean Oil, and Rosin Ester. *ACS Sustainable Chemistry & Engineering* **2015,** *3*, 2309-2320.

14. Schneiderman, D. K.; Hill, E. M.; Martello, M. T.; Hillmyer, M. A., Poly(lactide)-block-poly(ε-caprolactone-co-ε-decalactone)-block-poly(lactide) copolymer elastomers. *Polym. Chem.* **2015,** *6*, 3641-3651.

15. Schneiderman, D. K.; Hillmyer, M. A., Aliphatic Polyester Block Polymer Design. *Macromolecules* **2016,** *49*, 2419-2428.

16. Schneiderman, D. K.; Gilmer, C.; Wentzel, M. T.; Martello, M. T.; Kubo, T.; Wissinger, J. E., Sustainable Polymers in the Organic Chemistry Laboratory: Synthesis and Characterization of a Renewable Polymer from δ-Decalactone and l-Lactide. *Journal of Chemical Education* **2014,** *91*, 131-135.

17. Arrington, K. J.; Waugh, J. B.; Radzinski, S. C.; Matson, J. B., Photo- and Biodegradable Thermoplastic Elastomers: Combining Ketone-Containing Polybutadiene with Polylactide Using Ring-Opening Polymerization and Ring-Opening Metathesis Polymerization. *Macromolecules* **2017,** *50*, 4180-4187.

18. Wanamaker, C. L.; O'Leary, L. E.; Lynd, N. A.; Hillmyer, M. A.; Tolman, W. B., Renewable-Resource Thermoplastic Elastomers Based on Polylactide and Polymenthide. *Biomacromolecules* **2007,** *8*, 3634-3640.

19. Shin, J.; Martello, M. T.; Shrestha, M.; Wissinger, J. E.; Tolman, W. B.; Hillmyer, M. A., Pressure-Sensitive Adhesives from Renewable Triblock Copolymers. *Macromolecules* **2011,** *44*, 87-94.

20. Hillmyer, M. A.; Tolman, W. B., Aliphatic Polyester Block Polymers: Renewable, Degradable, and Sustainable. *Accounts of Chemical Research* **2014,** *47*, 2390-2396.

21. Cohn, D.; Hotovely-Salomon, A., Biodegradable multiblock PEO/PLA thermoplastic elastomers: molecular design and properties. *Polymer* **2005,** *46*, 2068-2075.

22. Lee, S.; Yuk, J. S.; Park, H.; Kim, Y.-W.; Shin, J., Multiblock Thermoplastic Elastomers Derived from Biodiesel, Poly(propylene glycol), and l-Lactide. *ACS Sustainable Chemistry & Engineering* **2017,** *5*, 8148-8160.

23. Frick, E. M.; Zalusky, A. S.; Hillmyer, M. A., Characterization of Polylactide-b-polyisoprene-b-polylactide Thermoplastic Elastomers. *Biomacromolecules* **2002,** *4*, 216-223.

24. Lebarbé, T.; Ibarboure, E.; Gadenne, B.; Alfos, C.; Cramail, H., Fully bio-based poly(l-lactide)-b-poly(ricinoleic acid)-b-poly(l-lactide) triblock copolyesters: investigation of solid-state morphology and thermo-mechanical properties. *Polymer Chemistry* **2013,** *4*, 3357.

25. Li, H.; Sun, J.-T.; Wang, C.; Liu, S.; Yuan, D.; Zhou, X.; Tan, J.; Stubbs, L.; He, C., High Modulus, Strength, and Toughness Polyurethane Elastomer Based on Unmodified Lignin. *ACS Sustainable Chemistry & Engineering* **2017,** *5*, 7942-7949.

26. Wang, Z.; Yuan, L.; Tang, C., Sustainable Elastomers from Renewable Biomass. *Acc Chem Res* **2017,** *50*, 1762-1773.

27. Zhu, Y.; Romain, C.; Williams, C. K., Sustainable polymers from renewable resources. *Nature* **2016,** *540*, 354-362.

28. Delidovich, I.; Hausoul, P. J. C.; Deng, L.; Pfützenreuter, R.; Rose, M.; Palkovits, R., Alternative Monomers Based on Lignocellulose and Their Use for Polymer Production. *Chemical Reviews* **2016,** *116*, 1540-1599.

29. Ganewatta, M. S.; Ding, W.; Rahman, M. A.; Yuan, L.; Wang, Z.; Hamidi, N.; Robertson, M. L.; Tang, C., Biobased Plastics and Elastomers from Renewable Rosin via "Living" Ring-Opening Metathesis Polymerization. *Macromolecules* **2016,** *49*, 7155-7164.

30. Bolton, J. M.; Hillmyer, M. A.; Hoye, T. R., Sustainable Thermoplastic Elastomers from Terpene-Derived Monomers. *ACS Macro Letters* **2014,** *3*, 717-720.

31. Shin, J.; Lee, Y.; Tolman, W. B.; Hillmyer, M. A., Thermoplastic Elastomers Derived from Menthide and Tulipalin A. *Biomacromolecules* **2012,** *13*, 3833-3840.

32. Ding, K.; John, A.; Shin, J.; Lee, Y.; Quinn, T.; Tolman, W. B.; Hillmyer, M. A., High-Performance Pressure-Sensitive Adhesives from Renewable Triblock Copolymers. *Biomacromolecules* **2015,** *16*, 2537-2539.

33. Mosnáček, J.; Yoon, J. A.; Juhari, A.; Koynov, K.; Matyjaszewski, K., Synthesis, morphology and mechanical properties of linear triblock copolymers based on poly(α-methylene-γ-butyrolactone). *Polymer* **2009,** *50*, 2087-2094.

34. Wilbon, P. A.; Chu, F.; Tang, C., Progress in Renewable Polymers from Natural Terpenes, Terpenoids, and Rosin. *Macromolecular Rapid Communications* **2013,** *34*, 8-37.

35. Ding, W.; Wang, S.; Yao, K.; Ganewatta, M. S.; Tang, C.; Robertson, M. L., Physical Behavior of Triblock Copolymer Thermoplastic Elastomers Containing Sustainable Rosin-Derived Polymethacrylate End Blocks. *ACS Sustainable Chemistry & Engineering* **2017,** *5*, 11470-11480.

36. Nasiri, M.; Reineke, T. M., Sustainable glucose-based block copolymers exhibit elastomeric and adhesive behavior. *Polym. Chem.* **2016,** *7*, 5233-5240.

37. Gallagher, J. J.; Hillmyer, M. A.; Reineke, T. M., Acrylic Triblock Copolymers Incorporating Isosorbide for Pressure Sensitive Adhesives. *ACS Sustainable Chemistry & Engineering* **2016,** *4*, 3379-3387.

38. Tian, Z.; Fattahi, A.; Lis, L.; Kass, S. R., Single-Centered Hydrogen-Bonded Enhanced Acidity (SHEA) Acids: A New Class of Brønsted Acids. *Journal of the American Chemical Society* **2009,** *131*, 16984-16988.

39. Nasiri, M.; Shakourian-Fard, M.; Fattahi, A., Influence of the hydrogen bonding on the basicity of selected macrocyclic amines. *Journal of Physical Organic Chemistry* **2012,** *25*, 803-810.

40. Parmar, D.; Sugiono, E.; Raja, S.; Rueping, M., Addition and Correction to Complete Field Guide to Asymmetric BINOL-Phosphate Derived Brønsted Acid and Metal Catalysis: History and Classification by Mode of Activation; Brønsted Acidity, Hydrogen Bonding, Ion Pairing, and Metal Phosphates. *Chemical Reviews* **2017,** *117*, 10608-10620.

41. Schreiner, P. R., Metal-free organocatalysis through explicit hydrogen bonding interactions. *Chemical Society Reviews* **2003,** *32*, 289-296.

42. Ting, J. M.; Tale, S.; Purchel, A. A.; Jones, S. D.; Widanapathirana, L.; Tolstyka, Z. P.; Guo, L.; Guillaudeu, S. J.; Bates, F. S.; Reineke, T. M., High-Throughput Excipient Discovery Enables Oral Delivery of Poorly Soluble Pharmaceuticals. *ACS Central Science* **2016,** *2*, 748-755.

43. Tale, S.; Purchel, A. A.; Dalsin, M. C.; Reineke, T. M., Diblock Terpolymers Are Tunable and pH Responsive Vehicles To Increase Hydrophobic Drug Solubility for Oral Administration. *Molecular Pharmaceutics* **2017,** *14*, 4121-4127.

44. Lillie, L. M.; Tolman, W. B.; Reineke, T. M., Structure/property relationships in copolymers comprising renewable isosorbide, glucarodilactone, and 2,5-bis(hydroxymethyl)furan subunits. *Polym. Chem.* **2017,** *8*, 3746-3754.

45. Beniah, G.; Fortman, D. J.; Heath, W. H.; Dichtel, W. R.; Torkelson, J. M., Non-Isocyanate Polyurethane Thermoplastic Elastomer: Amide-Based Chain Extender Yields Enhanced Nanophase Separation and Properties in Polyhydroxyurethane. *Macromolecules* **2017,** *50*, 4425-4434.

46. Hayashi, M.; Matsushima, S.; Noro, A.; Matsushita, Y., Mechanical Property Enhancement of ABA Block Copolymer-Based Elastomers by Incorporating Transient Cross-Links into Soft Middle Block. *Macromolecules* **2015,** *48*, 421-431.

47. Feldman, K. E.; Kade, M. J.; Meijer, E. W.; Hawker, C. J.; Kramer, E. J. Model Transient Networks from Strongly Hydrogen-Bonded Polymers. *Macromolecules* **2009,** *42*, 9072-9081.

48. Montarnal, D.; Delbosc, N.; Chamignon, C.; Virolleaud, M. A.; Luo, Y.; Hawker, C. J.; Drockenmuller, E.; Bernard, J. Highly Ordered Nanoporous Films from Supramolecular Diblock Copolymers with Hydrogen-Bonding Junctions. *Angew. Chem., Int. Ed.* **2015**, 54, 11117−11121.

49. Tong, J.-D.; Jerôme, R., Dependence of the Ultimate Tensile Strength of Thermoplastic Elastomers of the Triblock Type on the Molecular Weight between Chain Entanglements of the Central Block. *Macromolecules* **2000,** *33*, 1479-1481.

50. Tehrani, M.; Sarvestani, A., Effect of chain length distribution on mechanical behavior of polymeric networks. *European Polymer Journal* **2017,** *87*, 136-146.

51. Nasiri, M.; Bertrand, A.; Reineke, T. M.; Hillmyer, M. A., Polymeric nanocylinders by combining block copolymer self-assembly and nanoskiving. *ACS Appl Mater Interfaces* **2014,** *6*, 16283-8.

52. Mark, J. E., *Physical Properties of Polymers Handbook*. 2 ed.; Springer-Verlag New York: New York, NY, 2007.

53. Kaelble, D. H., Theory and Analysis of Peel Adhesion: Adhesive Thickness Effects. *The Journal of Adhesion* **1992,** *37*, 205-214.

54. Zhou, C.; Hillmyer, M. A.; Lodge, T. P., Micellization and Micellar Aggregation of Poly(ethylene-alt-propylene)-b-poly(ethylene oxide)-b-poly(N-isopropylacrylamide) Triblock Terpolymers in Water. *Macromolecules* **2011,** *44*, 1635-1641.

55. De Kimpe, N.; Van, T.; Claessens, S.; Habonimana, P.; Tehrani, K.; Van Puyvelde, L., Synthesis of Harounoside, A Naturally Occurring Pentalongin Hydroquinone Bisglucoside. *Synlett* **2006,** *2006*, 2469-2471.

Chapter 4

Polymeric Nanocylinders by Combining Block Copolymer Self-assembly and Nanoskiving*

* Reproduced in part with permission from Nasiri, M.; Bertrand, A.; Reineke, T. M.; Hillmyer, M. A. *ACS Appl Mater Interfaces* **2014,** *6*, 16283-8. DOI: 10.1021/am504486r

4.1 Introduction

Polymeric nanoparticles are utilized in different research disciplines, including delivery vehicles in the field of nanomedicine.[1] To fine-tune nanosystems for various applications, new methods are needed to fabricate particles with tunable sizes, specific shapes and homogenous surfaces. Nanoparticle fabrication methods are generally divided into "top–down" and "bottom–up" approaches. In top down methods, the desired dimensions are typically achieved by reducing the size of an object with larger dimensions in a mechanically controlled manner. Conversely, a bottom-up approach typically corresponds to self-assembly of molecular constituents into supramolecualr nanoscale assemblies.[2]

In general, bottom-up nanoparticle fabrication methods, based on precipitation methods, yield spherical nanoparticles of various sizes with narrow size distributions.[3] Also there are examples in the literature where cylindrical micelles are generated using dissolution techniques.[4-6] However, size control can be difficult to achieve and maintain due to molecular rearrangement and potential morphological transitions, although molecular exchange can be a very slow process as revealed by small-angle scattering experiments.[7,8] On the other hand, lithographic and imprinting methods are able to produce nanoparticles with controlled sizes and various shapes via top-down approaches. For example, in the photolithographic process, particles can be formed by irradiating a film of photo-resist with UV light through a mask of the desired shape. The nanoparticles can then be harvested by washing off the unexposed material along with the sacrificial layer underneath.[9] Although this technique has an excellent control over the size and shape of

the particles, a UV-curable material is required, thus dramatically restricting the range of particles achievable.[10] To resolve this issue, imprinting techniques have been developed where only the initial master template needs to be formed via lithography, such as soft lithography, and then particle replication in non-wetting templates (PRINT®) technology are used to form the nanoobjects of various sizes and shapes.[1]

With the ability to fabricate nearly monodisperse particles in the range of 10 nm–200 μm,[10] high precision and versatility on the shape of particles and scalability, PRINT technology is a leading method for nanoparticle fabrication. In the PRINT process, a patterned fluorocarbon-based mold is filled with the materials of interest followed by lamination with a high surface energy material. Peeling off the laminate material removes all the excess solution from the mold. After the curing and solidification steps an adhesive layer is used to harvest the cured particles. Dissolution of the adhesive layer results in a solution containing free particles.[11] PRINT employs several steps with particular requirements and access to the requisite fabrication equipment. While PRINT represents an elegant and successful strategy, a potential limitation for this and related top-down nanoparticle fabrication methods, is the generation of particles with imperfect surfaces.[3] On the other hand, generally, in a bottom-up approach, particles are formed in their thermodynamically stable state typically resulting in homogeneous surfaces with minimum defects.[12]

Because of their ability to self-organize into predictable nanostructures, block copolymers can adopt structures with controlled dimensions and high aspect ratios desirable for the fabrication of nanostructured materials.[13] In particular, several studies

demonstrated the possibility to macroscopically orientate the microstructure of self-assembled block copolymers.[14-16] With these properties of bulk block copolymers in mind, we were inspired by the work of Whitesides and coworkers, who developed a new technique for nanostructure fabrications called “nanoskiving”, combining deposition of metals on a substrate and thin sectioning with an ultramicrotome process.[18-20] They showed the applicability of this technique for simple structures such as nanowires, as well as more complex nanostructures.

Herein, a novel top-down particle fabrication approach combining bottom-up block copolymer self-assembly and nanoskiving is investigated. Monolithic specimens were generated from diblock copolymers with a composition tuned to self-assemble into a cylindrical morphology, followed by microstructural alignment using a channel die. Afterwards, the specimen was cut to thin slices with defined thicknesses using a microtome equipped with a diamond knife. Finally, dispersion of the cut slices into a selective solvent for the matrix block resulted in nanocylinders of the minor component with coronae of the major component (Figure 4.1). Unlike cylindrical micelles, our BCP-based strategy relies on bulk self-assembly and mechanical down-sizing, thus providing shape stability and some degree of length control of the nanocylinders.

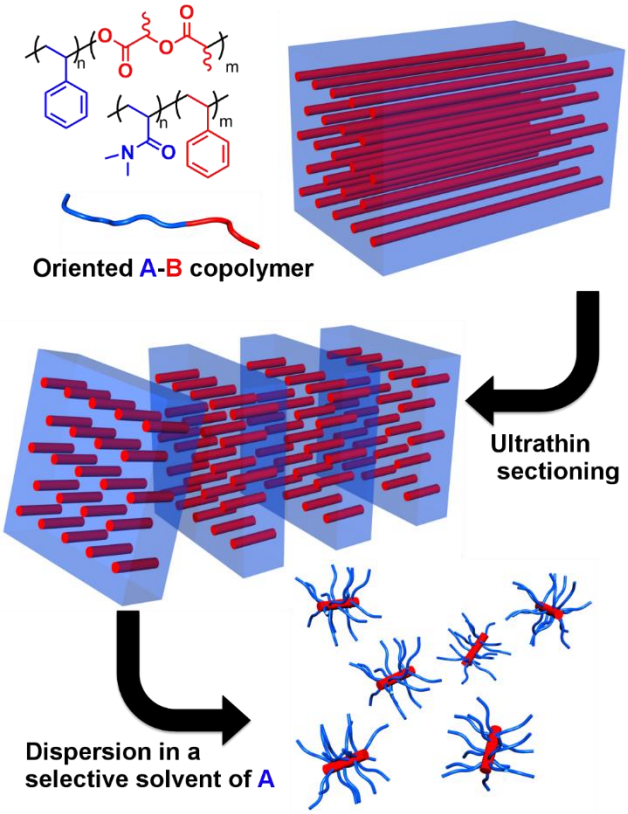

Figure 4.1. Schematic representation of nanoparticle generation combining block copolymer self-assembly and nanoskiving.

4.2 Results and Discussion

To explore the idea of nanoparticle fabrication via nanoskiving, bulk ordered block copolymer structures, a polystyrene-*b*-polylactide (PS-*b*-PLA) copolymer was synthesized according to a previously reported procedure by a combination of anionic and ring opening transesterification polymerization (ROTEP) techniques.[14] The molar masses for the PS and PLA blocks were determined to be 42 kg/mol and 18 kg/mol, respectively, by ^{1}H NMR spectroscopy (see Figure 4.S1 for polymer characterization details). Based on the calculated PLA volume fraction (0.26), a microstructure composed of PLA cylinders in a

PS matrix is expected.[14] The copolymer was processed in a home-built channel die at 130 °C to produce microstructurally-aligned PS-PLA monoliths (Figure 4.3a).[15] Microstructure characterization was performed via small-angle X-ray scattering (SAXS) analysis of the oriented PS-PLA monolith at 25 °C and revealed an intense primary peak at $q^* = 0.165$ nm^{-1} ($D^* = 38.1$ nm), along with a prominent peak at $\sqrt{7}q^*$, consistent with a cylindrical morphology (Figure 4.2). Both 2D patterns obtained perpendicular to the flow direction were anisotropic, and two sets of spots at scattering vectors were separated azimuthally by 180°, as expected for an oriented cylindrical morphology (Figure 4.S2). The 2D pattern obtained parallel to the direction of the flow exhibited an isotropic ring-like pattern, indicating a lack of long-range hexagonal packing of the oriented cylinders. Transmission electron microscopy (TEM) images, obtained both parallel and perpendicular to the flow direction of the oriented monolith, demonstrated alignment of the cylindrical domains along the shear direction (Figure 4.2). The diameter of the cylinders was estimated to 19 ± 6 nm from the TEM images, which was in agreement with the value extracted from the SAXS data (23.6 nm).

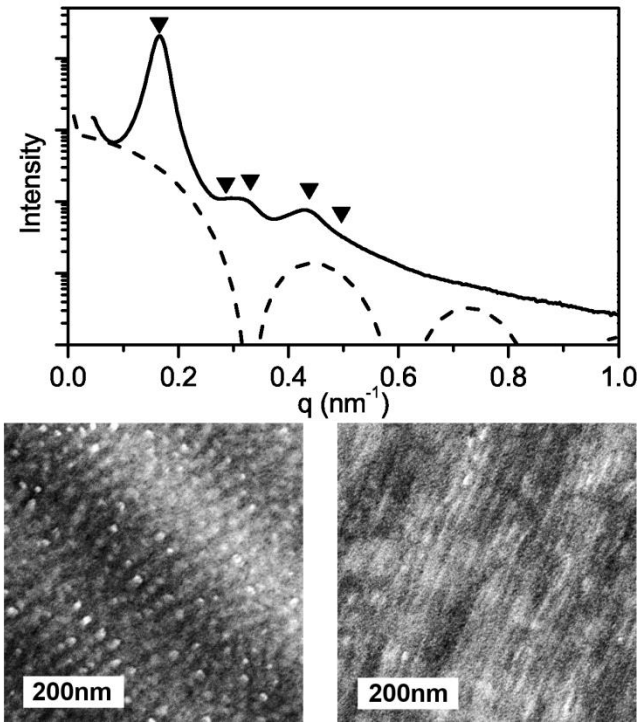

Figure 4.2. (Solid line) Experimental 1D synchrotron SAXS profile of shear-oriented PS-PLA monolith at 25°C and (dashed line) simulated form factor scattering curve generated for cylinders with a 11.8 nm radius (value extracted from the experimental SAXS profile). The black triangles indicate the expected reflections for a cylindrical morphology (√1; √3; √4; √7; √9). Corresponding TEM images of the material obtained (left) perpendicularly and (right) parallel to the shear direction (The PS matrix was stained by RuO_4 vapors).

4.2.1 Sectioning Procedure

Ultramicrotoming is routinely employed for preparing ultrathin sections of materials that can be subsequently observed by TEM. This instrument is based on precisely-controlled advancement of an arm holding the sample synchronized with an oscillatory movement applied to the arm. When the extremity of the arm goes down, the sample is forced on the edge of a knife, producing a thin slice of the material. The arm is then moved toward the knife according to the increment step defined by the user to produce the next slice. Using this instrument, we directly cut a 2 mm × 2 mm square cross-section

of our PS-PLA monolith. Diamond knives are usually designed with a cavity on the top called the boat that can be filled with water until the upper edge of the diamond blade is moistened. During the course of monolith microtoming, the sections are floated on the surface of water, which prevents the sections from sticking to the hydrophobic knife-edge. If this occurs the samples would crumple and quickly accumulate, a problem that would be particularly detrimental to our procedure, where high throughput with limited operator intervention is desirable (Figure 4.3c). When the desired number of sections was reached, the diamond knife is removed, and the water reservoir is emptied into a polypropylene tube, and the water was removed by freeze-drying.

The ability to cut ultrathin sections is largely affected by the mechanical properties of the material. If the material is too soft, it will tend to be deformed, resulting in thickness variations and missed cuts. This undesired behavior can be circumvented by decreasing the operating temperature with liquid nitrogen (cryo-microtomy). However, the water boat is important for our procedure, as it helps to maintain the edge of the knife clean, implying that the cutting process must be done at room temperature. With both PS and PLA blocks being glassy and stiff at room temperature ($T_{g(PS)}$= 100 °C[21], $T_{g(PLA)}$=55 °C[22]), PS-PLA block copolymers are good candidates for this purpose. We employed a 45° diamond knife with a clearance angle of 6° and a width of 3 mm. The cutting speed was typically set at 4 mm/s, producing about 25 sections/min. Each section was expected to contain about 2.4×10^9 individual cylinders, based on the monolith dimensions and the domain spacing extracted from the SAXS analysis of the PS-PLA copolymer. The theoretical particle production rate was estimated to 6×10^{10} particles/min (see Section 4.4.7 for details). A

binocular optical microscope allowed observation of the sections produced. Within each floating section, it appeared that some wrinkling occurred along with stripes of various thicknesses. The combined effects of the large sample width (~2 mm) and the knife likely produced such compression-induced defects.

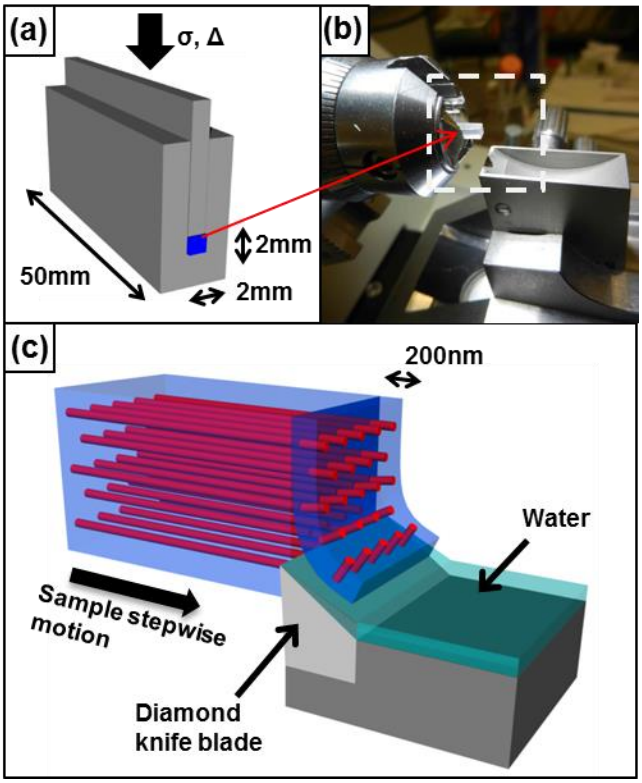

Figure 4.3. (a) Schematic view of the channel die employed for microstructural alignment (b) Close up photograph of the PS-PLA monolith mounted on the microtome arm that is about to be cut by the diamond knife (c) Schematic view of the sectioning procedure, the cut slices are floated on the water boat.

The dried sections were subsequently dispersed in cyclohexane, a selective solvent for the PS matrix. Particle sizes were estimated by dynamic light scattering (DLS). DLS experiments revealed a monomodal size distribution and a mean hydrodynamic diameter (D_h) of 75 ± 3 nm when the theoretical thickness of the cut slices was 200 nm. As DLS

measurements give only an average hydrodynamic size of the particles, TEM imaging was employed to visualize the cylinders in the dry state. TEM samples were prepared by drop-casting from the dilute cyclohexane solution onto copper grids with a Formvar® supportive layer. The grids were subsequently exposed to RuO_4 vapors, which selectively stains the PS shell (appears darker on the images, Figure 4.4).

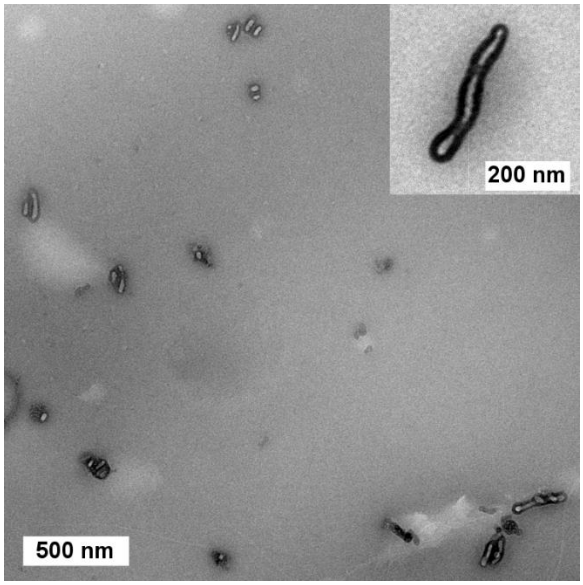

Figure 4.4. TEM image of PS-PLA nanoparticles casted from a cyclohexane solution (0.02 $g.L^{-1}$) for 200 nm-thick sections. The particles were stained with RuO_4. The TEM sample was prepared by absorbing the excess of solution with a piece of cleaning paper placed under the grid. Inset: A higher magnification view of an isolated cylindrical nanoparticle revealing its core-shell structure.

Isolated particles along with small aggregates were observed throughout the grid, and the core-shell structures of the nanoparticles were noticeable. Although the diameter of the PLA core (~18–20 nm) was consistent with the cylinder diameter measured for the monolith (19 ± 6 nm by TEM, 23.6 nm by SAXS), the length distribution was somewhat broad, ranging from ~30 nm to 400 nm. The thickness variations observed during the

cutting process could be the main reason for this result. In addition, the quality of the alignment can also affect the size distribution of the particles; first, if the cylinders are not completely parallel to the shear flow (perpendicular to the edge of knife), they will result in nanocylinders with longer lengths and consequently particles with greater average size. Second, smaller particles will be produced if the cylinders are not contiguous throughout the sample.

4.2.2 Aqueous System

As the PS-PLA copolymer showed promising results for nanocylinder fabrication via block copolymer self-assembly and nanoskiving, we also explored extension of our procedure for water-dispersable nanoparticles. To generate hydrophobic particle cores with water-soluble coronae a poly(N,N-dimethylacrylamide)-*b*-poly(styrene) (PDMA-PS) block copolymer was synthesized using reversible addition-fragmentation chain transfer (RAFT) controlled radical polymerization, with S-dodecyl-S′-(isobutyric acid) trithiocarbonate (DIBTTC) as the chain transfer agent (CTA) and α,α′-azobis(isobutyronitrile) (AIBN) as the initiator (Scheme 4.1).[23] Block molar masses for the copolymer used in this study, determined by NMR spectroscopy, were 25 kg/mol and 12 kg/mol for the PDMA and PS blocks, respectively, which corresponds to 36 volume percent of PS. The composition was tuned for cylindrical morphology, and this copolymer was expected to form hydrophobic PS cylinders into a water-soluble PDMA matrix.

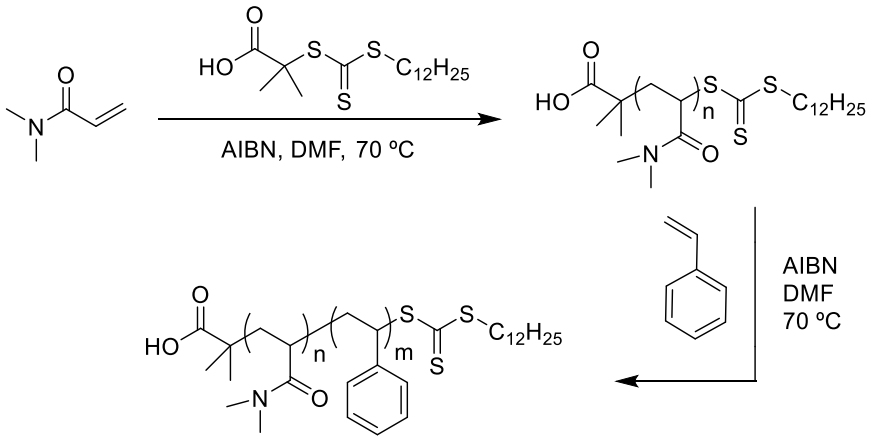

Scheme 4.1. Synthetic pathway for the synthesis of PDMA-PS block copolymer by RAFT polymerization.

The copolymer was processed at 160 °C in the same home-built channel die employed for the PS-PLA samples, and the microstructure of the resulting monolith was investigated by SAXS and TEM (sample A). To illustrate the consistency and reproducibility of our method, characterization details of second sample prepared in the same conditions is provided in the Supporting Information (referred to as sample B). SAXS analysis of the resulting monolith revealed an intense primary peak at q*=0.197 nm (D*=31.9 nm^{-1}) along with numerous higher order reflections at $\sqrt{4}q^*$, $\sqrt{7}q^*$, $\sqrt{9}q^*$, $\sqrt{12}q^*$, $\sqrt{13}q^*$ and $\sqrt{16}q^*$, unambiguously indicative of a cylindrical morphology (Figure 4.5, and Figure 4.S7 for Sample B). Similar to the PS-PLA monolith, the 2D SAXS patterns obtained parallel to the shear direction are anisotropic, hence demonstrating the microstructural alignment (Figure 4.S6). In agreement with SAXS results, TEM images showed a well-aligned specimen. In particular, hexagonally packed cylinders were evident when imaging in the shear flow direction. The cylinder diameter was estimated to be 19 ± 5 nm, in agreement with the value extracted from the SAXS data (22.6 nm).

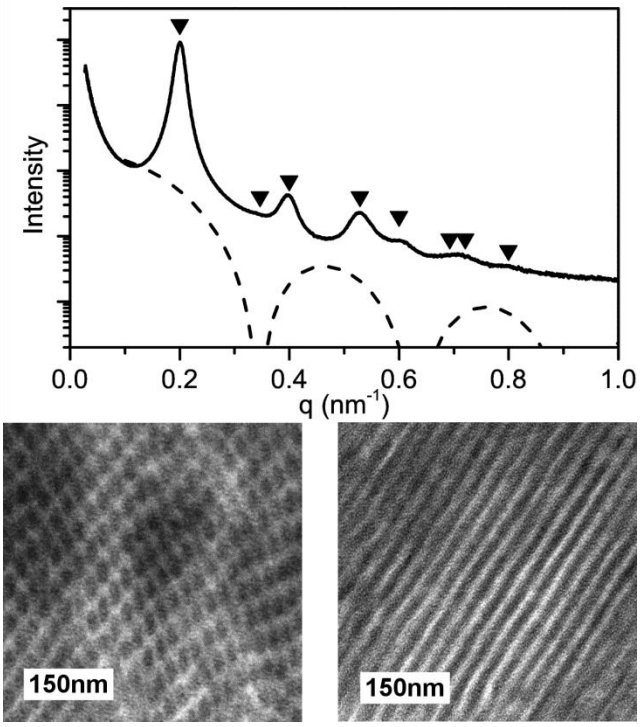

Figure 4.5. (Solid line) Experimental 1D synchrotron SAXS profile of shear-oriented PDMA-PS monolith (sample A) at 25 °C and (dashed line) simulated form factor scattering curve generated for cylinders with an 11.3 nm radius (value extracted from the experimental SAXS profile). The black triangles indicate the expected reflections for a cylindrical morphology (√1; √3; √4; √7; √9; √12; √13; √16). Corresponding TEM images of the material, obtained (left) perpendicularly and (right) parallel to the shear direction (PS domains, appearing darker, were stained by RuO_4 vapors).

Since both PDMA and PS are also glassy at room temperature ($T_{g(PDMA)}$ = 112 °C[24], $T_{g(PS)}$ = 100 °C[21]), the monolith was sectioned at room temperature. For the PDMA-PS copolymer, however, the water boat used to float the cut slices is also a selective solvent for the PDMA matrix, and this can potentially eliminate the need for freeze-drying as the dispersions can be formed in the water reservoir on the diamond knife upon sectioning. However, to prepare solutions with a known concentration, the resulting dispersions were freeze-dried, and the sample was diluted with water for DLS and TEM analyses. From the monolith dimensions, 2 mm×2 mm, and the domain spacing extracted from the SAXS

analysis, each section is expected to contain about 3.6×10^9 cylinders (9×10^{10} particles/min with 25 sections/min). Once a cut slice was introduced to the water boat, it did not immediately dissolve and appeared to be a highly swollen sheet floating on the water. Thus, to be certain that the cylinders were well dispersed in the solvent, the solutions were shaken for about 30 minutes after they were transferred into a plastic centrifuge tube.

Prior to TEM characterization of the samples, the carbon/Formvar-coated TEM grids were treated with air plasma (glow discharge) to improve their hydrophilicity. Two different sample preparation methods were used: (i) droplets of the solution were placed on the grid and the solvent was allowed to evaporate, and (ii) a piece of cleaning paper was placed under the grid to absorb the solvent. Figure 4.6 and Figure 4.S10 compare images acquired with these two different methods; these images were taken before sonication of the samples. As evident from the images, in the latter method (ii), due to the quick absorption of the solvent and removing most of the particles by the paper placed underneath, no accumulation of cylinders was observed. Whereas, in the former method (i), all of the particles dry on the grid and slow evaporation of the solvent allows the particles to aggregate. From the images (Figure 4.6b and 4.6c), the average length of the cylinders is estimated to be about 480 nm with ~10% variation. Although the size distribution seems to be off the targeted length of 200 nm, there is a reasonable control on the length of the cylinders. To produce longer cylinders, 300 nm-thick sections were also prepared. Similar to the aforementioned results, we observed by TEM cylinders relatively homogeneous in size, with an average length of approximately 600 nm (Figure 4.S12). It

is certainly possible to achieve fiber-like particles by increasing the thickness. However, targeting bigger particles might result in a higher proportion of defected structures.

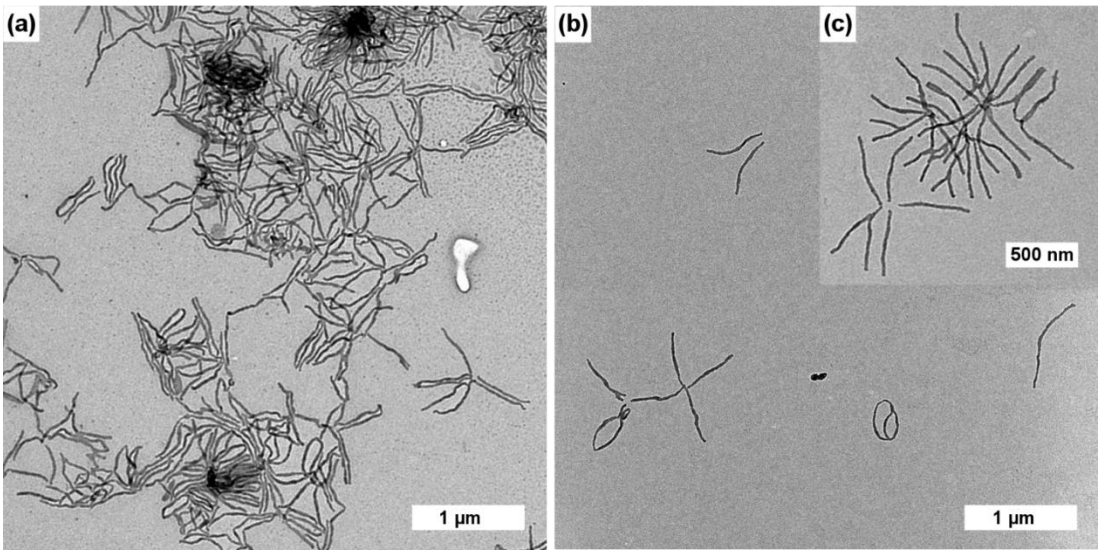

Figure 4.6. (a) TEM image of PS-PDMA nanoparticles (sample A) casted from an aqueous solution (0.2 $g.L^{-1}$). The carbon/Formvar-coated TEM grids were treated with air plasma to improve their hydrophilicity prior to use. The nanoparticles were stained with RuO_4. (a) Sample prepared through complete evaporation of the water in a droplet placed on the grid (method (i)). (b) and (c) Sample prepared by absorbing the excess of solution with a piece of paper placed under the grid (method (ii)).

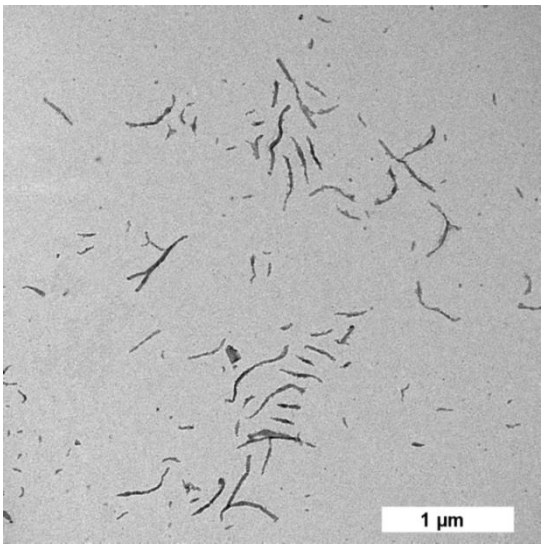

Figure 4.7. TEM image of PS-PDMA nanoparticles (sample A) casted from an aqueous solution (0.2 $g.L^{-1}$) after 5min of sonication. The carbon/Formvar-coated TEM grids were treated with air plasma to improve their hydrophilicity prior to use. The nanoparticles were stained with RuO_4. The sample was prepared by absorbing the excess of solution with a piece of paper placed under the grid (method (ii)).

In both cases, some nanocylinders seem to be aggregated at their ends, a possible indication of sample damage during the cutting step. To break any non-dispersed materials, the dispersions were sonicated for 3 to 5 minutes. Although sonication seems to be efficient in breaking aggregates, it results in appearance of smaller particles in a broader size range, implying that some of the cylinders are broken/damaged upon sonication (Figures 4.7, and Figure 4.S11 for Sample B). The average length of the cylinders was estimated to 290 ± 150 nm after sonication. The major variation observed in the size distribution of more than 50% is likely due to the breakage of the cylinders, an issue that could possibly be circumvented by optimizing the sonication conditions. According to DLS, the average size of the cylinders decreases from 189 ± 9 nm to 163 ± 8 nm with sonication (Figure 4.S8 and Figure 4.S9).

4.3 Conclusion

Herein, an approach for nanoparticle fabrication that combines block copolymer self-assembly and nanoskiving is introduced. This fabrication method allows a facile experimental procedure that does not require specialty fabrication equipment. While maintaining many advantages of the other top-down approaches, e.g., specific shape fidelity, and some degree of control on the size, our new approach utilizes block copolymer self-assembly to form the nanostructures in their thermodynamically stable state. This is advantageous because it is expected to result in nanoparticles with homogenous and optimized surfaces, the mechanical altering on the nanoparticles surface is minimized, and only the ends of the cylinders are formed in a non-optimal condition due to the cutting step. The production of particles that are surrounded by a stabilizing corona is another advantage of this approach to nanoparticle fabrication. Simple synthesis procedures and easy accessibility to cylindrical nanostructures in a range of compositions (~25–35%) through controlled polymerizations allow a versatile choice of materials for nanoparticle fabrications using this technique. Successfully illustrated with a PS-PLA and a PDMA-PS diblock copolymer, we expect this fabrication method to be usable with any glassy self-assembled block copolymer sample.

4.4 Materials and Methods

4.4.1 Materials

All the reagents were from Sigma-Aldrich and were used as received. N,N-dimethylacrylamide (DMA) and styrene were passed through an activated alumina column to remove the inhibitors and stored at –20 °C for future use.

4.4.2 Characterization

All NMR spectra were recorded from a Varian INOVA 300 MHz or a Brüker Avance III 500 MHz Spectrometer with $CDCl_3$ as solvent at room temperature. Chemical shifts are relative to the TMS peak at 0.00 ppm. Size-exclusion chromatography (SEC) was performed in THF using a Waters Styragel guard column and 3 Waters Styragel columns (HR6, HR4, and HR1) in series with an available of 100–10,000,000 $g.mol^{-1}$. The columns are contained in an Agilent 1260 Infinity liquid chromatograph equipped with a Wyatt Dawn Heleos II multiangle light scattering detector and a Wyatt Optilab T-rEX refractive index detector.

4.4.3 Transmission Electron Microscopy (TEM)

To investigate the microstructure of the shear-oriented specimens: ultrathin sections (ca. 70–100 nm) of the polymeric monoliths were cut using a Leica EM UC6 Ultramicrotome at –120 °C. Although both materials are already glassy at room temperature, cryomicrotomy helped to achieve the thickness desired for TEM imaging. The cut sections were placed on 400 mesh copper grids and subsequently stained with RuO_4

vapor for ~5 min by exposure to a 0.5% aqueous solution. For the nanocylinders after dissolution, 2–3 drops of the solution were placed on TEM grids with a Formvar® supporting film (~3 nm) and after complete evaporation of the solvent, or quick absorption of the solvent with a piece of cleaning paper under the grid, stained with RuO_4 vapor for ~5 min by exposure to a 0.5% aqueous solution. All of the TEM images were obtained with a FEI Tecnai G2 Spirit BioTWIN transmission electron microscope, operated at 120 kV.

4.4.4 Small-angle X-ray Scattering (SAXS)

All experiments were performed at the Sector 5-ID-D beamline of the Advanced Photon Source (APS) at Argonne National Laboratories, maintained by the Dow-Northwestern-Dupont Collaborative Access Team (DNDCAT). The source produces X-rays with 0.70 Å wavelengths. The sample to detector distance was fixed to 7.491 m. Scattering intensity was monitored using a Mar 165 mm diameter CCD detector operating with a resolution of 2048 by 2048. The two-dimensional scattering patterns were azimuthally integrated to afford one-dimensional profiles presented as spatial frequency (q) versus scattered intensity.

4.4.5 Dynamic Light Scattering (DLS)

Size distributions of the nanocylinders were investigated by DLS, in cyclohexane for PS-PLA and water for PDMA-PS samples. The solutions were passed through 0.45 μm filters into glass tubes. Light scattering was carried out in a Brookhaven BI-200SM DLS system equipped with a Mini L-30 HeNe laser operating at 637 nm, and a BI-NDO detector.

The sample tube was immersed in decalin. Experiments were performed at room temperature. Intensity correlation functions were recorded at scattering angle 90°, with an aperture size of 400 nm, and converted to size distributions using the CONTIN analysis program provided by the Brookhaven software.

4.4.6 Self-assembly, Channel-die Alignment, and Thermal Annealing

Polymer films were prepared by casting from chloroform solutions. The polymer films were collected and dried in a vacuum oven at 80 °C for the PS-PLA sample, and 130 °C for PDMA-PS samples, for 18 h. ~0.5 g of the polymer films were cut into small pieces (~0.5 cm^2) and placed in the center of a home-built channel die 2-mm wide and 5-cm long. The channel die was placed in a laboratory press at 130 ºC for the PS-PLA sample, and 160 ºC for the PDMA-PS samples, and the compression was started after 15 min. The sample was pressed for 1–2 mm every 10 min manually. Compression stopped when the melted polymers reached the ends of the channel die. The channel die was left in the laboratory press for 15 min without further pressing. The aligned specimens were left in the channel die and annealed under vacuum at 130 °C for the PS-PLA sample, and 160 ºC for the PDMA-PS samples, for 60 h. The aligned material was removed from the die with sample thickness of ~2 mm. In summary, the time required was 18 hours for solvent casting and drying the films, followed by 63 hours for channel die alignment and annealing, for theoretically about 6×10^{15} particles.

4.4.7 Nanoparticle Preparation by Nanoskiving

A Leica EM UC6 Ultramicrotome equipped with a diamond knife was used for sectioning the polymer specimens. The aligned specimen, with dimensions of ~ 2× 2 ×10 mm3, was mounted on the microtome arm. After the surface of the sample was leveled using a razor blade and smoothed with a glass knife, sections with the desired thicknesses were collected into a water-boat on the diamond knife. The microtome was set on the automatic setting with a 4 mm/s cutting speed. During the sectioning, some polymer sections were picked-up using an eyelash stick to prevent exceeding accumulation at the surface of the water and transferred into a plastic centrifuge tube. Sectioning was stopped after 1000 sections. The sections were then recovered by dumping the boat into the same plastic tube. The samples were then lyophilized to remove the water. Finally, solutions for DLS analysis were prepared by dissolving dry sections in 1 ml of the proper solvent, cyclohexane for PS-PLA and water for PDMA-PS samples. Further dilutions were used for TEM characterization. At a rate of 25 sections/min, the nanoparticle fabrication rate is estimated to 6×10^{10} particles/min for PS-PLA and 9×10^{10} particles/min for PDMA-PS. Freeze-drying (overnight) and dissolution (30 min) steps are independent from the number of sections and are not included in the rate calculations.

4.4.8 Synthesis of the Polymers

Poly(styrene)-b-poly(lactide)(PS-PLA). Following a previously reported protocol,[14] a hydroxyl-terminated polystyrene (PS-OH) was synthesized by anionic polymerization, and subsequently used as macroinitiator to polymerize D,L-lactide by ring

opening transesterification polymerization. Addition of PLA to the PS block was performed in a glove-box by mixing 3.27 g of PS-OH, 1.921 g of D,L-lactide, 20.0 µL of 1,8-diazabicycloundec-7-ene (DBU) with 35 mL of dichloromethane (anhydrous) at room temperature. The reaction was terminated with a spatula tip of benzoic acid (stirring 1–2 min) after 65 minutes. The polymer was precipitated into ~ 400ml of cold methanol (–20 to –30 °C). The D,L lactide conversion was determined to be 82.3%. M_nNMR= 60 kg/mol, f_{PLA}= 0.26 (calculated using ρ_{PLA}=1.25 g/cm^3,[25] ρ_{PS}=1.04g/cm^3 [26]). M_nSEC= 57 kg/mol, Đ =1.01. ^{1}HNMR ($CDCl_3$, 300 MHz): δ = 1.25−1.55 (br, CH_2-PS), 1.55−1.7 (m, CH_3-PLA), 1.7-2 (br, CH-PS), 5.1-5.3 (m, CH-PLA), 6.4−6.7 (br m, ArH-PS), 6.85-7.25 (br m, ArH-PS) ppm.

Poly(N,N-dimethylacrylamide)-b-poly(styrene)(PDMA-PS). To a 200 mL round-bottom flask equipped with a Teflon stirring bar was added DIBTTC (346 mg, 0.95 mmol), AIBN (16 mg, 0.098 mmol), and 30 mL of DMF. Next, DMA (30 mL, 291 mmol) was added and the flask was sealed and the mixture was degassed by bubbling nitrogen at room temperature for 2.5 hours. Subsequently, the reaction vessel was submerged into a thermostated oil bath at 70 °C for one hour. The polymerization was quenched by immediately placing the flask into liquid nitrogen and opening it to air. The obtained viscous bright yellow reaction mixture was diluted by adding 50 mL of methylene chloride, and subsequently the polymer was precipitated in four liters of ice-cold hexane/diethyl ether 50:50 (v/v). The yellow solid was isolated via filtration and dissolved in 200 ml of CH_2Cl_2 and precipitated in four liters of ice-cold cyclohexane. After reprecipitation in another four liters of ice-cold cyclohexane followed by filtration, the resulting PDMA-

CTA powder was dried in a vacuum oven at 40 °C for one week (~16 g, 67% yield). M_n= 25 kg/mol (80% conversion), Đ =1.10. ^{1}HNMR ($CDCl_3$, 500 MHz): δ = 1.1−1.9 (br m, CH_2), 2.4−2.9 (br m, CH), 2.9−3.4 (br m, CH_3) ppm. The product was stored under vacuum, in a desiccator, at room temperature until further use. To synthesize the final block copolymer, AIBN (3.6 mg, 0.022 mmol), the PDMA-CTA (5.99 g, 0.24 mmol), styrene (20 mL, 174 mmol) and 28 mL of DMF were mixed in a 200 ml round-bottom flask equipped with a Teflon stirring bar. The flask was sealed and the mixture was degassed under inert nitrogen at room temperature for one hour. Subsequently, the reaction vessel was submerged into a preheated, stirring oil bath maintained at 70 °C. After 31 hours, the reaction was quenched by immediately placing the flask into liquid nitrogen and opening it to air. 50 mL of CH_2Cl_2 was added to the mixture, and subsequently the polymer was precipitated in four liters of ice-cold hexane/diethyl ether 75:25 (v/v). After filtration, the polymer was redissolved in 150 mL of CH_2Cl_2 followed by precipitation in four liters of ice-cold hexane. After another precipitation in ice-cold hexane, the product was dried in a vacuum oven at 40 °C for one week (~6.5 g, 73% yield). M_n(PS)= 12 kg/mol (15% conversion), f_{PS}= 0.36 (calculated using ρ_{PDMA}=1.21 g/cm^3 [27], ρ_{PS}=1.04g/cm^3 [26]), Đ =1.12. ^{1}HNMR ($CDCl_3$, 500 MHz): δ = 1.1−2.75 (br m, CH_2-PDMA and PS, CH- PDMA and PS), 2.75−3.85 (br m, CH_3-PDMA), 6.3−6.9 (br m, ArH-PS), 6.9-7.25 (br m, ArH-PS) ppm. The final block copolymer was stored under vacuum, in a desiccator, at room temperature.

4.5 Supplementary Figures and Tables

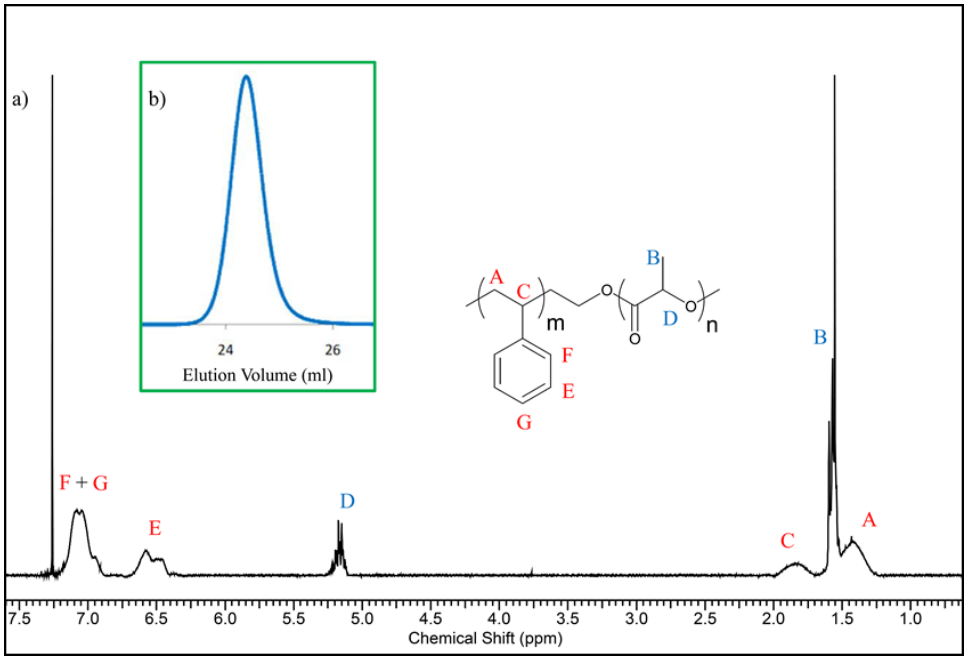

Figure 4.S1. a) ^{1}H NMR spectrum of the PS-PLA block copolymer (300 MHz, $CDCl_3$). b) SEC trace for the PS-PLA block copolymer (eluent: chloroform, at room temperature).

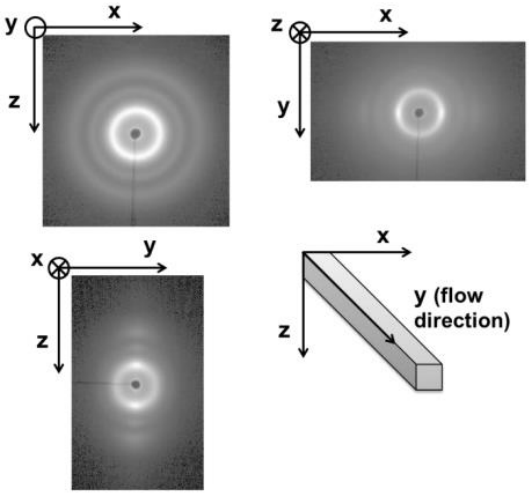

Figure 4.S2. 2D Synchrotron SAXS patterns of shear-oriented PS-PLA block copolymer.

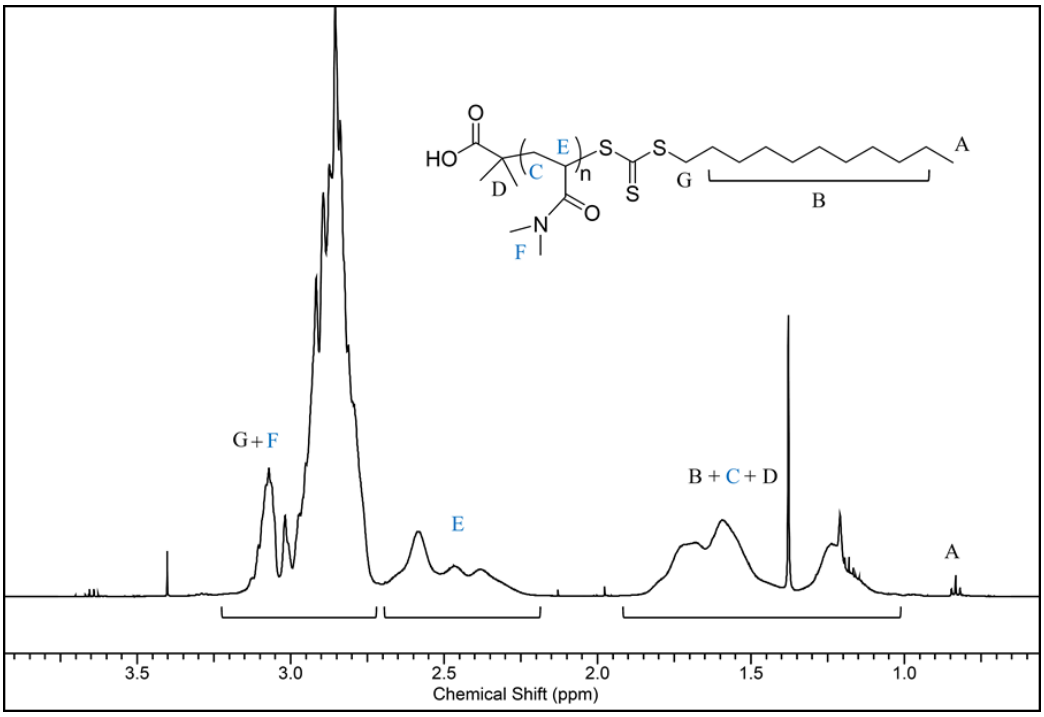

Figure 4.S3. ^{1}H NMR spectrum of the PDMA Macro-CTA (500 MHz, $CDCl_3$). Non-assigned peaks at 1.4, 1.9, 3.4, and 3.65 ppm correspond to residual solvents (cyclohexane, diethyl ether, dimethylformamide and diethyl ether, respectively)

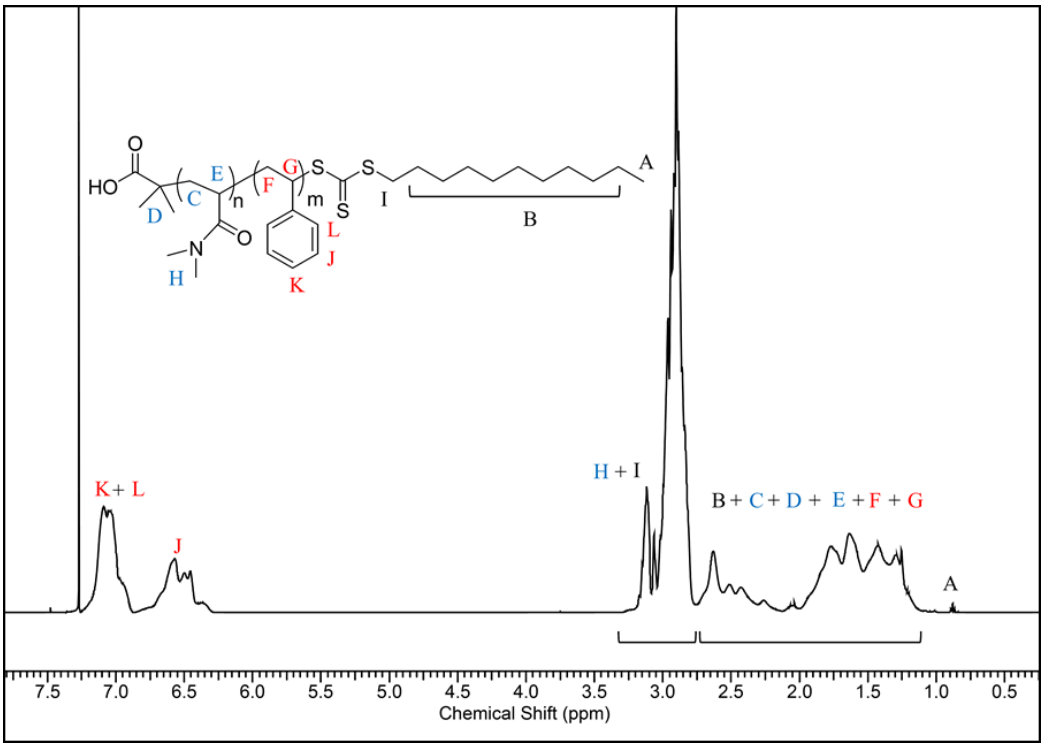

Figure 4.S4 .[1]H NMR spectrum of the PDMA-PS block copolymer (500 MHz, $CDCl_3$)

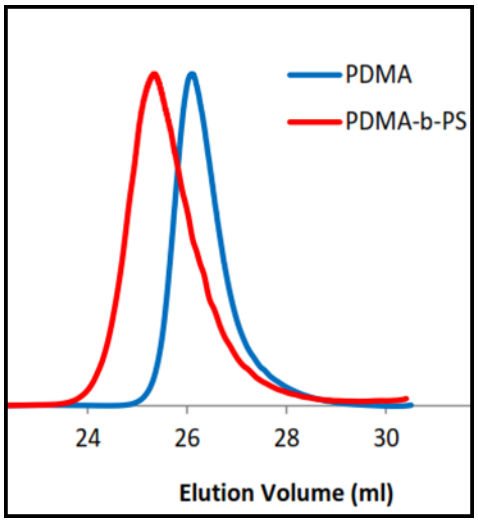

Figure 4.S5. SEC traces for the PDMA macro-CTA and the resulting PDMA- PS copolymer (eluent: THF, at room temperature).

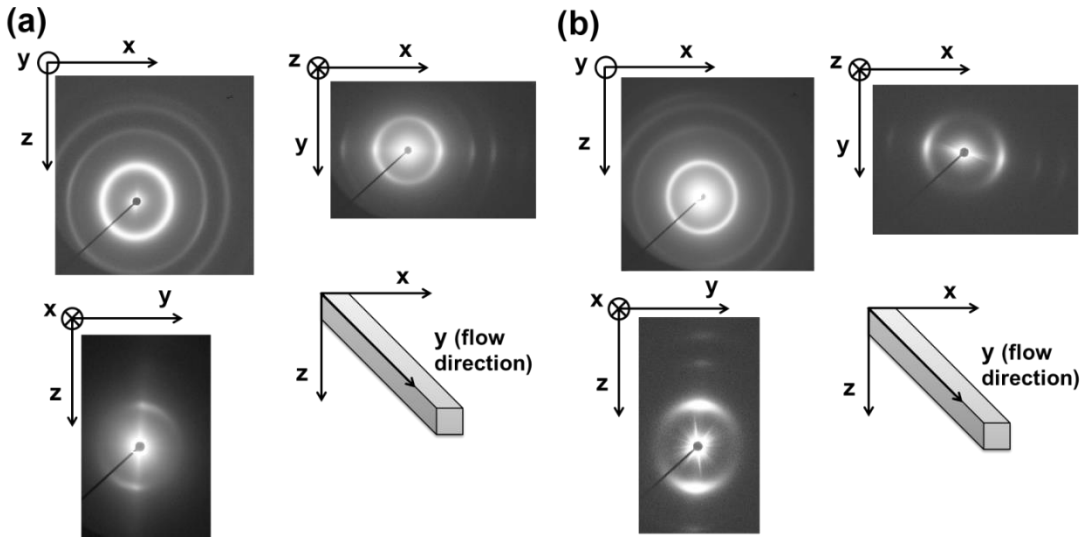

Figure 4.S6. 2D Synchrotron SAXS patterns of shear-oriented PDMA-PS block copolymer (a) Sample A and (b) Sample B.

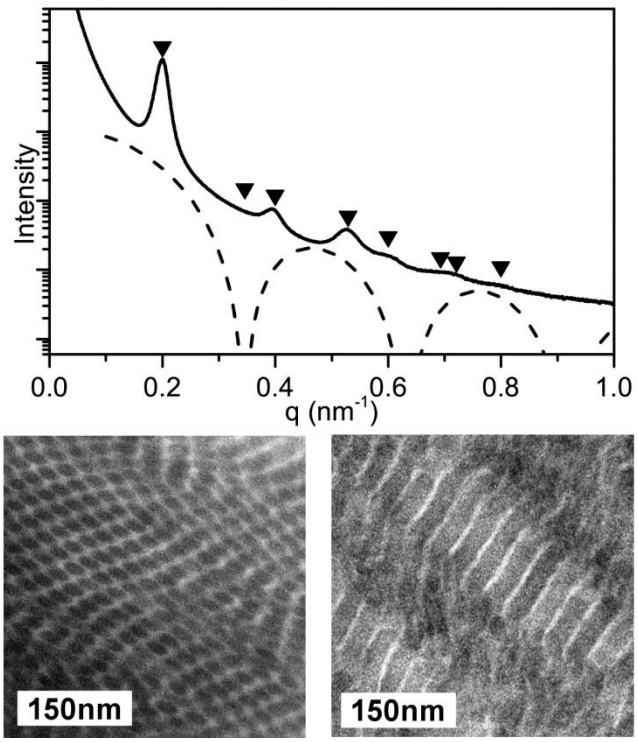

Figure 4.S7. (Solid line) Experimental 1D synchrotron SAXS profile of shear-oriented PDMA-PS sample B at 25°C and (dashed line) simulated form factor scattering curve generated for cylinders with a 10.8 nm radius (value extracted from the experimental SAXS profile). The triangle symbols indicate the expected reflections for a cylindrical morphology (√1; √3; √4; √7; √9; √12; √13; √16). Corresponding TEM images of the material, obtained (left) perpendicularly and (right) parallel to the shear direction (PS domains were stained by RuO_4 vapors).

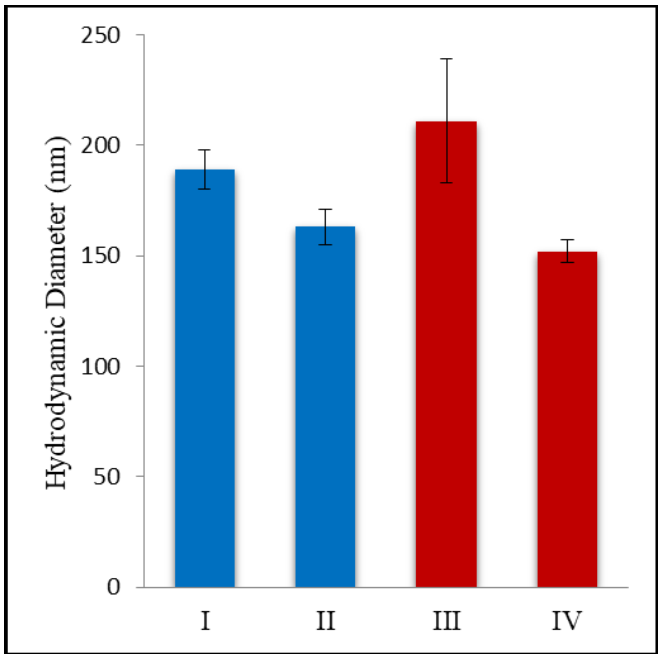

Figure 4.S8. Apparent size distribution of the PS nanocylinders dispersion in water by DLS, the error bars represent standard deviations for ten measurements. Scattering detection angle is 90° and λ= 637 nm. For the concentrations, see Table 4.S1. The theoretical thickness of the sections was set at 200 nm. I) Sample A, II) Sample A after sonication, III) Sample B, and IV) Sample B after sonication.

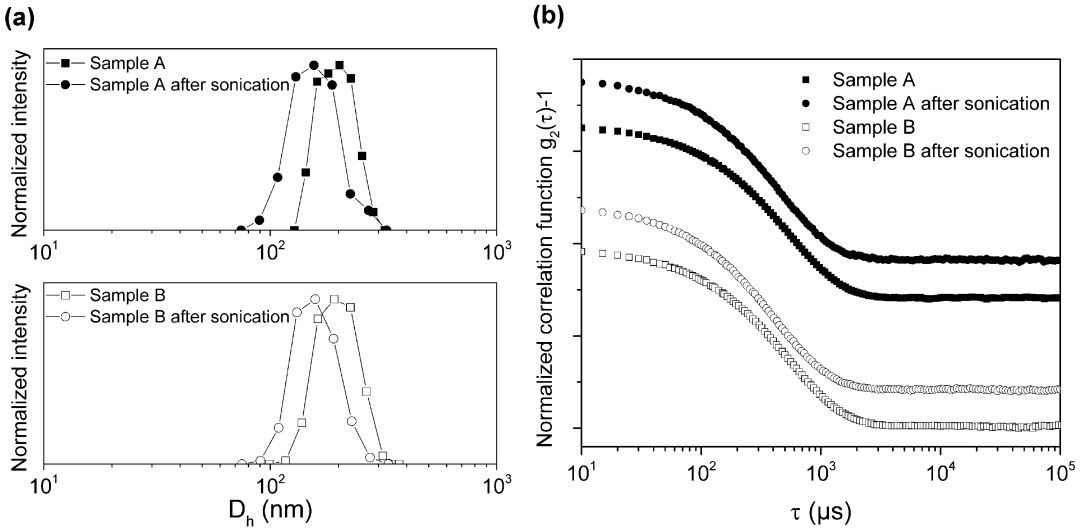

Figure 4.S9. (a) DLS size distribution profiles of the PS nanocylinders dispersions in water for samples A and B, before and after sonication. (b) Associated correlation functions. Scattering detection angle is 90° and λ= 637 nm. For the concentrations, see Table 4.S1. The theoretical thickness of the sections was set at 200 nm.

Table 4.S1. DLS characterization summary of the PS nanocylinders with PDMA coronae in water, for ten measurements for each sample. The laser beam wavelength was 637 nm and the scattered light was detected at 90°. I) Sample A, II) Sample A after sonication, III) Sample B, and IV) Sample B after sonication.

Sample	**D_h[a]** (nm)	**Peak Position** (nm)[b]	**Rel. Var.** [c]	**Conc. Wt.%**[d]
I	189 ± 9	201.4 ± 14.6	0.074 ± 0.043	0.09
II	163 ± 8	166.7 ± 12.8	0.119 ± 0.050	0.03
III	211 ± 28	204.5 ± 30.3	0.073 ± 0.066	0.09
IV	152 ± 5	154.2 ± 11.0	0.064 ± 0.041	0.03

[a]Average hydrodynamic diameters determined by the CONTIN analysis. [b] Position at which the highest scattering intensity occurs. [c] Particle dispersity (average value of the relative variances for 10 measurements). [d] Approximate weight percent of the polymer in solution.

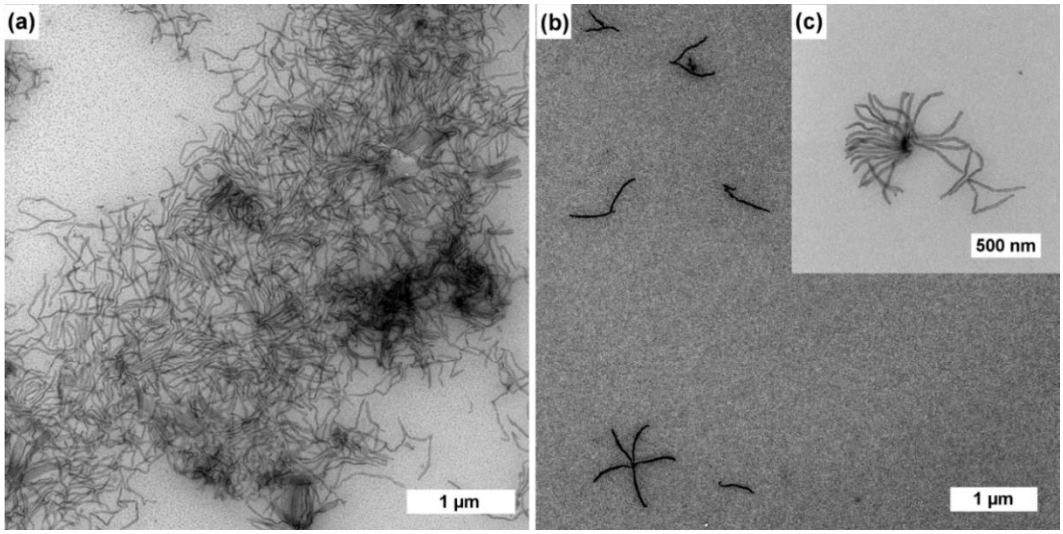

Figure 4.S10. TEM image of PDMA-PS nanoparticles (sample B) casted from an aqueous solution (0.2 $g.L^{-1}$). The nanoparticles were stained with RuO_4. (a) Sample prepared through complete evaporation of the water in a droplet placed on the grid. (b) Sample prepared by absorbing the excess of solution with a piece of paper placed under the grid. (c) Close-up view of end-aggregated cylinders, same sample preparation than b).

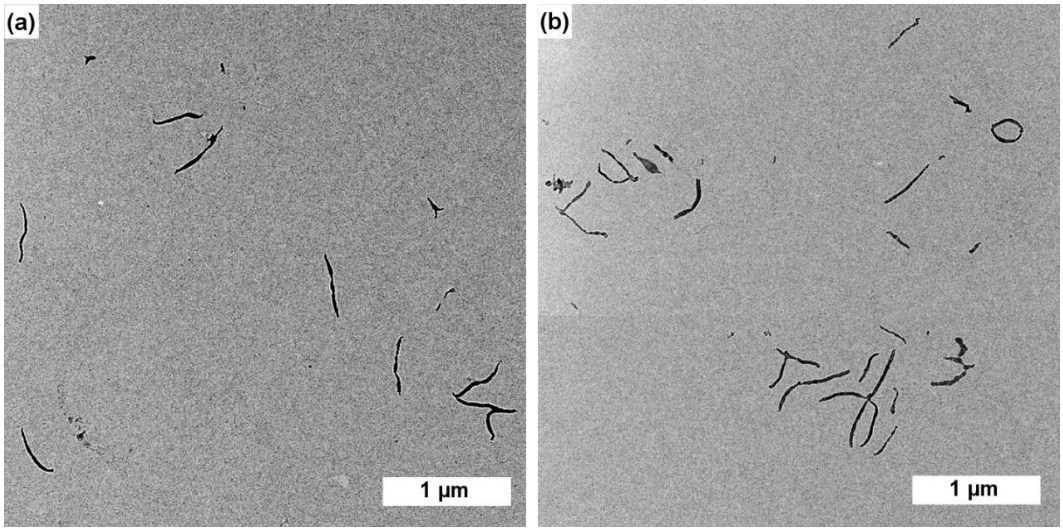

Figure 4.S11. (a) and (b) TEM images of PS-PDMA nanoparticles (sample B) casted from an aqueous solution (0.2 $g.L^{-1}$) after 5min of sonication. The carbon/Formvar-coated TEM grids were treated with air plasma to improve their hydrophilicity prior to use. The nanoparticles were stained with RuO_4. The sample was prepared by absorbing the excess of solution with a piece of paper placed under the grid.

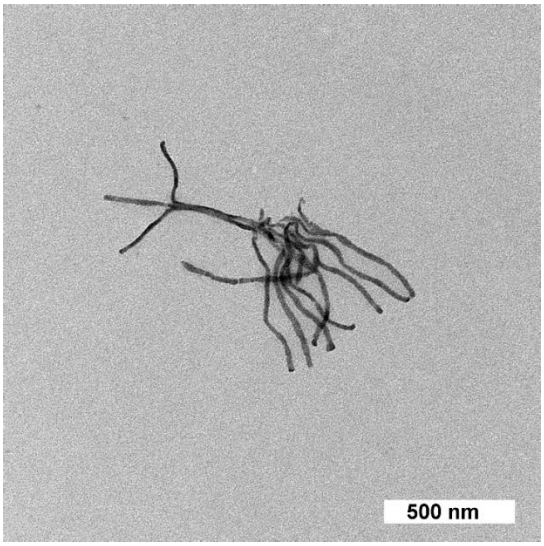

Figure 4.S12. TEM image of PDMA-PS nanoparticles (sample B) casted from an aqueous solution (0.2 $g.L^{-1}$). The carbon/Formvar-coated TEM grids were treated with air plasma to improve their hydrophilicity prior to use. The theoretical thickness of the sections was set on 300 nm and the nanoparticles were stained with RuO_4. Sample prepared by absorbing the excess of solution with a piece of paper placed under the grid.

4.6 References

1. Euliss, L. E.; DuPont, J. A.; Gratton, S.; DeSimone, J. M. Imparting Size, Shape, and Composition Control of Materials for Nanomedicine. *Chem. Soc. Rev.* **2006,** *35*, 1095-1104.

2. Biswas, A.; Bayer, I. S.; Biris, A. S.; Wang, T.; Dervishi, E.; Faupel, F. Advances in top-down and bottom-up surface nanofabrication: Techniques, Applications & Future Prospects. *Adv. Colloid Interface Sci.* **2012,** *170*, 2-27.

3. Devadasu, V. R.; Bhardwaj, V.; Kumar, M. N. V. R. Can Controversial Nanotechnology Promise Drug Delivery? *Chem. Rev.* **2013,** *113*, 1686-1735.

4. Zhang, L. F.; Eisenberg, A. Multiple Morphologies of Crew-cut Aggregates of Polystyrene-b-poly(acrylic acid) Block-copolymers. *Science* **1995**, 268, 1728-1731.

5. Hu, J.; Njikang, G.; Liu, G. Twisted ABC Triblock Copolymer Cylinders with Segregated A and C Coronal Chains. *Macromolecules* **2008**, 41, 7993-7999.

6. Li, X.; Liu, G.; Han, D. Wrapping Amino-bearing Block Copolymer Cylinders Around Carboxyl-bearing Nanofibers: A Case of Hierarchical Assembly. *Soft Matter* **2011**, 7, 8216-8223.

7. Choi, S.-H.; Bates, F. S.; Lodge, T. P. Molecular Exchange in Ordered Diblock Copolymer Micelles. *Macromolecules* **2011**, 44, 3594-3604.

8. Lund, R.; Willner, L.; Richter, D. In *Controlled Polymerization and Polymeric Structures*; Abe, A., Lee, K.-S., Leibler, L., Kobayashi, S., Eds.; Springer International Publishing: 2013; Vol. 259, pp 51-158.

9. Badaire, S.; Cottin-Bizonne, C.; Woody, J. W.; Yang, A.; Stroock, A. D. Shape Selectivity in the Assembly of Lithographically Designed Colloidal Particles. *J. Am. Chem. Soc.* **2007**, 129, 40-41.

10. Merkel, T. J.; Herlihy, K. P.; Nunes, J.; Orgel, R. M.; Rolland, J. P.; DeSimone, J. M. Scalable, Shape-Specific, Top-Down Fabrication Methods for the Synthesis of Engineered Colloidal Particles. *Langmuir* **2010,** *26*, 13086-13096.

11. Canelas, D. A.; Herlihy, K. P.; DeSimone, J. M. Top-down Particle Fabrication: Control of Size and Shape for Diagnostic Imaging and Drug Delivery. *Wiley Interdiscip. Rev. Nanomed. Nanobiotechnol.* **2009,** *1*, 391-404.

12. Varadan, V. K.; Chen, L.; Xie, J. *Nanomedicine: design and applications of magnetic nanomaterials, nanosensors and nanosystems*. John Wiley & Sons, Ltd: Chichester, UK, 2008.

13. Kim, H.-C.; Park, S.-M.; Hinsberg, W. D. Block Copolymer Based Nanostructures: Materials, Processes, and Applications to Electronics. *Chem. Rev.* **2010,** *110*, 146-177.

14. Zalusky, A. S.; Olayo-Valles, R.; Wolf, J. H.; Hillmyer, M. A. Ordered Nanoporous Polymers from Polystyrene-Polylactide Block Copolymers. *J. Am. Chem. Soc.* **2002,** *124*, 12761-12773.

15. Drzal, P. L.; Barnes, J. D.; Kofinas, P. Path Dependent Microstructure Orientation During Strain Compression of Semicrystalline Block Copolymers. *Polymer* **2001,** *42*, 5633-5642.

16. Rzayev, J.; Hillmyer, M. A. Nanochannel Array Plastics with Tailored Surface Chemistry. *J. Am. Chem. Soc.* **2005,** *127*, 13373-13379.

17. Bertrand, A.; Hillmyer, M. A. Nanoporous Poly(lactide) by Olefin Metathesis Degradation. *J. Am. Chem. Soc.* **2013,** *135*, 10918-10921.

18. Xu, Q. B.; Gates, B. D.; Whitesides, G. M. Fabrication of Metal Structures with Nanometer-Scale Lateral Dimensions by Sectioning Using a Microtome. *J. Am. Chem. Soc.* **2004,** *126*, 1332-1333.

19. Xu, Q.; Rioux, R. M.; Dickey, M. D.; Whitesides, G. M. Nanoskiving: A New Method To Produce Arrays of Nanostructures. *Acc. Chem. Res.* **2008,** *41*, 1566-1577.

20. Lipomi, D. J.; Martinez, R. V.; Whitesides, G. M. *Angew. Chem. Int. Ed.* **2011**, *50*, 8566-8583.

21. Shen, M. C.; Eisenberg, A. Glass Transitions in Polymers. *Rubber Chem. and Technol.* **1970,** *43*, 95-155.

22. Hyon, S. H.; Jamshidi, K.; Ikada, Y. Effects of Residual Monomer on the Degradation of DL-Lactide Polymer. *Polym. Int.* **1998,** *46*, 196-202.

23. Faber, M.; Hofman, A. H.; Polushkin, E.; van Ekenstein, G. A.; Seitsonen, J.; Ruokolainen, J.; Loos, K.; ten Brinke, G. Hierarchical Self-Assembly in Supramolecular Double-Comb Diblock Copolymer Complexes. *Macromolecules* **2013,** *46*, 500-517.

24. Chiantore, O.; Costa, L.; Guaita, M. Glass Temperatures of Acrylamide Polymers. *Makromol. Chem. Rapid Commun.* **1982,** *3*, 303-309.

25. Witzke, D. R.; Narayan, R.; Kolstad, J. J. Reversible Kinetics and Thermodynamics of the Homopolymerization of L-Lactide with 2-Ethylhexanoic Acid Tin(II) Salt. *Macromolecules* **1997,** *30*, 7075-7085.

26. Quach, A.; Simha, R. Pressure-Volume-Temperature Properties and Transitions of Amorphous Polymers; Polystyrene and Poly (orthomethylstyrene). *J. Appl. Phys.* **1971,** *42*, 4592-4606.

27. Gundogan, N.; Okay, O.; Oppermann, W. Swelling Elasticity and Spatial Inhomogeneity of Poly(N,N-dimethylacrylamide) Hydrogels Formed at Various Polymer Concentrations. *Macromol. Chem. Phys.* **2004,** *205*, 814-823.

Chapter 5

Summary and Outlook

5.1 Dissertation Summary

In summary, Chapters 2 and 3 describe development of block copolymers from biomass to produce functional elastomeric materials. Acrylic monomers of glucose and isosorbide were prepared and utilized as glassy components in thermoplastic elastomers. Comprehensive studies on the adhesion properties of the resulting polymers revealed characteristics that are comparable to many commercial pressure sensitive adhesives. The sugar-derived block copolymers were also investigated for their structure-properties relationship as well as their mechanical and elastomeric features. Enhancement of adhesion and mechanical properties via utilization of non-covalent interactions such as chain entanglements and self-complementary hydrogen bonding was demonstrated. Marked improvements in the performance of these materials as a result of such non-covalent interactions allows for improved design of sustainable, sugar-derived polymers as high performance TPEs. This study introduces a new platform of sugar-based ABA-type copolymers and demonstrates functionality of a bio-based feedstock for developing green polymeric materials, particularly for TPE applications.

Chapter 4 introduces a novel approach for nanoparticle fabrication that combines block copolymer self-assembly and nanoskiving. This fabrication method allows a facile experimental procedure that does not require specialty fabrication equipment. While maintaining many advantages of the other top-down approaches, such as size control and specific shape fidelity, our new approach utilizes block copolymer self-assembly to form the nanostructures in their thermodynamically stable state. This is advantageous because it is expected to result in nanoparticles with homogenous and optimized surfaces, since the

mechanical altering on the nanoparticles surface is minimized. The production of particles that are surrounded by a stabilizing corona is another advantage of this approach to nanoparticle fabrication. We expect this fabrication method to be usable with any glassy self-assembled block copolymer system.

5.2 Future Directions

As more of the world's population are entering the developed world, the demand for plastics continues to increase, so too are the environmental concerns associated with polymers. The crucial need for development of sustainable materials cannot be over-emphasized. The importance of this matter has led the scientists and engineers around the world to put forth significant efforts towards utilizing biomass to create greener alternatives to the commodity polymers. This field is rapidly expanding and there have been promising progresses in exploration of biomass as a green feedstock for sustainable polymers. The work presented here can significantly benefit from incorporation of a greener soft block. Although n-butyl acrylate can be produced from natural resources, the current industry mainly uses petroleum-based feedstock for its production. Alternatively, midblocks that are more sustainable and are produced from biomass can be copolymerized with the glucose- and isosorbide-based monomers reported here. For instance, γ-Methyl-ε-caprolactone (γMCL), which may be derived from lignin, can be polymerized via ring opening polymerization (ROP). Subsequently, macro-CTAs that are suitable for RAFT polymerization can be achieved via modification of the end groups of PγMCL. Afterward, chain-extension of such macro-CTAs with the GATA and AAI monomers would result in

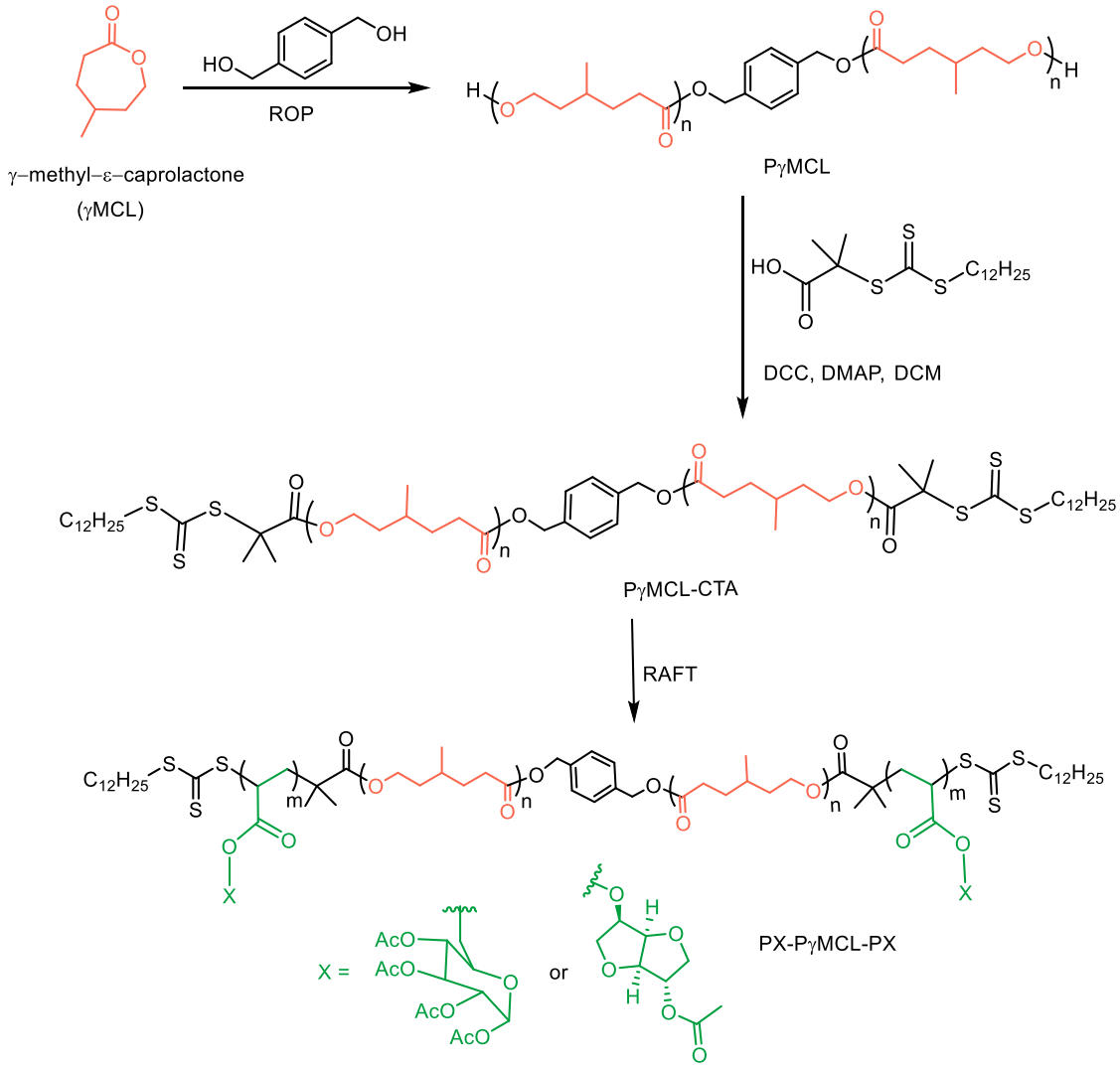

Scheme 5.1. A proposed route for copolymerization of GATA and AAI with γ-Methyl-ε-caprolactone.

fully sustainable and bio-derived TPEs. A proposed route for preparation of PGATA/AAI-PγMCL-PGATA/AAI triblock copolymers is shown in Scheme 5.1. Additionally, procedures that are more efficient and utilize safer chemistries are desirable, such as minimizing waste generation, reducing the number of steps required, and avoiding use of hazardous chemicals. Indeed, the research on adapting enzymatic one-pot pathways for

production of our sugar-based monomers has already begun and the initial results are very promising.

Moreover, further study on effects of hydrogen bonding incorporation within the glassy and/or soft domains of these TPEs could be another interesting avenue of research. Similar to GATA, the acetyl groups of the AAI units can be removed to study hydrogen bonding incorporation within the glassy segments of the PAAI-PnBA-PAAI copolymers. Also, GATA-based triblock copolymers with different adhesion or mechanical properties may be prepared by varying the degree of deacetylation in the glassy domains. This would allow for an optimized design of glucose-based polymers for a desired application. Additionally, partial deprotection of the PnBA midblocks may improve the mechanical strength in these materials, via transient networking formed by hydrogen bonding within the soft domains.

The nanoparticle fabrication method introduced here can serve as a useful tool for generating nanocarriers. The next step for this project will be fabrication of pre-loaded nanoparticles and study of their biological efficacy. Based on the chemistry of the drug and the polymeric structure, different strategies can be applied for loading a cargo into the nanocylinders. One way is to form polymer conjugates in which the drug is covalently bound to the polymer. If the drug molecules are bound to the shorter block end of the polymer chains, they will be entrapped inside the cylinders upon phase separation. Another simple way to load a drug into the nanocylinders is to mix the drug and the polymer before the self-assembly. This method of loading is appropriate for highly hydrophobic drugs, which are miscible with the short hydrophobic block and are immiscible with the long

hydrophilic block. Drug molecules will be trapped in the cylinders during the self-assembly and will be present inside of the nanocylinders at the end of the particle fabrication procedure.

Furthermore, given their hydrophobic nature, our sugar-derived monomers can be copolymerized with hydrophilic monomers, such as N,N-dimethylacrylamide, to produce amphiphilic polymers. Subsequently, our nanoparticle fabrication method can be employed to generate nanocylinders from these amphiphilic polymers. The resulting delivery vehicles could potentially exhibit high biocompatibility due to their sugar components. Utilization of this approach for a poly(acetylated acrylic isosorbide)-*b*-poly(N,N-dimethyl-acrylamide) copolymer is schematically presented in Figure 5.1.

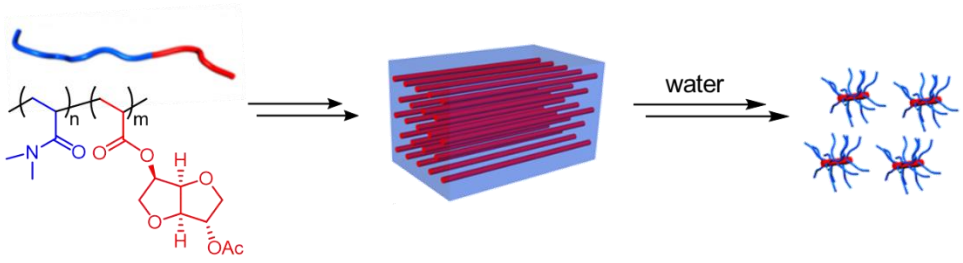

Figure 5.1. Proposed strategy for fabrication of isosorbide-based nanocylinders.

Bibliography

Chapter 1

(1) Elias, H.-G.; Mülhaupt, R., Ullmann's Encyclopedia of Industrial Chemistry (Plastics, General Survey, 2. Production of Polymers and Plastics). Wiley-VCH Verlag GmbH & Co. KGaA: Weinheim, Germany, 2015; Vol. 38.

(2) Xiong, M.; Schneiderman, D. K.; Bates, F. S.; Hillmyer, M. A.; Zhang, K., Scalable production of mechanically tunable block polymers from sugar. Proceedings of the National Academy of Sciences 2014, 111 (23), 8357-8362.

(3) Lichtenthaler, F. W., Ullmann's Encyclopedia of Industrial Chemistry (Carbohydrates as Organic Raw Materials). Wiley-VCH Verlag GmbH & Co. KGaA: Weinheim, Germany, 2010; Vol. 6.

(4) Kola, R.; Elsner, O. v.; Riepe, W.; Reuter, K., Ullmann's Encyclopedia of Industrial Chemistry (Raw Materials and Energy). Wiley-VCH Verlag GmbH & Co. KGaA: Weinheim, Germany, 2000.

(5) Mekonnen, T.; Mussone, P.; Khalil, H.; Bressler, D., Progress in bio-based plastics and plasticizing modifications. Journal of Materials Chemistry A 2013, 1 (43), 13379-13398.

(6) Fenouillot, F.; Rousseau, A.; Colomines, G.; Saint-Loup, R.; Pascault, J. P., Polymers from renewable 1,4:3,6-dianhydrohexitols (isosorbide, isomannide and isoidide): A review. Progress in Polymer Science 2010, 35 (5), 578-622.

(7) Natureworks Product and Applications http://www.natureworksllc.com/Product-and-Applications. (accessed November 29).

(8) Matsen, M. W.; Bates, F. S., Unifying weak- and strong-segregation block copolymer theories. Macromolecules 1996, 29 (4), 1091-1098.

(9) Bates, F. S., Polymer-polymer phase behavior. Science 1991, 251 (4996), 898-905.

(10) Bates, F. S.; Fredrickson, G. H., Block copolymers—designer soft materials. Physics Today 1999, 52 (2), 32.

(11) Zalusky, A. S. Nanoporous material from ordered polylactide containing block copolymer template. University of Minnesota, Minneapolis, 2003.

(12) Matsen, M. W.; Thompson, R. B., Equilibrium behavior of symmetric ABA triblock copolymer melts. The Journal of Chemical Physics 1999, 111 (15), 7139-7146.

(13) Holden, G.; Quirk, R. P.; Kricheldorf, H. R., Thermoplastic Elastomers. 3rd ed.; Hanser Gardner Publications: Cincinnati, 2004.

(14) Shin, J.; Kim, Y.-W.; Kim, G.-J., Sustainable Block Copolymer-based Thermoplastic Elastomers. Applied Chemical Engineering 2014, 25 (2), 121-133.

(15) Kinnaman, T. C., The Economics of Municipal Solid Waste Management. Waste Management 2009, 2615-2617.

(16) 16. Shin, J.; Martello, M. T.; Shrestha, M.; Wissinger, J. E.; Tolman, W. B.; Hillmyer, M. A., Pressure-Sensitive Adhesives from Renewable Triblock Copolymers. Macromolecules 2011, 44, 87-94.

(17) Euliss, L. E.; DuPont, J. A.; Gratton, S.; DeSimone, J., Imparting size, shape, and composition control of materials for nanomedicine. Chemical Society reviews 2006, 35 (11), 1095-104.

(18) Biswas, A.; Bayer, I. S.; Biris, A. S.; Wang, T.; Dervishi, E.; Faupel, F., Advances in top-down and bottom-up surface nanofabrication: techniques, applications & future prospects. Advances in colloid and interface science 2012, 170 (1-2), 2-27.

(19) Devadasu, V. R.; Bhardwaj, V.; Kumar, M. N., Can controversial nanotechnology promise drug delivery? Chemical reviews 2012, 113 (3), 1686–1735.

(20) Lee, J. Y.; Cho, E. C.; Cho, K., Incorporation and release behavior of hydrophobic drug in functionalized poly(D,L-lactide)-block-poly(ethylene oxide) micelles. Journal of Controlled Release 2004, 94 (2-3), 323-335.

(21) Akagi, T.; Kaneko, T.; Kida, T.; Akashi, M., Preparation and characterization of biodegradable nanoparticles based on poly(gamma-glutamic acid) with L-

phenylalanine as a protein carrier. Journal of Controlled Release 2005, 108 (2-3), 226-236.

(22) Merkel, T. J.; Herlihy, K. P.; Nunes, J.; Orgel, R. M.; Rolland, J. P.; DeSimone, J. M., Scalable, shape-specific, top-down fabrication methods for the synthesis of engineered colloidal particles. Langmuir 2010, 26 (16), 13086-13096.

(23) Hernandez, C. J.; Mason, T. G., Colloidal alphabet soup: monodisperse dispersions of shape-designed LithoParticles. Journal of Physical Chemistry C 2007, 111 (12), 4477-4480.

(24) Badaire, S.; Cottin-Bizonne, C.; Woody, J. W.; Yang, A.; Stroock, A. D., Shape selectivity in the assembly of lithographically designed colloidal particles. Journal of the American Chemical Society 2007, 129 (1), 40-41.

(25) Dumond, J.; Low, H. Y., Residual layer self-removal in imprint lithography. Advanced Materials 2008, 20 (7), 1291-1297.

(26) Canelas, D. A.; Herlihy, K. P.; DeSimone, J. M., Top-down particle fabrication: control of size and shape for diagnostic imaging and drug delivery. Wiley Interdisciplinary Reviews-Nanomedicine and Nanobiotechnology 2009, 1 (4), 391-404.

(27) Varadan, V. K.; Chen, L.; Xie, J., Nanomedicine: design and applications of magnetic nanomaterials, nanosensors and nanosystems. Wiley: Chichester, 2008.

Chapter 2

(1) Shin, J.; Kim, Y.-W.; Kim, G.-J., Sustainable Block Copolymer-based Thermoplastic Elastomers. *Applied Chemical Engineering* **2014,** *25*, 121-133.

(2) Shin, J.; Martello, M. T.; Shrestha, M.; Wissinger, J. E.; Tolman, W. B.; Hillmyer, M. A., Pressure-Sensitive Adhesives from Renewable Triblock Copolymers. *Macromolecules* **2011,** *44*, 87-94.

(3) Bates, F. S.; Fredrickson, G. H., Block Copolymers-Design Soft Materials. *Physics Today* **1999,** *52*, 32-38.

(4) Li, H. X.; Getzinger, G. J.; Ferguson, P. L.; Orihuela, B.; Zhu, M.; Rittschof, D., Effects of Toxic Leachate from Commercial Plastics on Larval Survival and Settlement of the Barnacle Amphibalanus amphitrite. *Environmental science & technology* **2016,** *50*, 924-31.

(5) Miller, S. A., Sustainable Polymers: Opportunities for the Next Decade. *ACS Macro Letters* **2013,** *2*, 550-554.

(6) Saito, T.; Brown, R. H.; Hunt, M. A.; Pickel, D. L.; Pickel, J. M.; Messman, J. M.; Baker, F. S.; Keller, M.; Naskar, A. K., Turning renewable resources into value-added polymer: development of lignin-based thermoplastic. *Green Chemistry* **2012,** *14*, 3295.

(7) Gandini, A., The irruption of polymers from renewable resources on the scene of macromolecular science and technology. *Green Chemistry* **2011,** *13*, 1061.

(8) Liu, Y.; Yao, K.; Chen, X.; Wang, J.; Wang, Z.; Ploehn, H. J.; Wang, C.; Chu, F.; Tang, C., Sustainable thermoplastic elastomers derived from renewable cellulose, rosin and fatty acids. *Polymer Chemistry* **2014,** *5*, 3170.

(9) Wang, Z.; Yuan, L.; Jiang, F.; Zhang, Y.; Wang, Z.; Tang, C., Bioinspired High Resilient Elastomers to Mimic Resilin. *ACS Macro Letters* **2016,** *5*, 220-223.

(10) Mauck, S. C.; Wang, S.; Ding, W.; Rohde, B. J.; Fortune, C. K.; Yang, G.; Ahn, S.-K.; Robertson, M. L., Biorenewable Tough Blends of Polylactide and Acrylated Epoxidized Soybean Oil Compatibilized by a Polylactide Star Polymer. *Macromolecules* **2016,** *49*, 1605-1615.

(11) Miller, S. A., <Sustainable polymers replacing polymers derived.pdf>. *Polymer Chemistry* **2014,** *5*, 3117-3118.

(12) Haitao, Q.; Jianzhong, B.; Shenguo, W., Synthesis, characterization and degradation of ABA block copolymer of l-lactide and ε-caprolactone. *Polymer Degradation and Stability* **2000,** *68*, 423-429.

(13) Cohn, D.; Hotovely-Salomon, A., Biodegradable multiblock PEO/PLA thermoplastic elastomers: molecular design and properties. *Polymer* **2005,** *46*, 2068-2075.

(14) Frick, E. M.; Hillmyer, M. A., Synthesis and characterization of polylactide-block-polyisoprene-block-polylactide triblock copolymers: new thermoplastic elastomers containing biodegradable segments. *Macromolecular Rapid Communications* **2000,** *21*, 1317-1322.

(15) Frick, E. M.; Zalusky, A. S.; Hillmye, M. A., Characterization of Polylactide-b-polyisoprene-b-polylactide Thermoplastic Elastomers. *Biomacromolecules* **2002,** *4*, 216-223.

(16) Lebarbé, T.; Ibarboure, E.; Gadenne, B.; Alfos, C.; Cramail, H., Fully bio-based poly(l-lactide)-b-poly(ricinoleic acid)-b-poly(l-lactide) triblock copolyesters: investigation of solid-state morphology and thermo-mechanical properties. *Polymer Chemistry* **2013,** *4*, 3357.

(17) Mosnáček, J.; Yoon, J. A.; Juhari, A.; Koynov, K.; Matyjaszewski, K., Synthesis, morphology and mechanical properties of linear triblock copolymers based on poly(α-methylene-γ-butyrolactone). *Polymer* **2009,** *50*, 2087-2094.

(18) Gallagher, J. J.; Hillmyer, M. A.; Reineke, T. M., Isosorbide-based Polymethacrylates. *ACS Sustainable Chemistry & Engineering* **2015,** *3*, 662-667.

(19) Gallagher, J. J.; Hillmyer, M. A.; Reineke, T. M., Acrylic Triblock Copolymers Incorporating Isosorbide for Pressure Sensitive Adhesives. *ACS Sustainable Chemistry & Engineering* **2016,** *4*, 3379-3387.

(20) Wang, S.; Ding, W.; Yang, G.; Robertson, M. L., Biorenewable Thermoplastic Elastomeric Triblock Copolymers Containing Salicylic Acid-Derived End-Blocks and a Fatty Acid-Derived Midblock. *Macromolecular Chemistry and Physics* **2016,** *217*, 292-303.

(21) Bolton, J. M.; Hillmyer, M. A.; Hoye, T. R., Sustainable Thermoplastic Elastomers from Terpene-Derived Monomers. *ACS Macro Letters* **2014,** *3*, 717-720.

(22) Martello, M. T.; Schneiderman, D. K.; Hillmyer, M. A., Synthesis and Melt Processing of Sustainable Poly(ε-decalactone)-block-Poly(lactide) Multiblock Thermoplastic Elastomers. *ACS Sustainable Chemistry & Engineering* **2014,** *2*, 2519-2526.

(23) Maisonneuve, L.; Lebarbé, T.; Grau, E.; Cramail, H., Structure–properties relationship of fatty acid-based thermoplastics as synthetic polymer mimics. *Polymer Chemistry* **2013,** *4*, 5472.

(24) Satoh, K.; Sugiyama, H.; Kamigaito, M., Biomass-derived heat-resistant alicyclic hydrocarbon polymers: poly(terpenes) and their hydrogenated derivatives. *Green Chemistry* **2006,** *8*, 878.

(25) Satoh, K.; Matsuda, M.; Nagai, K.; Kamigaito, M., AAB-Sequence Living Radical Chain Copolymerization of Naturally Occurring Limonene with Maleimide: An End-to-End Sequence-Regulated Copolymer. *Journal of the American Chemical Society* **2010,** *132*, 10003-10005.

(26) Matsuda, M.; Satoh, K.; Kamigaito, M., Periodically Functionalized and Grafted Copolymers via 1:2-Sequence-Regulated Radical Copolymerization of Naturally Occurring Functional Limonene and Maleimide Derivatives. *Macromolecules* **2013,** *46*, 5473-5482.

(27) Shearouse, W. C.; Lillie, L. M.; Reineke, T. M.; Tolman, W. B., Sustainable Polyesters Derived from Glucose and Castor Oil: Building Block Structure Impacts Properties. *ACS Macro Letters* **2015,** *4*, 284-288.

(28) Wang, S.; Vajjala Kesava, S.; Gomez, E. D.; Robertson, M. L., Sustainable Thermoplastic Elastomers Derived from Fatty Acids. *Macromolecules* **2013,** *46*, 7202-7212.

(29) Wang, Z.; Yuan, L.; Trenor, N. M.; Vlaminck, L.; Billiet, S.; Sarkar, A.; Du Prez, F. E.; Stefik, M.; Tang, C., Sustainable thermoplastic elastomers derived from plant oil and their "click-coupling" via TAD chemistry. *Green Chem.* **2015,** *17*, 3806-3818.

(30) Yuan, L.; Wang, Z.; Trenor, N. M.; Tang, C., Robust Amidation Transformation of Plant Oils into Fatty Derivatives for Sustainable Monomers and Polymers. *Macromolecules* **2015,** *48*, 1320-1328.

(31) Lee, S.; Lee, K.; Kim, Y.-W.; Shin, J., Preparation and Characterization of a Renewable Pressure-Sensitive Adhesive System Derived from ε-Decalactone,l-Lactide, Epoxidized Soybean Oil, and Rosin Ester. *ACS Sustainable Chemistry & Engineering* **2015,** *3*, 2309-2320.

(32) Schneiderman, D. K.; Hill, E. M.; Martello, M. T.; Hillmyer, M. A., Poly(lactide)-block-poly(ε-caprolactone-co-ε-decalactone)-block-poly(lactide) copolymer elastomers. *Polym. Chem.* **2015,** *6*, 3641-3651.

(33) Schneiderman, D. K.; Hillmyer, M. A., Aliphatic Polyester Block Polymer Design. *Macromolecules* **2016,** *49*, 2419-2428.

(34) Shin, J.; Lee, Y.; Tolman, W. B.; Hillmyer, M. A., Thermoplastic elastomers derived from menthide and tulipalin A. *Biomacromolecules* **2012,** *13*, 3833-40.

(35) Ding, K.; John, A.; Shin, J.; Lee, Y.; Quinn, T.; Tolman, W. B.; Hillmyer, M. A., High-Performance Pressure-Sensitive Adhesives from Renewable Triblock Copolymers. *Biomacromolecules* **2015,** *16*, 2537-9.

(36) Lee, C.-C.; Liu, Y.; Reineke, T. M., Glucose-Based Poly(ester amines): Synthesis, Degradation, and Biological Delivery. *ACS Macro Letters* **2012,** *1*, 1388-1392.

(37) Wu, Y.; Wang, M.; Sprouse, D.; Smith, A. E.; Reineke, T. M., Glucose-containing diblock polycations exhibit molecular weight, charge, and cell-type dependence for pDNA delivery. *Biomacromolecules* **2014,** *15*, 1716-26.

(38) Yin, L.; Dalsin, M. C.; Sizovs, A.; Reineke, T. M.; Hillmyer, M. A., Glucose-Functionalized, Serum-Stable Polymeric Micelles from the Combination of Anionic and RAFT Polymerizations. *Macromolecules* **2012,** *45*, 4322-4332.

(39) Ting, J. M.; Navale, T. S.; Bates, F. S.; Reineke, T. M., Design of Tunable Multicomponent Polymers as Modular Vehicles To Solubilize Highly Lipophilic Drugs. *Macromolecules* **2014,** *47*, 6554-6565.

(40) Shi, H.; Liu, L.; Wang, X.; Li, J., Glycopolymer–peptide bioconjugates with antioxidant activity via RAFT polymerization. *Polymer Chemistry* **2012,** *3*, 1182.

(41) Mahkam, M., New pH-Sensitive Glycopolymers for Colon-Specific Drug Delivery. *Drug Delivery* **2007,** *14*, 147-153.

(42) J, B.; E, I.; E, G.; A, A.; D, B., *Polymer Handbook*. 4th ed.; Wiley: New York, 1999; Vol. 49.

(43) Hiemenz, P. C.; Lodge, T. P., *Polymer Chemistry*. CRC Press: Boca Raton, FL, 2007.

(44) Nakamura, Y.; Sakai, Y.; Adachi, M.; Fujii, S.; Sasaki, M.; Urahama, Y., Effects of Compatibility of Acrylic Block Copolymer and Tackifier on Phase Structure and Peel Adhesion of Their Blend. *Journal of Adhesion Science and Technology* **2008,** *22*, 1313-1331.

(45) Malic, N.; Evans, R. A., Synthesis of Carboxylic Acid and Ester Mid-Functionalized Polymers using RAFT Polymerization and ATRP. *Australian Journal of Chemistry* **2006,** *59*, 763–771.

(46) Li, Y.; Peng, B.; Chen, Y., Encapsulation properties of reverse-amphiphilic core/shell polymeric nanoobjects with different shapes. *Journal of Materials Chemistry B* **2013,** *1*, 5694.

(47) Nasiri, M.; Bertrand, A.; Reineke, T. M.; Hillmyer, M. A., Polymeric nanocylinders by combining block copolymer self-assembly and nanoskiving. *ACS Appl Mater Interfaces* **2014,** *6*, 16283-8.

(48) Zhang, J.; Sides, S.; Bates, F. S., Ordering of Sphere Forming SISO Tetrablock Terpolymers on a Simple Hexagonal Lattice. *Macromolecules* **2012,** *45*, 256-265.

(49) Hayashi, M.; Matsushima, S.; Noro, A.; Matsushita, Y., Mechanical Property Enhancement of ABA Block Copolymer-Based Elastomers by Incorporating Transient Cross-Links into Soft Middle Block. *Macromolecules* **2015,** *48*, 421-431.

(50) Hayashi, M.; Noro, A.; Matsushita, Y., Highly Extensible Supramolecular Elastomers with Large Stress Generation Capability Originating from Multiple Hydrogen Bonds on the Long Soft Network Strands. *Macromol Rapid Commun* **2016,** *37*, 678-84.

Chapter 3

(1) Nakajima, N.; Babrowicz, R.; Harrell, E. R., Rheology, composition, and peel-mechanism of block copolymer–tackifier-based pressure sensitive adhesives. *Journal of Applied Polymer Science* **1992,** *44*, 1437-1456.

(2) Gibert, F. X.; Marin, G.; Derail, C.; Allal, A.; Lechat, J., Rheological properties of hot melt pressure-sensitive adhesives based on styrene--isoprene copolymers. Part 1: A rheological model for [sis-si] formulations. *The Journal of Adhesion* **2003,** *79*, 825-852.

(3) Derail, C.; Cazenave, M. N.; Gibert, F. X.; Marin, G.; Kappes, N.; Lechat, J., Rheological Properties of Hot-melt Pressure-sensitive Adhesive (HMPSAS) Based on Styrene–Isoprene Copolymers. Part 2: Innovative Molecular Design from Predictive Formulation. *The Journal of Adhesion* **2004,** *80*, 1131-1151.

(4) Daoulas, K. C.; Theodorou, D. N.; Roos, A.; Creton, C., Experimental and Self-Consistent-Field Theoretical Study of Styrene Block Copolymer Self-Adhesive Materials. *Macromolecules* **2004,** *37*, 5093-5109.

(5) Jeusette, M.; Leclère, P.; Lazzaroni, R.; Simal, F.; Vaneecke, J.; Lardot, T.; Roose, P., New "All-Acrylate" Block Copolymers: Synthesis and Influence of the Architecture on the Morphology and the Mechanical Properties. *Macromolecules* **2007,** *40*, 1055-1065.

(6) Creton, C.; Hu, G.; Deplace, F.; Morgret, L.; Shull, K. R., Large-Strain Mechanical Behavior of Model Block Copolymer Adhesives. *Macromolecules* **2009,** *42*, 7605-7615.

(7) Holden, G.; Quirk, R. P.; Kricheldorf, H. R., *Thermoplastic Elastomers*. 3rd ed.; Hanser Gardner Publications: Cincinnati, 2004.

(8) Shin, J.; Kim, Y.-W.; Kim, G.-J., Sustainable Block Copolymer-based Thermoplastic Elastomers. *Applied Chemistry for Engineering* **2014,** *25*, 121-133.

(9) Tang, B.; Schneiderman, D. K.; Zare Bidoky, F.; Frisbie, C. D.; Lodge, T. P., Printable, Degradable, and Biocompatible Ion Gels from a Renewable ABA Triblock Polyester and a Low Toxicity Ionic Liquid. *ACS Macro Letters* **2017,** *6*, 1083-1088.

(10) Watts, A.; Kurokawa, N.; Hillmyer, M. A., Strong, Resilient, and Sustainable Aliphatic Polyester Thermoplastic Elastomers. *Biomacromolecules* **2017,** *18*, 1845-1854.

(11) Haitao, Q.; Jianzhong, B.; Shenguo, W., Synthesis, characterization and degradation of ABA block copolymer of l-lactide and ε-caprolactone. *Polymer Degradation and Stability* **2000,** *68*, 423-429.

(12) Lee, S.; Lee, K.; Jang, J.; Choung, J. S.; Choi, W. J.; Kim, G.-J.; Kim, Y.-W.; Shin, J., Sustainable poly(ε-decalactone)−poly(l-lactide) multiarm star copolymer architectures

for thermoplastic elastomers with fixed molar mass and block ratio. *Polymer* **2017,** *112*, 306-317.

(13) Lee, S.; Lee, K.; Kim, Y.-W.; Shin, J., Preparation and Characterization of a Renewable Pressure-Sensitive Adhesive System Derived from ε-Decalactone,l-Lactide, Epoxidized Soybean Oil, and Rosin Ester. *ACS Sustainable Chemistry & Engineering* **2015,** *3*, 2309-2320.

(14) Schneiderman, D. K.; Hill, E. M.; Martello, M. T.; Hillmyer, M. A., Poly(lactide)-block-poly(ε-caprolactone-co-ε-decalactone)-block-poly(lactide) copolymer elastomers. *Polym. Chem.* **2015,** *6*, 3641-3651.

(15) Schneiderman, D. K.; Hillmyer, M. A., Aliphatic Polyester Block Polymer Design. *Macromolecules* **2016,** *49*, 2419-2428.

(16) Schneiderman, D. K.; Gilmer, C.; Wentzel, M. T.; Martello, M. T.; Kubo, T.; Wissinger, J. E., Sustainable Polymers in the Organic Chemistry Laboratory: Synthesis and Characterization of a Renewable Polymer from δ-Decalactone and l-Lactide. *Journal of Chemical Education* **2014,** *91*, 131-135.

(17) Arrington, K. J.; Waugh, J. B.; Radzinski, S. C.; Matson, J. B., Photo- and Biodegradable Thermoplastic Elastomers: Combining Ketone-Containing Polybutadiene with Polylactide Using Ring-Opening Polymerization and Ring-Opening Metathesis Polymerization. *Macromolecules* **2017,** *50*, 4180-4187.

(18) Wanamaker, C. L.; O'Leary, L. E.; Lynd, N. A.; Hillmyer, M. A.; Tolman, W. B., Renewable-Resource Thermoplastic Elastomers Based on Polylactide and Polymenthide. *Biomacromolecules* **2007,** *8*, 3634-3640.

(19) Shin, J.; Martello, M. T.; Shrestha, M.; Wissinger, J. E.; Tolman, W. B.; Hillmyer, M. A., Pressure-Sensitive Adhesives from Renewable Triblock Copolymers. *Macromolecules* **2011,** *44*, 87-94.

(20) Hillmyer, M. A.; Tolman, W. B., Aliphatic Polyester Block Polymers: Renewable, Degradable, and Sustainable. *Accounts of Chemical Research* **2014,** *47*, 2390-2396.

(21) Cohn, D.; Hotovely-Salomon, A., Biodegradable multiblock PEO/PLA thermoplastic elastomers: molecular design and properties. *Polymer* **2005,** *46*, 2068-2075.

(22) Lee, S.; Yuk, J. S.; Park, H.; Kim, Y.-W.; Shin, J., Multiblock Thermoplastic Elastomers Derived from Biodiesel, Poly(propylene glycol), and l-Lactide. *ACS Sustainable Chemistry & Engineering* **2017,** *5*, 8148-8160.

(23) Frick, E. M.; Zalusky, A. S.; Hillmyer, M. A., Characterization of Polylactide-b-polyisoprene-b-polylactide Thermoplastic Elastomers. *Biomacromolecules* **2002,** *4*, 216-223.

(24) Lebarbé, T.; Ibarboure, E.; Gadenne, B.; Alfos, C.; Cramail, H., Fully bio-based poly(l-lactide)-b-poly(ricinoleic acid)-b-poly(l-lactide) triblock copolyesters: investigation of solid-state morphology and thermo-mechanical properties. *Polymer Chemistry* **2013,** *4*, 3357.

(25) Li, H.; Sun, J.-T.; Wang, C.; Liu, S.; Yuan, D.; Zhou, X.; Tan, J.; Stubbs, L.; He, C., High Modulus, Strength, and Toughness Polyurethane Elastomer Based on Unmodified Lignin. *ACS Sustainable Chemistry & Engineering* **2017,** *5*, 7942-7949.

(26) Wang, Z.; Yuan, L.; Tang, C., Sustainable Elastomers from Renewable Biomass. *Acc Chem Res* **2017,** *50*, 1762-1773.

(27) Zhu, Y.; Romain, C.; Williams, C. K., Sustainable polymers from renewable resources. *Nature* **2016,** *540*, 354-362.

(28) Delidovich, I.; Hausoul, P. J. C.; Deng, L.; Pfützenreuter, R.; Rose, M.; Palkovits, R., Alternative Monomers Based on Lignocellulose and Their Use for Polymer Production. *Chemical Reviews* **2016,** *116*, 1540-1599.

(29) Ganewatta, M. S.; Ding, W.; Rahman, M. A.; Yuan, L.; Wang, Z.; Hamidi, N.; Robertson, M. L.; Tang, C., Biobased Plastics and Elastomers from Renewable Rosin via "Living" Ring-Opening Metathesis Polymerization. *Macromolecules* **2016,** *49*, 7155-7164.

(30) Bolton, J. M.; Hillmyer, M. A.; Hoye, T. R., Sustainable Thermoplastic Elastomers from Terpene-Derived Monomers. *ACS Macro Letters* **2014,** *3*, 717-720.

(31) Shin, J.; Lee, Y.; Tolman, W. B.; Hillmyer, M. A., Thermoplastic Elastomers Derived from Menthide and Tulipalin A. *Biomacromolecules* **2012,** *13*, 3833-3840.

(32) Ding, K.; John, A.; Shin, J.; Lee, Y.; Quinn, T.; Tolman, W. B.; Hillmyer, M. A., High-Performance Pressure-Sensitive Adhesives from Renewable Triblock Copolymers. *Biomacromolecules* **2015,** *16*, 2537-2539.

(33) Mosnáček, J.; Yoon, J. A.; Juhari, A.; Koynov, K.; Matyjaszewski, K., Synthesis, morphology and mechanical properties of linear triblock copolymers based on poly(α-methylene-γ-butyrolactone). *Polymer* **2009,** *50*, 2087-2094.

(34) Wilbon, P. A.; Chu, F.; Tang, C., Progress in Renewable Polymers from Natural Terpenes, Terpenoids, and Rosin. *Macromolecular Rapid Communications* **2013,** *34*, 8-37.

(35) Ding, W.; Wang, S.; Yao, K.; Ganewatta, M. S.; Tang, C.; Robertson, M. L., Physical Behavior of Triblock Copolymer Thermoplastic Elastomers Containing Sustainable Rosin-Derived Polymethacrylate End Blocks. *ACS Sustainable Chemistry & Engineering* **2017,** *5*, 11470-11480.

(36) Nasiri, M.; Reineke, T. M., Sustainable glucose-based block copolymers exhibit elastomeric and adhesive behavior. *Polym. Chem.* **2016,** *7*, 5233-5240.

(37) Gallagher, J. J.; Hillmyer, M. A.; Reineke, T. M., Acrylic Triblock Copolymers Incorporating Isosorbide for Pressure Sensitive Adhesives. *ACS Sustainable Chemistry & Engineering* **2016,** *4*, 3379-3387.

(38) Tian, Z.; Fattahi, A.; Lis, L.; Kass, S. R., Single-Centered Hydrogen-Bonded Enhanced Acidity (SHEA) Acids: A New Class of Brønsted Acids. *Journal of the American Chemical Society* **2009,** *131*, 16984-16988.

(39) Nasiri, M.; Shakourian-Fard, M.; Fattahi, A., Influence of the hydrogen bonding on the basicity of selected macrocyclic amines. *Journal of Physical Organic Chemistry* **2012,** *25*, 803-810.

(40) Parmar, D.; Sugiono, E.; Raja, S.; Rueping, M., Addition and Correction to Complete Field Guide to Asymmetric BINOL-Phosphate Derived Brønsted Acid and Metal Catalysis: History and Classification by Mode of Activation; Brønsted Acidity, Hydrogen Bonding, Ion Pairing, and Metal Phosphates. *Chemical Reviews* **2017,** *117*, 10608-10620.

(41) Schreiner, P. R., Metal-free organocatalysis through explicit hydrogen bonding interactions. *Chemical Society Reviews* **2003,** *32*, 289-296.

(42) Ting, J. M.; Tale, S.; Purchel, A. A.; Jones, S. D.; Widanapathirana, L.; Tolstyka, Z. P.; Guo, L.; Guillaudeu, S. J.; Bates, F. S.; Reineke, T. M., High-Throughput Excipient Discovery Enables Oral Delivery of Poorly Soluble Pharmaceuticals. *ACS Central Science* **2016,** *2*, 748-755.

(43) Tale, S.; Purchel, A. A.; Dalsin, M. C.; Reineke, T. M., Diblock Terpolymers Are Tunable and pH Responsive Vehicles To Increase Hydrophobic Drug Solubility for Oral Administration. *Molecular Pharmaceutics* **2017,** *14*, 4121-4127.

(44) Lillie, L. M.; Tolman, W. B.; Reineke, T. M., Structure/property relationships in copolymers comprising renewable isosorbide, glucarodilactone, and 2,5-bis(hydroxymethyl)furan subunits. *Polym. Chem.* **2017,** *8*, 3746-3754.

(45) Beniah, G.; Fortman, D. J.; Heath, W. H.; Dichtel, W. R.; Torkelson, J. M., Non-Isocyanate Polyurethane Thermoplastic Elastomer: Amide-Based Chain Extender Yields Enhanced Nanophase Separation and Properties in Polyhydroxyurethane. *Macromolecules* **2017,** *50*, 4425-4434.

(46) Hayashi, M.; Matsushima, S.; Noro, A.; Matsushita, Y., Mechanical Property Enhancement of ABA Block Copolymer-Based Elastomers by Incorporating Transient Cross-Links into Soft Middle Block. *Macromolecules* **2015,** *48*, 421-431.

(47) Feldman, K. E.; Kade, M. J.; Meijer, E. W.; Hawker, C. J.; Kramer, E. J. Model Transient Networks from Strongly Hydrogen-Bonded Polymers. *Macromolecules* **2009,** *42*, 9072-9081.

(48) Montarnal, D.; Delbosc, N.; Chamignon, C.; Virolleaud, M. A.; Luo, Y.; Hawker, C. J.; Drockenmuller, E.; Bernard, J. Highly Ordered Nanoporous Films from Supramolecular Diblock Copolymers with Hydrogen-Bonding Junctions. *Angew. Chem., Int. Ed.* **2015**, 54, 11117−11121.

(49) Tong, J.-D.; Jerôme, R., Dependence of the Ultimate Tensile Strength of Thermoplastic Elastomers of the Triblock Type on the Molecular Weight between Chain Entanglements of the Central Block. *Macromolecules* **2000,** *33*, 1479-1481.

(50) Tehrani, M.; Sarvestani, A., Effect of chain length distribution on mechanical behavior of polymeric networks. *European Polymer Journal* **2017,** *87*, 136-146.

(51) Nasiri, M.; Bertrand, A.; Reineke, T. M.; Hillmyer, M. A., Polymeric nanocylinders by combining block copolymer self-assembly and nanoskiving. *ACS Appl Mater Interfaces* **2014,** *6*, 16283-8.

(52) Mark, J. E., *Physical Properties of Polymers Handbook*. 2 ed.; Springer-Verlag New York: New York, NY, 2007.

(53) Kaelble, D. H., Theory and Analysis of Peel Adhesion: Adhesive Thickness Effects. *The Journal of Adhesion* **1992,** *37*, 205-214.

(54) Zhou, C.; Hillmyer, M. A.; Lodge, T. P., Micellization and Micellar Aggregation of Poly(ethylene-alt-propylene)-b-poly(ethylene oxide)-b-poly(N-isopropylacrylamide) Triblock Terpolymers in Water. *Macromolecules* **2011,** *44*, 1635-1641.

(55) De Kimpe, N.; Van, T.; Claessens, S.; Habonimana, P.; Tehrani, K.; Van Puyvelde, L., Synthesis of Harounoside, A Naturally Occurring Pentalongin Hydroquinone Bisglucoside. *Synlett* **2006,** *2006*, 2469-2471.

Chapter 4

(1) Euliss, L. E.; DuPont, J. A.; Gratton, S.; DeSimone, J. M. Imparting Size, Shape, and Composition Control of Materials for Nanomedicine. *Chem. Soc. Rev.* **2006,** *35*, 1095-1104.

(2) Biswas, A.; Bayer, I. S.; Biris, A. S.; Wang, T.; Dervishi, E.; Faupel, F. Advances in top-down and bottom-up surface nanofabrication: Techniques, Applications & Future Prospects. *Adv. Colloid Interface Sci.* **2012,** *170*, 2-27.

(3) Devadasu, V. R.; Bhardwaj, V.; Kumar, M. N. V. R. Can Controversial Nanotechnology Promise Drug Delivery? *Chem. Rev.* **2013,** *113*, 1686-1735.

(4) Zhang, L. F.; Eisenberg, A. Multiple Morphologies of Crew-cut Aggregates of Polystyrene-b-poly(acrylic acid) Block-copolymers. *Science* **1995**, 268, 1728-1731.

(5) Hu, J.; Njikang, G.; Liu, G. Twisted ABC Triblock Copolymer Cylinders with Segregated A and C Coronal Chains. *Macromolecules* **2008**, 41, 7993-7999.

(6) Li, X.; Liu, G.; Han, D. Wrapping Amino-bearing Block Copolymer Cylinders Around Carboxyl-bearing Nanofibers: A Case of Hierarchical Assembly. *Soft Matter* **2011**, 7, 8216-8223.

(7) Choi, S.-H.; Bates, F. S.; Lodge, T. P. Molecular Exchange in Ordered Diblock Copolymer Micelles. *Macromolecules* **2011**, 44, 3594-3604.

(8) Lund, R.; Willner, L.; Richter, D. In *Controlled Polymerization and Polymeric Structures*; Abe, A., Lee, K.-S., Leibler, L., Kobayashi, S., Eds.; Springer International Publishing: 2013; Vol. 259, pp 51-158.

(9) Badaire, S.; Cottin-Bizonne, C.; Woody, J. W.; Yang, A.; Stroock, A. D. Shape Selectivity in the Assembly of Lithographically Designed Colloidal Particles. *J. Am. Chem. Soc.* **2007**, 129, 40-41.

(10) Merkel, T. J.; Herlihy, K. P.; Nunes, J.; Orgel, R. M.; Rolland, J. P.; DeSimone, J. M. Scalable, Shape-Specific, Top-Down Fabrication Methods for the Synthesis of Engineered Colloidal Particles. *Langmuir* **2010,** *26*, 13086-13096.

(11) Canelas, D. A.; Herlihy, K. P.; DeSimone, J. M. Top-down Particle Fabrication: Control of Size and Shape for Diagnostic Imaging and Drug Delivery. *Wiley Interdiscip. Rev. Nanomed. Nanobiotechnol.* **2009,** *1*, 391-404.

(12) Varadan, V. K.; Chen, L.; Xie, J. *Nanomedicine: design and applications of magnetic nanomaterials, nanosensors and nanosystems*. John Wiley & Sons, Ltd: Chichester, UK, 2008.

(13) Kim, H.-C.; Park, S.-M.; Hinsberg, W. D. Block Copolymer Based Nanostructures: Materials, Processes, and Applications to Electronics. *Chem. Rev.* **2010,** *110*, 146-177.

(14) Zalusky, A. S.; Olayo-Valles, R.; Wolf, J. H.; Hillmyer, M. A. Ordered Nanoporous Polymers from Polystyrene-Polylactide Block Copolymers. *J. Am. Chem. Soc.* **2002,** *124*, 12761-12773.

(15) Drzal, P. L.; Barnes, J. D.; Kofinas, P. Path Dependent Microstructure Orientation During Strain Compression of Semicrystalline Block Copolymers. *Polymer* **2001,** *42*, 5633-5642.

(16) Rzayev, J.; Hillmyer, M. A. Nanochannel Array Plastics with Tailored Surface Chemistry. *J. Am. Chem. Soc.* **2005,** *127*, 13373-13379.

(17) Bertrand, A.; Hillmyer, M. A. Nanoporous Poly(lactide) by Olefin Metathesis Degradation. *J. Am. Chem. Soc.* **2013,** *135*, 10918-10921.

(18) Xu, Q. B.; Gates, B. D.; Whitesides, G. M. Fabrication of Metal Structures with Nanometer-Scale Lateral Dimensions by Sectioning Using a Microtome. *J. Am. Chem. Soc.* **2004,** *126*, 1332-1333.

(19) Xu, Q.; Rioux, R. M.; Dickey, M. D.; Whitesides, G. M. Nanoskiving: A New Method To Produce Arrays of Nanostructures. *Acc. Chem. Res.* **2008,** *41*, 1566-1577.

(20) Lipomi, D. J.; Martinez, R. V.; Whitesides, G. M. *Angew. Chem. Int. Ed.* **2011**, *50*, 8566-8583.

(21) Shen, M. C.; Eisenberg, A. Glass Transitions in Polymers. *Rubber Chem. and Technol.* **1970,** *43*, 95-155.

(22) Hyon, S. H.; Jamshidi, K.; Ikada, Y. Effects of Residual Monomer on the Degradation of DL-Lactide Polymer. *Polym. Int.* **1998,** *46*, 196-202.

(23) Faber, M.; Hofman, A. H.; Polushkin, E.; van Ekenstein, G. A.; Seitsonen, J.; Ruokolainen, J.; Loos, K.; ten Brinke, G. Hierarchical Self-Assembly in Supramolecular Double-Comb Diblock Copolymer Complexes. *Macromolecules* **2013,** *46*, 500-517.

(24) Chiantore, O.; Costa, L.; Guaita, M. Glass Temperatures of Acrylamide Polymers. *Makromol. Chem. Rapid Commun.* **1982,** *3*, 303-309.

(25) Witzke, D. R.; Narayan, R.; Kolstad, J. J. Reversible Kinetics and Thermodynamics of the Homopolymerization of L-Lactide with 2-Ethylhexanoic Acid Tin(II) Salt. *Macromolecules* **1997,** *30*, 7075-7085.

(26) Quach, A.; Simha, R. Pressure-Volume-Temperature Properties and Transitions of Amorphous Polymers; Polystyrene and Poly (orthomethylstyrene). *J. Appl. Phys.* **1971,** *42*, 4592-4606.

(27) Gundogan, N.; Okay, O.; Oppermann, W. Swelling Elasticity and Spatial Inhomogeneity of Poly(N,N-dimethylacrylamide) Hydrogels Formed at Various Polymer Concentrations. *Macromol. Chem. Phys.* **2004,** *205*, 814-823.